UNIVERSITY OF THE
WITWATERSRAND,
JOHANNESBURG

Taphonomy and palaeoecology of a monospecific microvertebrate bonebed: behavioural implications for the late Permian (Lopingian) parareptiles

by

Lutendo Mukwevho

(1944548)

0000-0003-2927-7057

A dissertation submitted to the Faculty of Science, University of the Witwatersrand, in fulfilment of the requirements for the degree of Master of Science in Palaeontology

Supervisors: Professor Jonah Choiniere & Professor Roger Smith

DECLARATION

I declare that this dissertation is my own, unaided work. It is being submitted for the Degree of Master of Science at the University of the Witwatersrand Johannesburg. It has not been submitted before for any degree of examination at any other University.

_____

Signed on the 05th June 2024 at the Evolutionary Studies Institute, University of the Witwatersrand, Johannesburg.

ABSTRACT

Sociality in the vertebrate fossil record is a dynamic and fast-expanding area of research. Natural history observations of living animals are crucial for understanding and categorizing sociality, but these observations are not feasible for extinct species. Monotaxic bonebeds provide unique opportunities to conceptualize the social behaviours of these extinct animals. An unusual bonebed (SAM-PK-K11289) discovered in the uppermost Permian strata of the Balfour Formation, Karoo Supergroup, in the Eastern Cape presents a window into the sociality of Late Permian reptiles. The use of propagation phase-contrast synchrotron X-ray microcomputed tomography permitted the 3D reconstruction of skeletal elements in SAMPK-K11289, allowing the taxonomic identification of the individuals in the bonebed as most likely belonging to *Owenetta.* This is the largest aggregation of *Owenetta* individuals known to date, with a minimum number of 31, which are all very similar in body size. The ontogenetic profile of SAM-PK-K11289 was interpreted by analysing the size distribution of duplicate elements and by making comparisons with other *Owenetta* and procolophonid specimens. The specimens in the bonebed are all osteologically immature, indicating that they are juveniles. The bonebed occurs in a pedogenically modified ripple cross-laminated siltstone suggesting that a low-energy fluvial sedimentation likely contributed to the modification, disturbance and disarticulation of elements before the bonebed was buried at or very close to the death site. This bonebed provides novel information that directly challenges the popular belief that reptiles and their ancestors are non-social or asocial. Considering the overall circumstances of the bonebed, I hypothesize that *Owenetta rubidgei* juveniles were socially gregarious and this behaviour may have been induced or influenced by environmental changes during the early extinction phase of the end Permian mass extinction in the Karoo Basin.

ACKNOWLEDGEMENTS

Academic research has been equally challenging as it is rewarding. I am indebted to multiple people for their invaluable contributions to the successful conclusion of my project. To begin with, I would like to thank my supervisors Professor Jonah Choiniere and Professor Roger Smith. I have learnt so much under your supervision. Thank you for your guidance, patience, and the opportunities you provided. Thank you for fostering an environment that motivates me to think critically and creatively.

To beam scientists Kathleen Dollman and Vincent Fernandez from the European Synchrotron Facility of Radiation, thank you for working tirelessly to provide me with the best synchrotron data possible. Thank you for always being available to answer questions and share data processing techniques.

To my lab mates, Bailey Weis, Rick Tolchard, Atashni Moopen, Wade Harris, Chandele Montgomary, Brandon Stuart, Dr Kimberly Chapelle and Enele Twala, thank you for your continued support, friendship, and willingness to share your different skill sets. It has been an absolute privilege to know and learn from you. To honorary members of the lab and visiting researchers, your interest in my project motivated me.

Thank you to the following collection managers and curators for granting me access to their material. Zaituna Skosan and Claire Browning from the Iziko South African Museum, Dr Sifelani Jireh and Dr Bernhard Zipfel from the Evolutionary Studies Institute and Dr Heidi Fourie from the Ditsong Museum. Thank you to Dr Marc Van den Brandt who helped take images of the specimens from the Wellwood collection.

Prof Roger Benson and Dr Christian Kammerer, thank you for the thought-provoking conversations that have given me much to ponder. Your perspectives and insight challenged me to think critically.

To my mother Flora Mukwevho, thank you for supporting me unconditionally.

Lastly this project would have not been possible without Genus (the DSI-NRF Centre of Excellence, Palaeosciences). Thank you for the financial support.

TABLE OF CONTENTS

LIST OF FIGURES

LIST OF TABLES

INTRODUCTION AND LITERATURE REVIEW

INTRODUCTION

Animal behaviour is a long-established scientific field and has been an integral part of Evolutionary Biology since the publication of Charles Darwin's seminal work, "On the Origin of Species", in the mid 1800's (Darwin, 1965, Ord et al., 2005, Darwin and Quammen, 2008). Biologists are particularly interested in the behaviour of modern animals because it provides insights into their ecology and biodiversity consequently helping them design conservation and management strategies (Dawkins, 2003, Barnard, 2007, Fraser, 2009, Davies et al., 2012, Nelson, 2014, Greggor et al., 2016).

Palaeontologists on the other hand are interested in studying the behaviour of ancient animals because it provides insights about the origins of behaviour and how it became modified over time (Barnard, 2012). Examples of interesting behaviours documented in the fossil record abound. For example, the drought-afflicted *Lystrosaurus* bonebeds from the earliest Triassic Karoo Basin of South Africa were interpreted as original behavioural aggregations that may have resulted from herd living behaviour of non-migratory herbivores, which is also observed in modern large herbivores (Smith et al., 2022). The discovery of an entombed *Diictodon* in a helical burrow provides the oldest evidence for helical burrowing in tetrapods and allows us to trace such burrowing behaviours to long before the age of mammals (Smith, 1987, Smith et al., 2021, Smith et al., 2022). Behaviours exhibited by modern birds have been observed in extinct theropod dinosaur fossils. For example a specimen of *Mei long,* a theropod dinosaur from the Early Cretaceous of the Yixian Formation in China, is preserved in a bird-like sleeping posture (Xu and Norell, 2004).

Animal behaviour is extremely diverse, encompassing a wide range of encounters and activities (Sparks, 1984). Examples of the more common animal behaviours include foraging, learned behaviour, territoriality, altruism, reproductive behaviours and social behaviours (Stamps, 1994, Hafez and Hafez, 2000, Okasha, 2003, van

Schaik, 2010, Kamil et al., 2012, Tinbergen, 2012). This study focuses on the social behavioural aspects (Frank, 2007, Wey et al., 2008, Ward and Webster, 2016) of a long extinct reptilian taxon that encompasses interactions between multiple individuals of the same species.

Actual observational data are required to study the social behaviour of extant animals (Hsieh and Plotnick, 2020). The social behaviours of ancient animals cannot be observed in real-time, making it challenging to reconstruct social behavioural repertoires from the fossil record (Benton, 2010, Hsieh and Plotnick, 2020). Fortunately, aggregations of the skeletons of multiple animals, here referred to as bonebeds (Rogers and Kidwell, 2007) offer a unique opportunity to study, conceptualize and categorize sociality in ancient animals. Various methods are utilized to study bonebeds, including investigating the taphonomy, morphology, taxonomy and palaeoenvironmental setting. This study uses classical methods coupled with synchrotron computer tomography scanning- a technique that is relatively new to the field of palaeontology- to investigate a late Permian microvertebrate bonebed from the South African Karoo basin (see Figure 1) containing hundreds of skeletal elements. This technique allows us to sharply image what would otherwise be invisible or poorly defined by conventional micro-computed X-ray scanning. It has been successfully applied to other fossil specimens and produced exceptional results (refer to Tafforeau et al. (2006) for review).

Ventral view

Dorsal view

Figure 1: Bonebed SAM-PK-K11289, the main focus of the current study, before preparation.

Late Permian microvertebrate bonebed. (A) Convex ventral view of bonebed SAMPK-K11289 and (B) Concave ventral view of bonebed SAM-PK-K11289.

LITERTURE REVIEW

Taphonomy of bonebeds

Taphonomy was originally defined by Efremov (1940) when he recognized the challenges that arise while studying and interpreting the deposition and preservation of organic matter. A more recent definition that extends the field to include plant and animal remains is “the comprehensive study of information from the time an organism dies to the time it is discovered in the fossil record” (Lawrence, 1968). It is an integrative field that includes but is not limited to collecting information from a fossil’s sedimentology, ecology, stratigraphy, geochemistry, ichnology and morphology. It is thus an important aspect in the field of palaeontology as it allows us to study fossils holistically. Early taphonomic research stressed the contribution of taphonomic processes to the loss of information and therefore focused primarily on studying the preservation bias in the fossil record. The breadth of study in taphonomy has since expanded while still being cognizant of the importance of this sort of data. Although taphonomy originated as a “new branch of palaeontology”, it has now become prevalent in other research domains such as archaeology and forensic science (Janaway et al., 2009).

Reconstructing the taphonomic history in palaeontology allows us to gather information about a fossil beyond that of taxonomic identification. It allows us to retrace the chain of occurrences leading to the preservation of an organism as a fossil and draw palaeontological conclusions (Fernández-Jalvo et al., 2011). The nature and extent of taphonomic history that can be recovered will vary between fossil specimens because of differential preservation. Generally, the taphonomic history of a fossil specimen provides information about the palaeoecology and palaeobiology of the organism, so that inferences may be made about the cause of the death, how long the organismal remains have been exposed to subaerial environmental factors and the processes leading to the final burial of the remains in the host sediment.

As opposed to single fossil specimens, the unique taphonomic signatures of bonebeds provides us with a more dynamic view of ancient life (Rogers et al., 2007).

In addition to the information listed above, bonebed assemblages occasionally capture short-term events, providing us with a glimpse of real-time moments in the ancient world. Some of the events captured include biological activities or catastrophes during ancient times. For recent examples, Smith et al. (2022) identified the monotaxic *Lystrosaurus* bonebeds from the lowermost Triassic of the Katberg Formation of the Karoo Basin and interpreted them as drought-induced mass death assemblages. A multitaxon aggregation of *Owenetta kitchingorum* (now synonymised with *Saurodektes kitchingorum*) and *Galesaurus planiceps* from early Triassic of the Katberg Formation has been interpreted as the likely the first evidence for shelter sharing in tetrapods (Abdala et al., 2006).

The taphonomy of bonebeds includes the investigation of the geochemical conditions of the locality and it allows us to infer how the accumulated bones became fossilized and how much reworking occurred before final burial. Eberth et al. (2010) defined a bonebed as any aggregation of vertebrate skeletal material belonging to multiple individuals. Bonebeds are reported throughout the marine and terrestrial deposits of the Phanerozoic (Rogers et al., 2007). The oldest reported vertebrate bonebeds are from the Ordovician and Devonian marine deposits and consist of multiple jawless fishes (Behre and Johnson, 1933, Allulee and Holland, 2005).

Following the size-based categories outlined by Behrensmeyer (2007), vertebrate skeletal accumulations are categorized as either microfossil bonebeds or macrofossil bonebeds (Rogers et al., 2007). This microfossil and macrofossil bonebed dichotomy is recognised by many palaeontologists. A macrofossil bonebed is a concentration of vertebrate skeletal elements that are larger than 5 cm in length and width and belong to more than two individuals. Some of the most famous examples of macrofossil bonebeds include the Liscomb bonebed assigned to the late Campanian Maastrichtian of the Prince Creek Formation and the *Albertosaurus* bonebed from the upper Horseshoe Canyon Formation. The Liscomb bonebed is a monodominant accumulation of over 600 dinosaur specimens. The assemblage is dominated by late juvenile *Edmontosaurus*. Gangloff and Fiorillo (2010) concluded that this was a mass mortality caused by overbank flooding. They also hypothesized that dinosaurs living in high altitudes were social and formed aggregations (Rogers,

1990, Sander, 1992, Gangloff and Fiorillo, 2010, Bell and Campione, 2014). The *Albertosaurus* bonebed is a multitaxic bonebed of 1340 specimens belonging to *Albertosaurus* and other taxa. The taphonomic signature observed in this bonebed could not be used to confidently suggest gregariousness in *Albertosaurus* (Eberth and Currie, 2010).

The South African Karoo Basin also preserves exemplary macrofossil bonebeds that have contributed significantly to the global understanding of the End Permian mass extinction, considered by many researchers as the most catastrophic extinction event in history. (Stanley and Yang, 1994, Retallack, 1995, Benton and Twitchett, 2003, Erwin, 2015). One such example is the *Lystrosaurus* bonebed (SAM-PKK8551) from the earliest Triassic of the South African Karoo basin. This bonebed encompasses 9 subadult individuals identified as *Lystrosaurus declivis*. This assemblage was interpreted as a behavioural aggregation that occurred in response to a cold snap (Viglietti et al., 2013). Subsequent, more detailed analysis of the distribution of skeletal elements and their stratification has concluded that the 9 subadults most likely succumbed to hunger and died around a shrinking waterhole on a drought-stricken Karoo floodplain, their disarticulated bones then further concentrated by sheet wash (Smith et al., 2022). This bonebed was recovered close to an exposure of the Permo-Triassic boundary, ultimately contributing to our understanding of the survival and recovery of fauna after the End-Permian mass extinction (Viglietti et al., 2013).

Microfossil bonebeds or vertebrate microsites contain 75% or more of vertebrate skeletal elements that are individually no larger than 5 cm in length and width, and which are substantially complete (Eberth et al., 2010). Microfossil bonebeds are crucial for reconstructing terrestrial communities of vertebrate palaeofauna and have been used to estimate the once-living species abundance and richness (Rogers and Brady, 2010). The two most prevailing theories regarding the genesis of microfossil bonebeds include fluvial processes and scatological origins (Mellett, 1974, Korth, 1979). For a long time, these theories have served as the foundation of microfossil bonebed interpretation. However, the composition of some microfossil bonebeds does not align with these two theories, requiring an alternative explanation. For example, the Judith River microfossil bonebeds from the Upper Cretaceous of

Montana do not exhibit any features compatible with the scenarios mentioned above and are instead interpreted as assemblages accumulated by low-energy aquatic systems such as ponds and lakes (Rogers and Brady, 2010).

In addition to the size of the preserved skeletal elements, the origins of a bonebed are widely used for classification. The origin of bonebeds can be classified as either biogenetic or physical. Biogenetic concentrations are vertebrate skeletal accumulations that result from the activities of the animal. Biogenic concentrations can either be intrinsic or extrinsic. Intrinsic biogenic concentrations are essentially a record of the biological activity performed by the individuals in the concentration. Extrinsic biogenetic concentrations are a record of the biological activities of other vertebrates performed on the vertebrates in the bonebed (Rogers et al., 2007). Physical concentrations are vertebrate skeletal accumulations that are generated by physical processes such as fluvial systems and the accumulation of sediments. Vertebrate skeletal parts that accumulate as a result of the fluvial systems are categorized as hydraulic accumulations and those that concentrate due to the accumulation of sediments are categorized as sedimentologic concentrations (Rogers and Kidwell, 2007). These categories are not mutually exclusive, every bonebed is unique and can satisfy multiple criteria resulting in it fitting in more than one category.

Bonebed aggregations from the Main Karoo Basin and their behavioural interpretations

Bonebed aggregations are significant indicators of sociality in animals. However fossil vertebrate bonebeds may also originate from long-term accumulation of vertebrate material with no behavioural significance, therefore we must be careful of over-interpretation. Different lines of evidence must be used to collect information about the structure and composition of an assemblage to achieve accurate palaeobiological reconstructions and make behavioural inferences that are as close to the truth as possible (Jasinoski and Abdala, 2017). Extensive research has been conducted on the social behaviours of modern animals. Although this research primarily focuses on birds and mammals, it has allowed us to develop a framework

of present-day animal behaviour that can be used to identify the social behaviours represented in the fossil record (Gaston, 1992, Bonnet et al., 2002, Pawar, 2003).

The South African Karoo basin has produced fossil aggregations that have presented compelling evidence for social behaviour in ancient organisms. Perhaps the first report of a social aggregation from the South African Karoo Basin was made in 1954 when J.W Kitching discovered a nodule containing one large individual and three similar-sized smaller individuals of the Early Triassic cynodont *Thrinaxodon*. At the time of the discovery, the specimen was used for morphological description (Brink, 1954), later Jasinoski and Abdala (2017) reviewed this specimen and hypothesized that the two different size classes are indicative of parental care. More specimens of *Thrinaxodon* juvenile aggregations have since been discovered suggesting that the juveniles of this genus behaviourally aggregated underground most likely for temperature regulation (Smith and Botha, 2005) but possibly some form of gregarious social behaviour (Jasinoski and Abdala, 2017). Such specimens provide unique and direct evidence of a behaviour.

The discovery of an aggregate of five articulated juveniles of the sauropsid reptile *Youngina capensis* from the late Permian strata of the Karoo is a notable instance (see Figure 2A and B for reference). The parallel alignment and the high degree of articulation of the *Youngina* skeletons, coupled with the presence of the floating sternal plates suggests that they were buried in their ‘life positions’ and had minimal to no exposure to processes that are responsible for destruction and dispersal (Smith and Evans, 1996). Analysis of the aggregation’s structure, composition and morphology revealed that every individual has the same level of skeletal development, conveying juvenility. Palaeoenvironmental interpretations of the host strata suggest that this was probably a method of minimising water loss during periods of drought on the semi-arid floodplains of the southern Karoo Basin. The identical ontogenetic stage of the five individuals suggests that they are from the same parent as observed in extant juvenile amniotes (Coombs, 1982, Gardner et al., 2001). The absence of multi-ontogenetic classes suggests and reflects a social behaviour known as brooding, also observed in their contemporary analogues. This *Youngina* assemblage is evidence that monospecific juvenile aggregation behaviour was practised by diapsid reptiles at least 255 million years ago.

Botha-Brink and Modesto (2009) described an aggregate of five articulated individuals of the varanopid *Heleosaurus scholtzi* from the middle Permian Abrahamskraal Formation (see Figure 2B and C for reference) in the southern Karoo Basin. The preservation style is like that of the *Youngina* specimen, revealing minimal disturbance and dispersal. However, this aggregation has preserved two ontogenetic classes. One individual, identified as the adult, is 50% larger than the other four individuals and has skeletal elements with a higher degree of ossification. The close association of an adult and 4 juveniles of the same age classes is suggestive of a brood aggregation with an attendant adult that could have been a parent (Botha-Brink and Modesto, 2009). Prior to the description of this specimen, only more recently branching vertebrates were known to exhibit this parental care behaviour (Ar and Yom-Tov, 1978, Clutton-Brock, 1991, Meng et al., 2004, Gubernick, 2013). There had been no prior reports of parental care in older Palaeozoic synapsids such that this may be the oldest fossil evidence of parental care in vertebrates.

Studying and understanding the social behaviours represented in the fossil record is crucial and enables us to form hypotheses about the origins of these behaviours in the vertebrate lineage, how the behaviour has evolved over time, the selective advantage of such behaviours and more.

Animal behaviour

The study of animal behaviour is necessarily interdisciplinary, with implications for understanding evolutionary processes, ecological dynamics, conservation biology and ultimately the natural world. Sociality evolved independently in different lineages, serving different purposes for different species. There are various benefits of forming social aggregations, including increased success in reproduction, predator deterrent, enhanced resource acquisition, thermoregulation, and transmission of knowledge, however, the overarching goal is survival. The same form of sociality may appear across different species (Doody et al., 2013). For instance, parental care – a social behaviour in which parents tend to their young is exhibited in different ways. In some species of Osteichthyes, the male parent looks after the offspring (Blumer, 1979, Blumer, 1982), while in other species it is the

female (Balshine, 2012). Brooding is also exhibited differently, some species such as the Japanese quail retain brooding in adulthood while others like the White-browed scrubwren, exhibit brooding only in juvenility (Leedman and Magrath, 2003, Ruscio and Adkins-Regan, 2004).

Making real-time observations of extinct organisms aggregating is impossible, making it challenging to study their social behaviours. However, bonebeds composed of multiple individuals can, in certain circumstances, represent aggregations. Bonebed assemblages have been used to infer complex social behaviours in ancient organisms (Ibiricu et al., 2013). For example, a Cretaceousaged assemblage with 21 subadult individuals of *Sinornithomimus dongi* from western Inner Mongolia was interpreted as a social aggregation representing herding in subadults and possibly extensive extended parental care (Varricchio et al., 2008). Inferring the behaviour of extinct organisms can be challenging due to limited information, but it is undeniable that fossils and their taphonomy provide us with novel information about behaviour and function (Benton, 2010, Hsieh and Plotnick, 2020). Understanding the social behaviours of ancient organisms requires collecting taphonomic data, morphological data, spatial data, assemblage data and making comparisons with their modern analogues (Benton, 2010, Rogers et al., 2010).

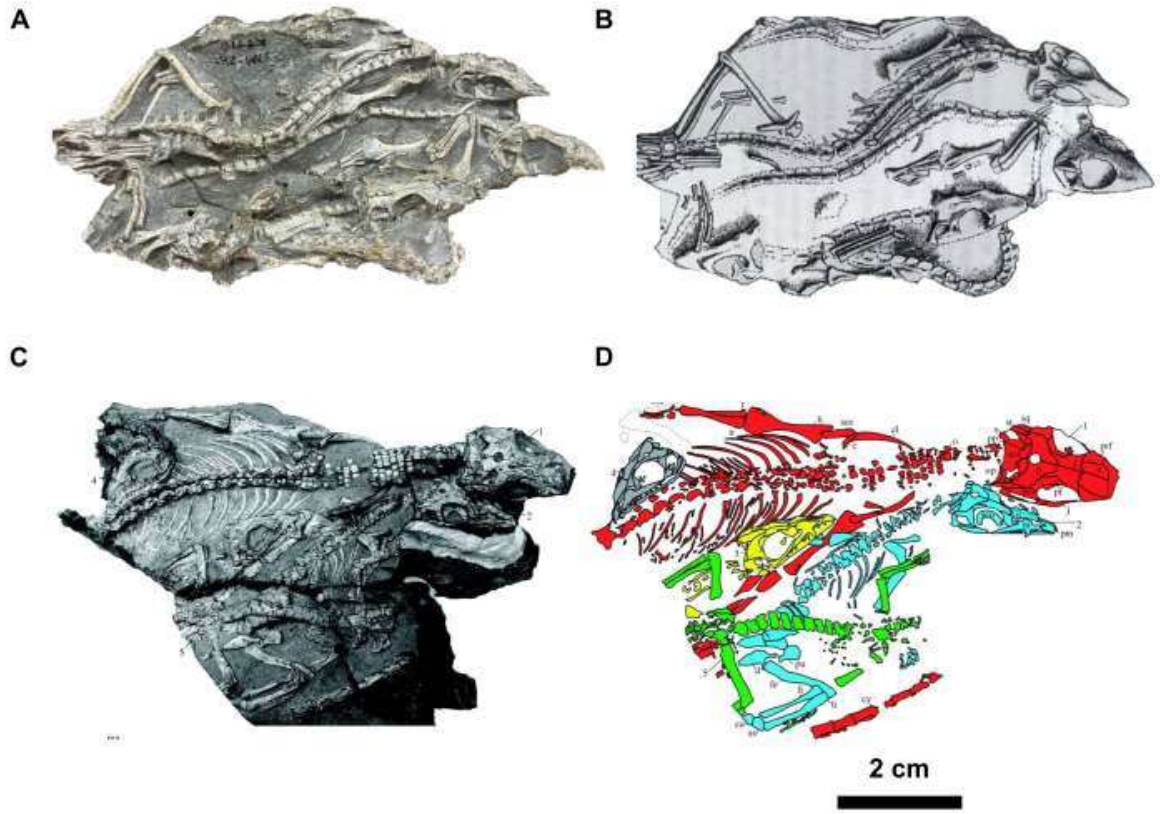

Figure 2: Examples of reptile aggregations with possible social significance from the South African Main Karoo.

(A) Dorsal view of an aggregation of five articulated juvenile *Youngina* (SAM-PK-K7710) from the Late Permian strata of the Karoo, here interpreted as a brood, from Smith and Evans (1996), (B) Drawing of dorsal side of SAM-PK-K7710 from Smith and Evans 1996 (C), An aggregate of five articulated varanopid individuals *Heleosaurus scholtzi* (SAM-PK-K8305) from the middle Permian Abrahamskraal Formation, interpreted as exhibiting extended parental care, from Botha-Brink and Modesto (2009) and (D) Interpretive drawing of SAM-PK-K8305 from Botha-Brink and Modesto 2009.

Body Size and Ecophysiology

Body size is an important metric for a host of evolutionary, ecological and physiological factors in vertebrates (Peters, 1986, Sauer and Slade, 1987, Brown et al., 1993, Currie, 1993, Blackburn and Gaston, 1994, Marquet et al., 1995, Burness et al., 2001, Gillooly et al., 2001, Speakman, 2005, White et al., 2007). This correlation is firmly established by research on extant taxa which reveals that it is strongly correlated to the organism's growth rate, metabolic rate, population diversity and density, clutch size and fecundity (Kleiber, 1947, Blackburn et al., 1990, Currie,

1993, Honěk, 1993, Martin and Palumbi, 1993, Elliott and Hurley, 1995, Marquet et al., 1995, Lafferty and Kuris, 2002, Davidowitz and Nijhout, 2004, Kozłowski et al., 2020, Preziosi et al., 1996).

The body size of extinct taxa cannot be directly measured, but because of its strong correlation to the biology of an organism and its potential to inform us of palaeobiology, researchers have devised several methods to estimate it (Campione and Evans, 2012). Volumetric reconstructions and skeletal scaling relationships are the most common methods used to estimate body size in extinct taxa (Folland et al., 2008, Brassey, 2016, Romano and Rubidge, 2021). This study uses skeletal scaling relationships. Skeletal scaling relationships were adopted from the pioneering work of Anderson et al. (1985) which found high regression coefficients between the circumference of the stylopodia and body mass. This method was traditionally used to estimate the body size of mammals, birds and their ancestors (Finarelli and Flynn, 2006, Millien and Bovy, 2010, De Esteban-Trivigno et al., 2008, Gingerich, 1990, Campbell and Marcus, 1992). Campione and Evans (2012) tested the applicability of this technique to distant taxa and revealed that it can be confidently applied to all terrestrial vertebrates, despite their variable evolutionary histories and gaits, and with subsequent modification of predictor variables even different limb postures (Campione et al., 2014). Body size estimates of extinct taxa have been used to comprehend, conceptualize and interpret large-scale evolutionary patterns, survivorship patterns, trophic structure of palaeoenvironments, and postural estimation (Benson et al., 2014, Campione and Evans, 2020).

MATERIALS

The Late Permian bonebed specimen (SAM-PK-K11289 accessioned at the Iziko South African Museum) consists of at least 316 skeletal elements in varying degrees of articulation and association (Figures 3 and 4). The entire bonebed SAM-PKK11289 is dish-shaped, 160 mm long, 85 mm wide and 55 mm thick with an elliptical planimetric shape. Although the specimen was found ex-situ it is most likely that the concave surface of the dish structure is the original dorsal surface of the bonebed. Some elements on the upper and lower surface are preserved in articulation such that their “life positions” can be inferred. Other elements are strongly associated but not in their natural or “life” positions. Elements on the surface exhibit dark grey and brown colour. The majority of the bones overlap and are in direct contact with one another. The matrix surrounding the skeletal elements is greenish grey micrite most likely precipitated by paedogenic processes during early diagenesis (Smith, 1990b).

Figure 3: Bonebed SAM-PK-11289 in ventral view, after surface preparation.

Figure 4: Bonebed SAM-PK-K11289 in dorsal view, after surface preparation.

AIMS AND OBJECTIVES

The main objectives of this research include: 1) documenting and characterising the hundreds of skeletal elements in bonebed SAM-PK-K11289; 2) identifying the taxonomic make-up of the bonebed; and 3) reconstructing the taphonomic pathway that led to the accumulation of this bonebed. These data were then used to develop a hypothesis that infers the potential social behaviours in Late Permian reptiles represented by the bonebed.

GEOLOGICAL SETTING

The South African Karoo basin is an intracratonic retro-arc foreland basin with an accumulative sedimentary thickness of 12 km and a spatial distribution of 300 000 km^{l}(Smith, 1990b, Johnson, 1976, Johnson et al., 1997). The main Karoo basin formed as a result of processes relating to the subduction of the palaeo-pacific margin of the supercontinent Gondwana (Catuneanu et al., 2005). This basin documents a sedimentary succession from the Late Carboniferous to the Middle Jurassic, including the Dwyka, Ecca, Beaufort (subdivided into the Adelaide and Tarkastad subgroups) and Stormberg units (Johnson, 1976, Tankard et al., 1982, Cole, 1992, Smith et al., 1993, Catuneanu et al., 1998). The Beaufort strata comprises predominately mudrocks and fluvial sandstone deposited on wide alluvial plains on the landward side of the mountains of Gondwana (Catuneanu et al., 2005). The Adelaide Subgroup contains the late Permian succession of the Karoo Basin east of 24 degrees E. It consists of the Koonap, Middleton and Balfour formations. The Balfour formation is the uppermost succession of the Adelaide Subgroup and is Changhsingian in age. It comprises four members: The Ouderberg, Daggaboesnek, Ripplemead, and Elandsberg.

The South African Karoo Basin is world-renowned for its continuous and most complete palaeontological record spanning over 100 million years from the Permian to the Jurassic (Smith, 1990a). Discoveries from the Karoo have contributed significantly to our understanding of the biodiversity, biostratigraphy, and biogeography of ancient life forms, ultimately leading to the understanding of the evolution of life on Earth (Hancox and Rubidge, 2001). The Beaufort Group, spanning from the Middle Permian to the Middle Triassic, records a period that is crucial to the evolutionary history of the Earth. This period of time is especially famous for documenting the appearance of mammals and dinosaurs, the most catastrophic mass extinction (End-Permian Mass Extinction) and the Permo-Triassic boundary (Erwin, 1990, Smith and Botha-Brink, 2014). This has advanced our knowledge of vertebrae extinction patterns, survival strategies, environmental turnover, the survival and recovery of fauna post the EPME (Smith, 1987, Smith and Ward, 2001).

Bonebed SAM-PK-K1289 is from an arenaceous member in the upper Balfour, informally named the Ripplemead member by Viglietti et al. (2017). Bonebed SAMPK-K11289 was recovered on the farm Osfontein, 30 km north of Graaf-Reinet in the Eastern Cape Province (See figure 5). A nearby farm, Doornplaats was designated as the type locality for the original *Dicynodon* Assemblage Zone (DiAZ) (Smith, 1995) and was retained when the name was revised to *Daptocephalus* Assemblage Zone (DaAZ) by Viglietti et al. (2016). The locality of SAM-PK-K11289 has recently been identified as part of the *Lystrosaurus maccaigi- Moschorhinus* subzone (Viglietti, 2020). Radiometric dating of the Ripplemead Member yielded dates of 255.24 Ma and 255.22 Ma, placing it in Changhsingian of the late Permian Lopingian epoch (Rubidge et al., 2013). SAM-PK-K11289 was recovered at approximately 20 m above the base of the Ripplemead member (Viglietti, 2016) at the base of a siltstone cliff in a mudstone interval between the two lowermost sandstones of that member (see Fig 5A and C) . The mudstone interval has isolated smooth surfaced calcareous nodules; this is a conspicuous characteristic of the palaeosols of the upper DaAZ (Smith and Botha-Brink, 2014). Three depositional environments have been identified for the upper *Daptocephalus* Assemblage Zone. The locality of SAMPK-K11289 is characteristic of ‘facies association two’ outlined by Viglietti et al. (2018). This facies association is a floodplain deposit and is reflective of increasing aridity, decrease in mean annual rainfall and the loss of large bodies of standing waters. Smith and Botha-Brink (2014) suggest that these changing conditions were a prelude to a larger-scale environmental change that ultimately led to Phase 1 of the End-Permian mass extinction.

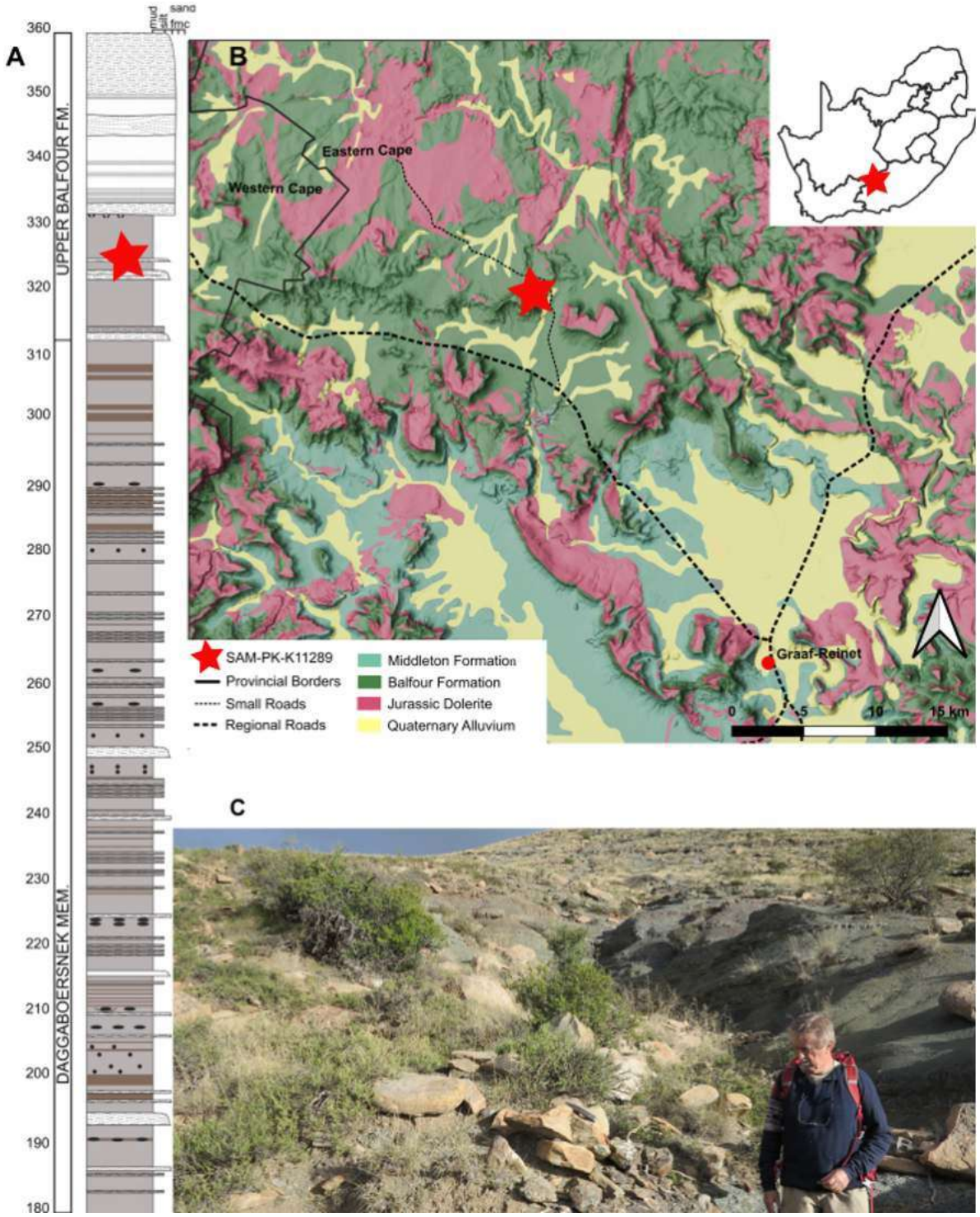

Figure 5: Geological setting and locality of SAM-PK-K11289.

(A) Stratigraphic section from Viglietti (2016) was measured on the farm Doornplaats 3 km west of the SAM-PK-K11289 locality, near Graaf-Reinet, (B) Geographic location of bonebed. (C) Field locality of SAM-PK-K11289, note Dr Mike Strong the finder of the bonebed bottom right for scale. Note the erosion gully into dark grey overbank siltstone beds from which the bonebed was eroded out. The red stars indicate SAM-PK-K111289.

METHODS

Synchrotron computer tomography scanning of fossils

Computed tomography is the visualization technique of representing three-dimensional materials a sequence of two-dimensional images that are parallel to one another (Sutton, 2008). The introduction of this technique to the field of palaeontology had yielded exceptional results, revealing novel information that would otherwise be invisible using conventional study methods. Conventional study methods have limitations, as they will only provide information about the external morphology of fossil specimens. While this is important it underestimates the information that can be recovered from fossil specimens. Understanding the internal structures of fossils has increasingly become important as it maximizes our comprehension of ancient life forms. The methods used to study the internal structures are often invasive, leading to the ultimate destruction of specimens (Tafforeau et al., 2006). While we want to obtain this information, we recognize the importance of preserving natural heritage resources. Computed tomography provides a solution to these limitations. It allows palaeontologists to visualize and reconstruct two-dimensionally fossilized specimens in three-dimension and reveals the internal morphology in a non-destructive fashion (Tafforeau et al., 2006).

Even though high quality data can be obtained through standard computer tomography, because this method was developed for medical and industrial use there are still limitations to imaging fossil specimens this way (Tate and Cann, 1982, Smith et al., 2009a). Due to their complex composition, the variable minerals within fossils may cause weak absorption contrast resulting in poor images that are difficult to reconstruct (Tafforeau et al., 2006). Imaging using propagation phase-contrast synchrotron X-ray micro-computed tomography is an enhanced technique that is particularly well suited for palaeontological research applications (Snigirev et al., 1995, Cloetens et al., 1996, Smith et al., 2009a). The use of a monochromatic beam source in propagation phase-contrast synchrotron X-ray micro-computed tomography instead of a polychromatic one, eliminates the “beam hardening effect”, allowing the differentiation of material with different densities within a sample.

Additionally, it makes use of a very high beam intensity, allowing a greater range of sample sizes that can imaged and a higher resolution. This tomography technique allows insights into palaeoneurology, palaehistology, the microstructure of fossil tissue, visualize soft tissue preservation in 3D and much more.

Synchrotron X-ray micro-computed tomography has been successfully applied to over 350 Southern African fossil specimens, advancing our understanding of extinct life forms (von der Heyden et al., 2020). Since African scientists do not have a synchrotron facility of their own, access to such data occurs through collaboration with international synchrotron facilities such as the European Synchrotron Facility of Radiation in France Grenoble. This collaboration has yielded world-class research outputs, exemplified by specimen BP/1/5558 from the Triassic, popularly known as the “Early Triassic Odd Couple”. This specimen was scanned at the ESRF and described by Fernandez et al. (2013) as a mixed species association. The use of synchrotron tomography made it possible to visualize the inhabitants of this burrow specimen and make taxonomic identifications without destroying it. Since ancient life forms cannot be observed in real-time, such interactions help conceptualize their behaviour (Hsieh and Plotnick, 2020). This contributes valuable insight into the palaeoecology of tetrapods post the End-Permian extinction event (Fernandez et al., 2013).

The use of synchrotron tomography scanning has allowed for great strides to be made in comprehending the palaeoneurology of synapsids, contributing to our ultimate understanding of mammalian neurology (Benoit et al., 2016, Benoit et al., 2018, Benoit et al., 2020, Benoit, 2023). This technique has allowed us to virtually reconstruct branches of the nervous system in 3D. From this, many inferences have been drawn including the evolution of the infraorbital foramen in mammals and their ancestors, the evolution of the brain in mammals, the evolution of facial nerves in some therapsids and much more.

Another area of palaeontology that has benefitted tremendously from synchrotron scanning is the study of coprolites (fossilized faeces). It allowed the 3D visualization of fossil inclusions in the coprolite (Qvarnström et al., 2017). Contents recovered

from the coprolite inclusions include bivalves, insects, fish, and plant material (Bajdek et al., 2017, Qvarnström et al., 2019, Qvarnström et al., 2021).
Adding to the long of specimens that have been scanned at the ESRF is bonebed SAM-PK-K11289. The successful record that synchrotron microtomography has had in imaging sensitive fossils makes it a suitable technique for this specimen (Smith et al., 2009b, Tafforeau et al., 2006). The application of propagation phase-contrast micro-computed tomography to this specimen has allowed for the holistic assessment of this bonebed.

Parameters for propagation phase-contrast X-ray micro-computed tomography of SAM-PK-K11289

SAM-PK-K11289 was imaged using propagation phase-contrast synchrotron X-ray micro-computed tomography on the BM18 beamline of the European Synchrotron Radiation Facility (ESRF, Grenoble, France). The beamline configuration consisted of: a white beam from a tripole wiggler (central pole 1.56 T, two lateral poles at 0.85 T, fixed gap) filtered with W 0.3 mm and Mo 1.3 mm, resulting in an averaged detected energy of ca. 159 keV; indirect detector comprising a 2 mm LuAG:Ce crystal scintillator coated with a layer of aluminium oxide, a visible light zoom lens (variable magnification from x1 to x0.26) and a PCO.edge 4.2 sCMOS (PCO, Kelheim, Germany) generating images with a measured isotropic pixel size of 23 µm; with a sample-detector distance of 28 m for phase-contrast images. Acquisition consisted of 7000 projections with a total exposure time of 130 msec (accumulation of 10 images of 13 msec each); continuous rotation over 360°. Flatfield images (n=41, image of the beam with no sample) and dark current images (n=20, images with no X-ray beam) were acquired for each scan. Given the size of the sample and the limited field of view at this resolution (v x h : 512 x 2048 pixels, ~11.8 x 47.1 mm) 26 acquisitions were necessary, moving the specimen on the vertical axis of the sample stage between each scan by 5.36 mm. Moving by ca. 50% of the vertical field of view limited artefacts induced by the vertical intensity profile of the beam. Additionally, an offset of 21.85 mm (corresponding to 950 pixels on the detector) was applied to the center of rotation, allowing an increase in the horizontal field of view for the reconstructed slices by 1900 pixels by stitching projections recorded

180° apart. Tomographic reconstruction was performed using PyHST2 and the single distance phase retrieval approach (Mirone et al., 2014, Paganin et al., 2002). The delta/beta value was set to 1200 as a priori knowledge for the phase retrieval. Postprocessing of the 32-bit tomograms included: ring correction (Lyckegaard et al., 2011), change of the dynamic range to 16-bits based on 0.001% saturation values of the 32-bit histograms, cropping of the data as close as possible to the export of the final complete stack at 16-bit jpeg2000 images. Additionally, a binning 2x2x2 version of the data was generated, allowing for quicker load time and processing when necessary. Matlab codes used for ring correction, binning and cropping can be found at https://github.com/HiPCTProject/Tomo_Recon.

Table 1: Parameters used for the characterisation of bonebed SAM-PK-K11289 at BM18

Parameters	**SAM-PK-K11289**
Filter	W 0.3 mm and Mo 1.3 mm
Average detected energy	159 keV
Scintillator	LuAG:Ce
Isotropic voxel size	23 µm
Sample to detector distance	28 m
Projections per scan	7000
Offset	21.85
Accumulation	10
Exposure time per frame	13 msec
Size of radiograph	512 x 2048 pixels

Comparative gross anatomy

The referred material in this project is all from the Karoo Supergroup and housed in several South African collections (see Table 2). Historically collected specimens from collections, particularly from the Iziko South African Museum, Evolutionary Studies Institute, Ditsong Museum and the Wellwood Collection were used to gather anatomical data used for the taxonomic identification of the elements in the bonebed. Specimens were physically observed through light microscopy and digital photographs. Additionally, a selection of published literature, including the original descriptions of late Permian reptiles from the South African Karoo basin, was used to collect comparative anatomical data. For the anatomical analysis on bonebed SAMPK-K111289, three-dimensional renderings of individual elements were obtained using manual segmentation in VGStudioMax 3.2.3. This enabled the assessment of the gross morphology of each element and ultimately the taxonomic identification of the individuals in the bonebed.

Separate terminology is used for the visualisation of the overall bonebed and for individual bones. For the bonebed, the terms “dorsal” and “ventral” are used to describe the view of the bonebed in the coronal plane, with reference to the depositional position, where “dorsal” indicates the upward facing surface and “ventral” indicates the downward facing surface. Adjectives like long and short are used to describe the variation of length of individual elements. Thin and broad are used to describe the diameter of individual elements. Proximal and distal are used to refer to the ends of individual long bones.

Table 2: Comparative specimens used in this study and their sources.

Taxon	Source
Owenetta kitchingorum (synonymised with *Saurodektes kitchingorum*)	BP1/1/4195a, 4195b, 5398; Reisz and Scott (2002)
Owenetta rubidgei	Broom (1939), RC 50 and SAM-PK-K7582
Saurictus australis	Modesto and Smith (2001)
Saurodectes rogersorum (synonymised with *Saurodektes kitchingorum*)	Hamley at al. (2021); Gardner et al. (2010); Goodrich (1942); Olson (1936); Evans (1987); RC 91, 626,625,627; BP/1/70, 2871,3859,2459; SAM-PK-K7578,10777 & 10651, Hunt et al. (2023)

Representation of skeletal elements in the bonebed and MNI estimates

To quantify the abundance of individuals in the bonebed the Minimum Number of Individuals (MNI) index was used. As suggested by Lyman (1994) MNI ought to account for all the skeletal elements present in the skeleton of the identified taxa. The MNI was calculated from the most abundant element from one side of the body (Badgley, 1986, Blob et al., 2007). NISP is an abbreviation for the number of individually identifiable specimens, this was used to quantify individually identifiable specimens.

Body size distribution

Data compilation and statistical analysis

For further analysis, reconstructed elements were exported to the software Avizo 8.1 as 3D models using .stl files. Duplicate elements (e.g. femora, humeri, tibiae, fibulae, ulnae and radii) were sorted into their respective files. To analyse the size frequency, a data set of limb bone measurements was compiled. Measurements were taken from stylopodial elements. These measurements include the maximum femoral length, midshaft femoral diameter, maximum humeral length, and midshaft humeral diameter. The 3D measurement tool of Avizo was used to collect these measurements. The diameter measurements were taken at the thinnest point along the diaphysis, in most cases approximately at mid-shaft. The distribution of variables measured was analysed using statistical methods implemented in R. Elements from each side of the body were statistically analysed to see if they belonged to the same population. Body size distributions are a key piece of evidence for inferring age distribution in a population, and this is relevant for understanding whether the specimens in the bonebed are of a similar developmental stage.

Additionally, the maximum cranial lengths were measured and compared with the size distribution of *Owenetta* specimens. This is because the fossil record for parareptilian post-cranial is relatively poor, therefore comparative post cranial data is limited.

Body mass estimation

Body mass estimates were made from the skeletal scaling relationships outlined by Campione and Evans (2012). Stylopodial circumferences exhibit the strongest relationship to body mass hence it was used in this study Accepting that the cross section of the stylopodial elements in the bonebed is circular, the diameter (d) was used to calculate the circumference (C) using the following equation:

$$C = \pi d$$

The stylopodial circumferences were fitted into the appropriate equations to estimate body mass. To estimate body mass from the femora this equation was used:

$$2.8479 * logC_{"} - 0.4587$$

Where $C_{"}$ is the femoral circumference in mm.

To estimate body mass from the humerus this equation was used:

$$2.6861 * logC_{\#} - 0.1438$$

Where $C_{\#}$ is the humeral circumference in mm.

For individuals whose femur and humerus could be positively identified the following equation for body mass estimation in quadrupedal tetrapods proposed by Campione and Evans (2012) was used:

$$logBM = 2.749.\ logC_{\#\$"} - 1.104$$

Taphonomic Analysis

To categorise the taphonomic signatures represented in bonebed SAM-PK-K11289 standard taphonomic procedures outlined by Behrensmeyer (1978), Eberth et al. (2007), Ryan et al. (2001), Brandt (1989), Smith and Botha-Brink (2014), and Lyman (1994) were used as guidelines. The skeletal elements on the surface of the bonebed were qualitatively assessed under a light microscope, recording each element's relative articulation, breakage, fracture, abrasion, weathering and bioerosion. Criteria outlined by Ryan et al. (2001) were used to classify breakage, abrasion and weathering. Taphonomic classes from Smith and Botha-Brink (2014) were used to classify articulation styles in the bonebed.

RESULTS

Image reconstruction from the bonebed scan

The quality of the propagation phase contrast scan was optimal for bonebed specimen SAM-PK-K11289. The scanning conditions (refer to Table 1) enabled the differentiation of the majority of the skeletal elements from the bonebed matrix (see Figure 6). It also enabled the visualization of elements buried in the matrix instead of just elements on the surface. Bone walls are thin and bone endoseal cavities variably contained a black dense mineral infill, likely manganese dioxide that made the segmentation of some individual elements particularly challenging. Many of the long bones (femur, humerus, radius, ulna, tibia, fibula and pedal phalanges) were particularly easy to segment as they were fully permineralized. In these cases, the entire length of the bone appears bright on the scan slices so it was easy to grab and reconstruct. Vertebrae, crania and ribs were often impossible to segment as the edges of the bone image were represented by patchy disconnected lines.

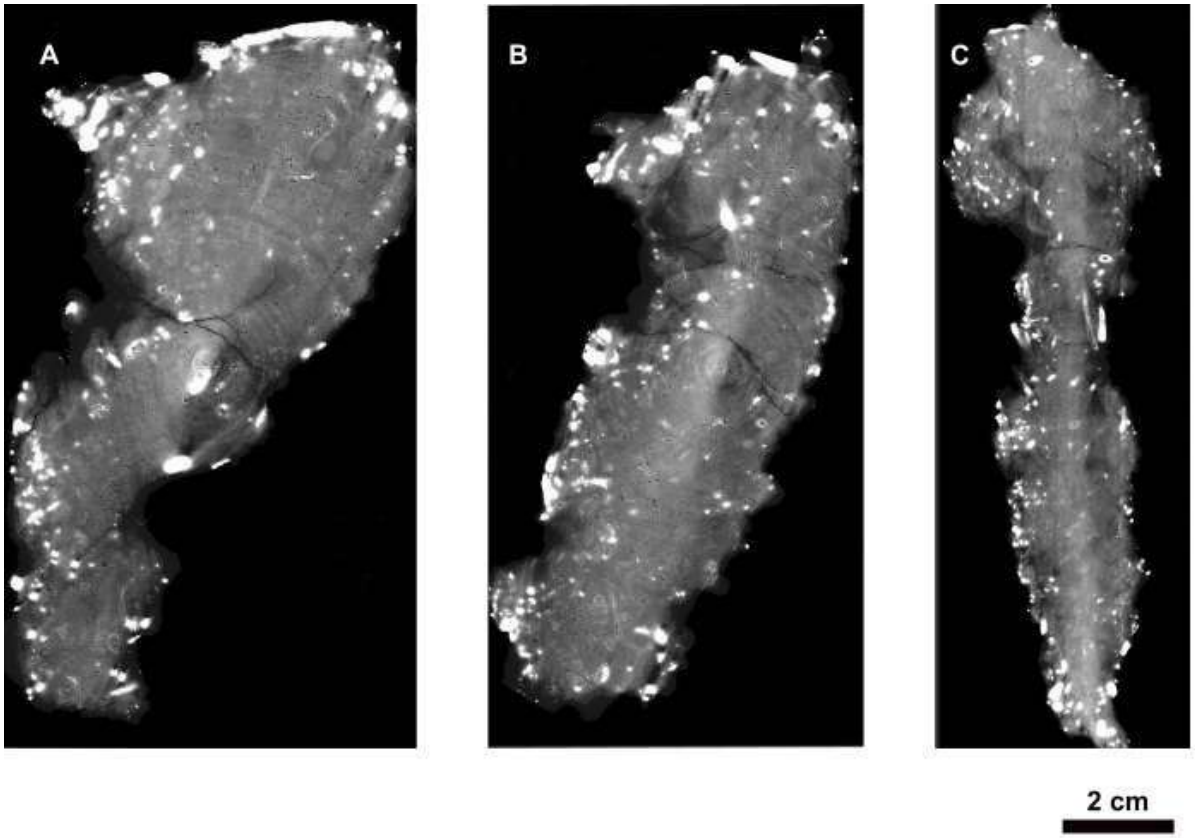

Figure 6: Single slices from image stacks reconstructed from the synchrotron scans of bonebed SAMPK-K11289.

Reconstructed image of bonebed scan (refer to Table 1 for scanning conditions) Cross sections in the X (A), Y(B) and Z (C) directions.

3D Reconstruction from the bonebed scan

3D renderings of elements in the bonebed SAM-PK-K11289 were produced from the scans (Figures 7,8 and 9). The 3D renderings of the elements in the bonebed allow the differentiation of some discrete elements (e.g. femur, humerus, tibia, fibula, radius, ulna and elements of the manus and pes). The distribution of these elements in the plain view of the bonebed is uniform, such that is there is no portion of the sample that appeared to contain denser concentrations of any individual limb element (Figure 10A and B). Stylopodial elements (femur and humerus Figure 10A), zeugopodial elements (tibia and fibula and radius and ulna Figure 10B) and autopodial elements (metapodials and phalanges (Figure 10C) are all evenly distributed throughout in the plain view of the bonebed. However, in the lateral view

(see Figure 11), limb elements are densely packed at the ventral surface and become less dense as you move more dorsally.

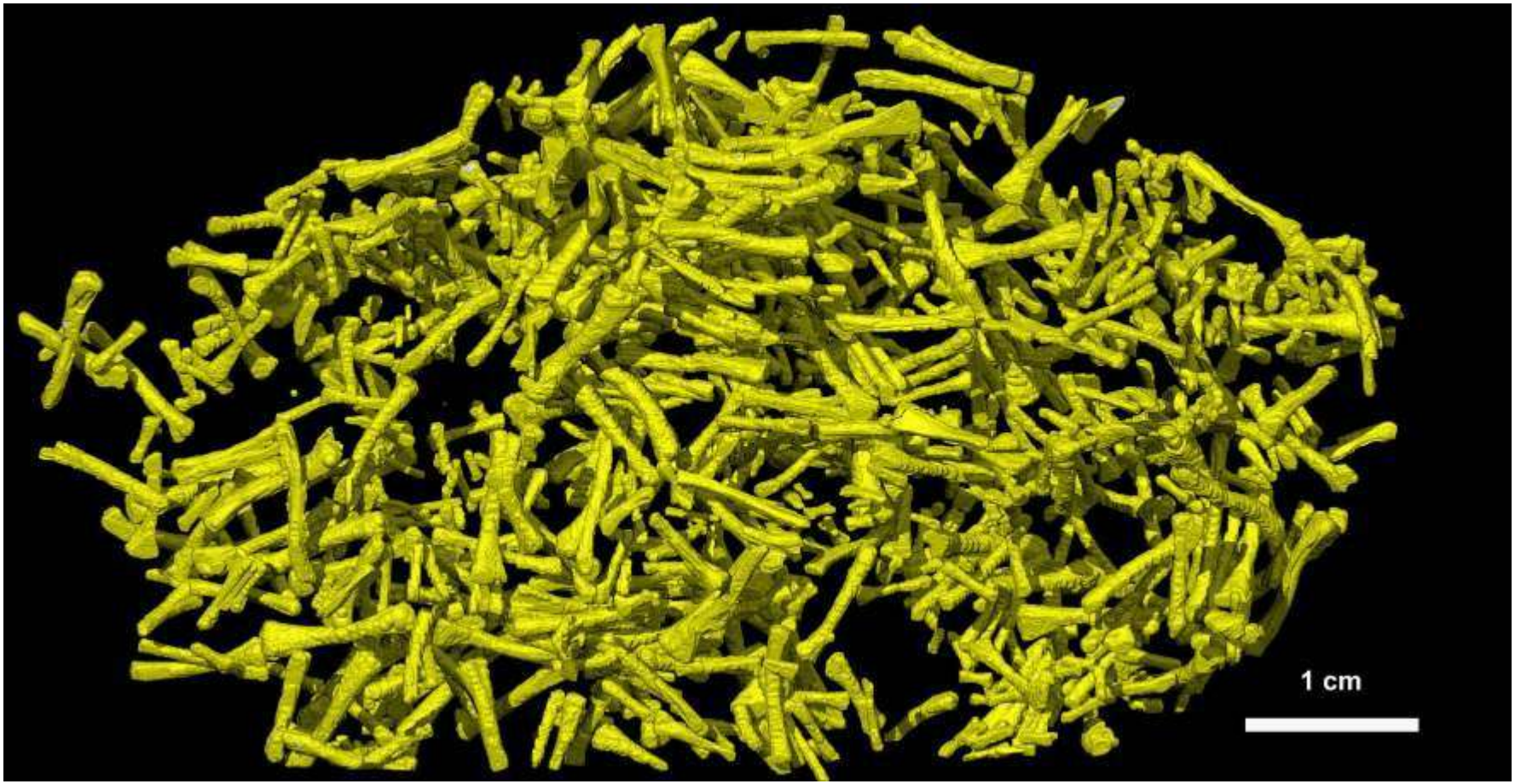

Figure 7: Three-dimensional renderings of skeletal elements in the ventral view.

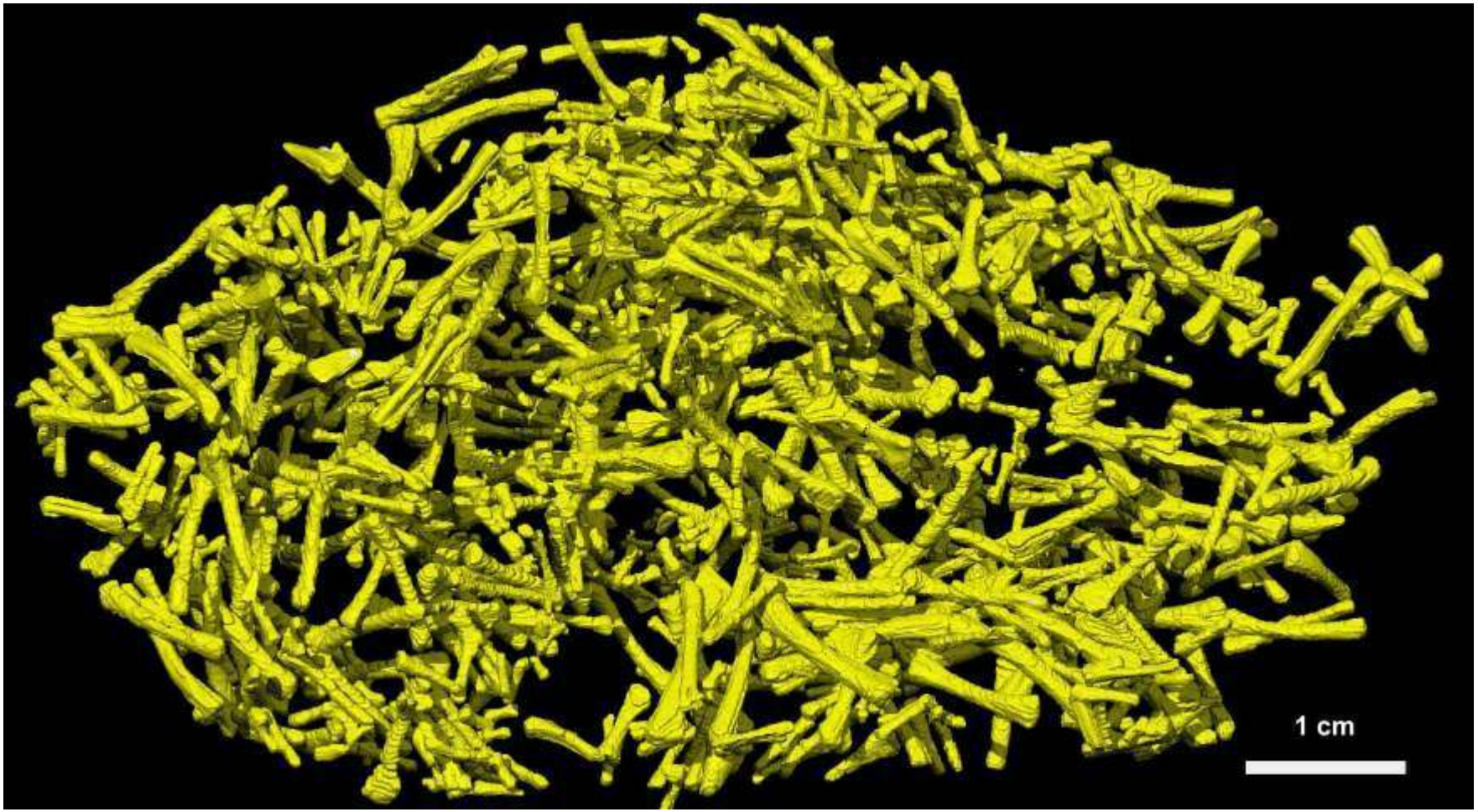

Figure 8: Three-dimensional renderings of skeletal elements in the dorsal view.

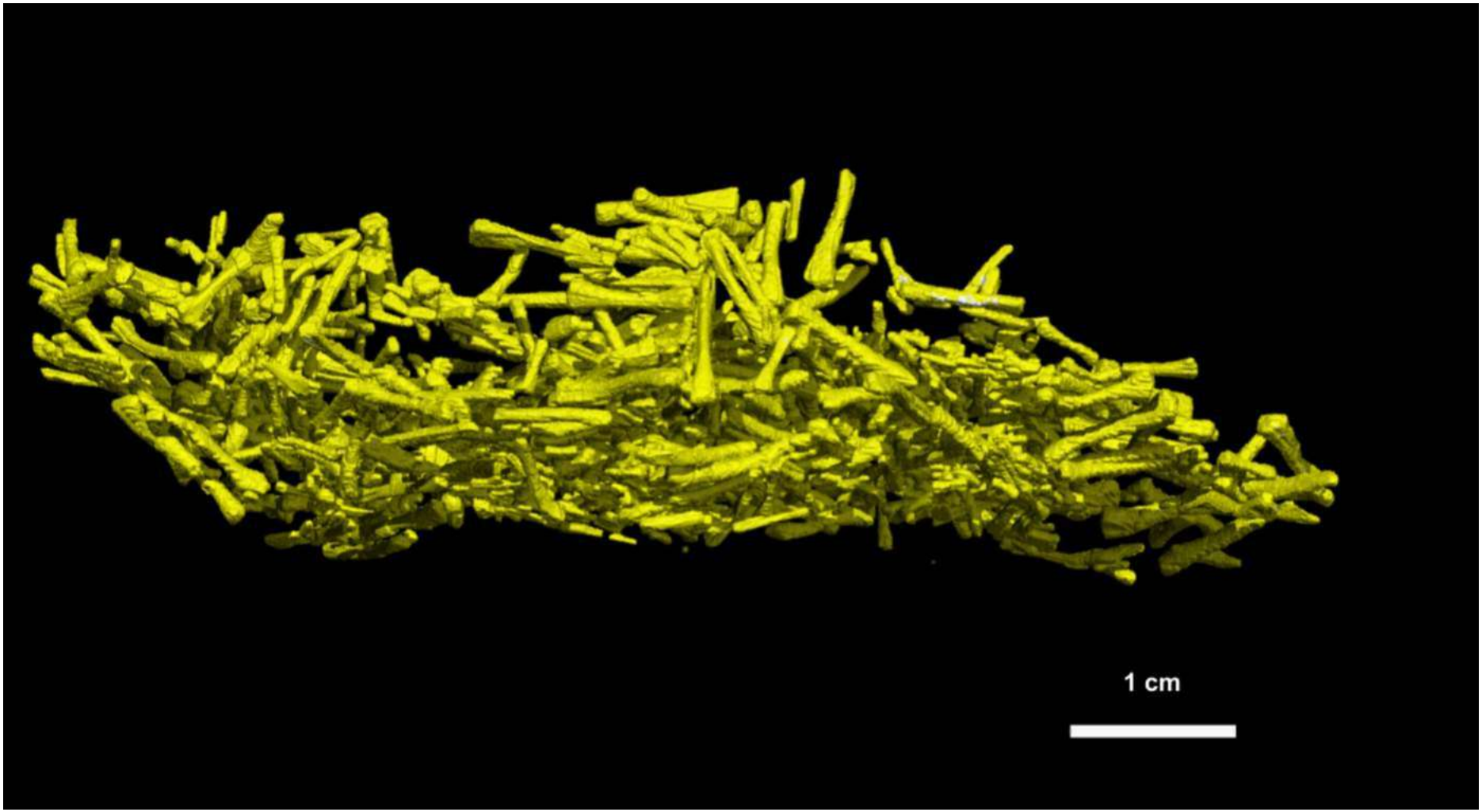

Figure 9: Three-dimensional renderings of the accumulation of skeletal elements in lateral view. Dorsal surface at the top.

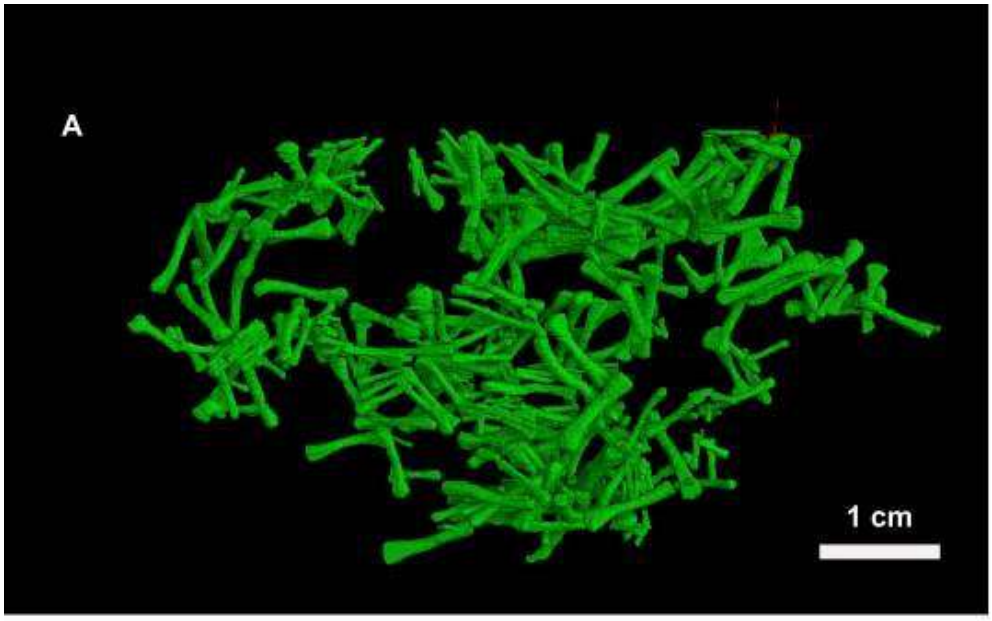
A
1 cm

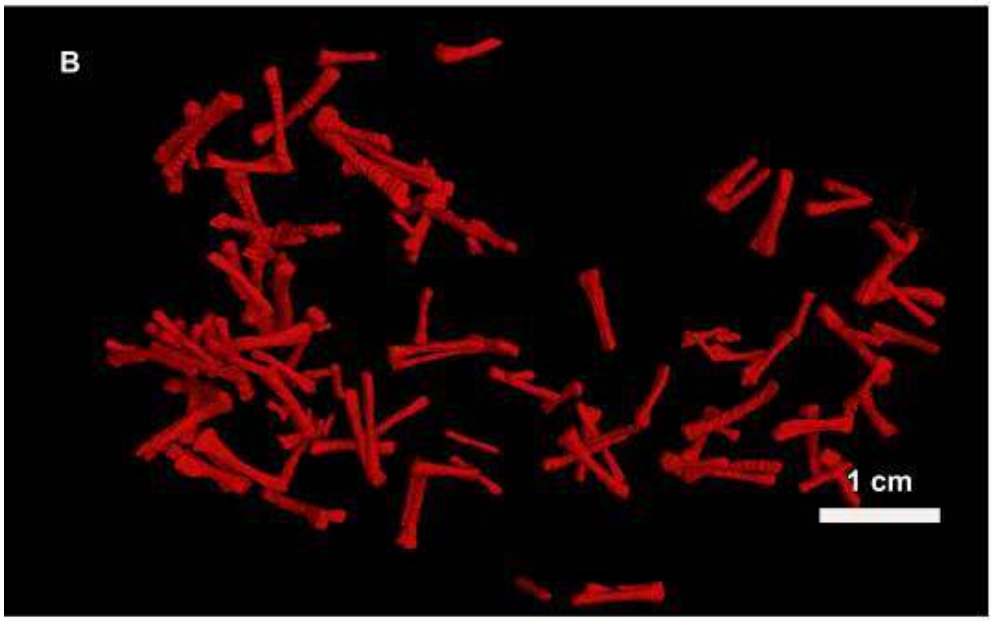
B
1 cm

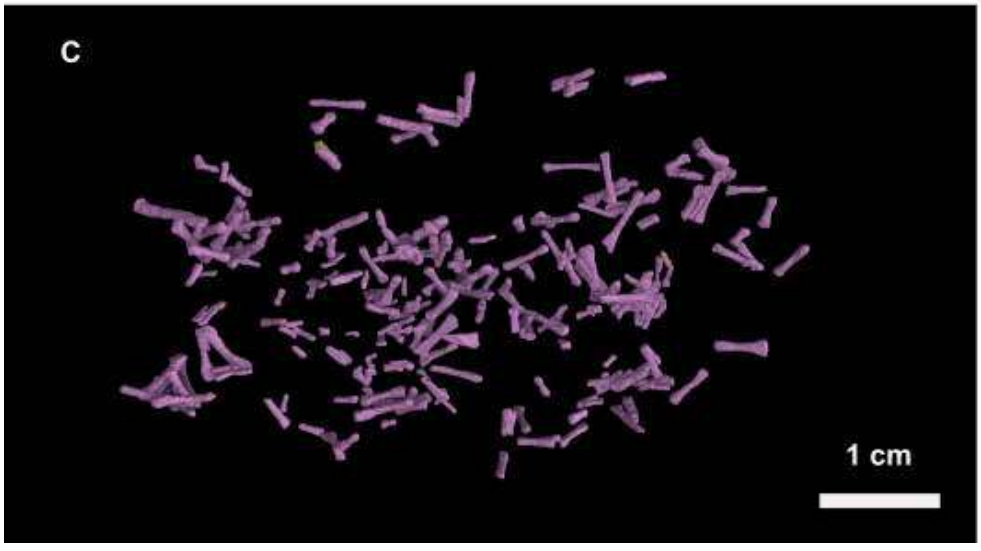
C
1 cm

Figure 10: Distribution of limb elements in plain view.

Uniform distribution of different elements in the bonebed in plain view. (A) Distribution of stylopodia in the bonebed in green, (B) Distribution of zeugopodia in the bonebed in red, and (C) Distribution of autopodia in the bonebed in purple.

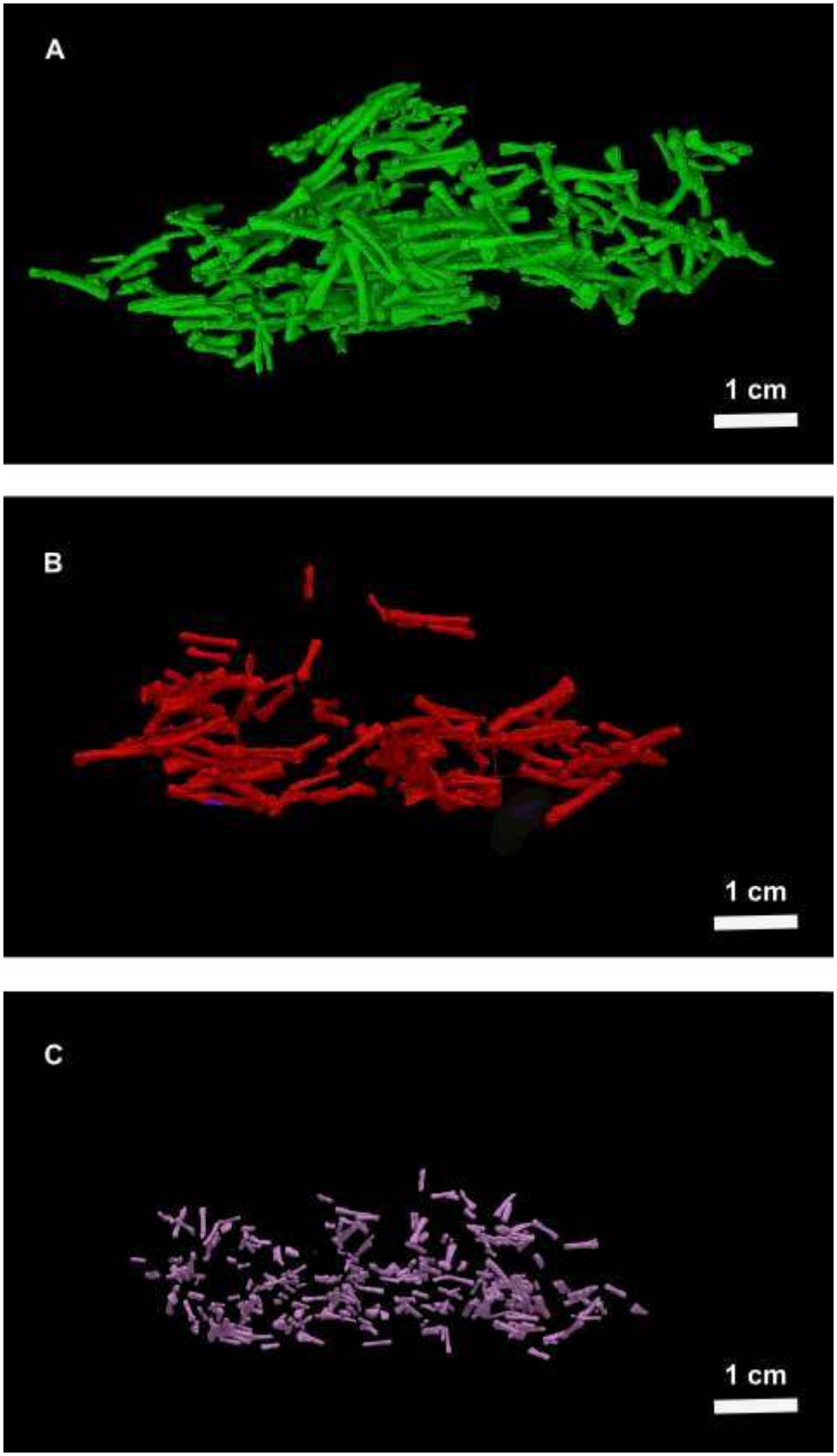

Figure 11: Distribution of elements in lateral view, dorsal surface at the top.

Limb elements are densely packed at the base and become less dense as you move higher up. A) Distribution of stylopodia in the bonebed in green, (B)

Distribution of zeugopod in the bonebed in red and (C) Distribution of autopods in the bonebed in purple.

Taxonomic make-up of the bonebed

Comparative description of the crania

All the identifiable skeletal elements in bonebed SAM-PK-K11289 are ascribed to *Owenetta*. The following specimens were used for comparison: *Owenetta rubidgei*, specimens RC and SAM-PK-K7582 and *Saurodektes kitchingorum* BP/1/4195a and BP/1/4195b (see Table 2 for a complete list of all the taxa and specimens used for comparative purposes). Note that *Saurodektes kitchingorum* was previously known as *Owenetta kitchingorum,* then Hamley, Cisnero & Damiani (2020) transferred it to the genus *Saurodektes* yielding *Saurodektes kitchingorum*. Additionally, *Saurodektes rogersorum* and *Saurodektes kitchingorum* were synonymised. Where data collection was possible the skulls in bonebed SAM-PK-K11289, whether partial or complete had a maximum cranial length ranging from 17 mm to 21 mm. The maximum cranial length collected from other owenettid specimens ranges from 17 mm to 49 mm (Cisneros et al., 2004) (see Figure 12 for comparisons). None of the cranial material in the following figures are attributed to individuals O1 and O2 later in the thesis.

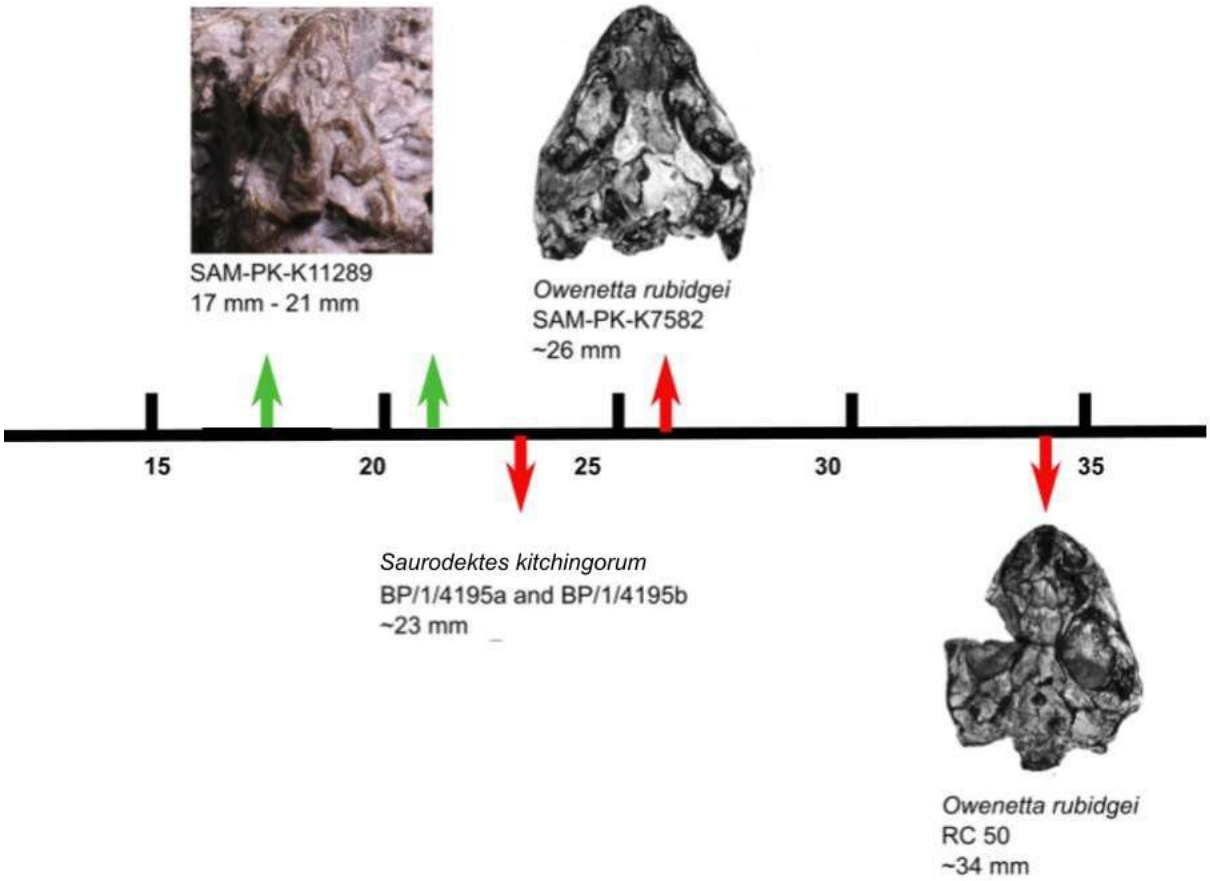

Figure 12: Range of maximum cranial length observed in *Owenetta* and other procolophonid parareptiles.

The maximum cranial length of *Owenettid* specimens whose crania is almost complete or complete, in comparison with the maximum cranial lengths observed in bonebed SAM-PK-K11289. The red arrows indicate the maximum cranial length of other *Owenetta* specimens. The green arrows indicate the range of maximum cranial observed in SAM-PK-K11289.

There are a few skulls in bonebed SAM-PK-K111289 that are orientated such that the dermal roof can be observed. Unfortunately, some of the elements are distorted and displaced, making it challenging to accurately determine suture lines however, some diagnoses can still be made with confidence. The skulls lack obvious cranial ornamentation. This is also observed in *Owenetta rubidgei* exemplified by holotype specimen RC 50 (see Figure 13 for a comparison between *Owenetta rubidgei* holotype and a skull from bonebed). Other parareptiles such as *Colobomycter pholeter* have very obvious ornamentation. This taxon exhibits shallow round pits on the skull roof (Modesto and Reisz, 2008). Refer to Figure 12 for comparisons

between the skull roofs of *Owenetta* and *Colobomycter pholeter.* In *Owenetta* the posterior portion of the frontal region is large, contributing significantly to the dorsal orbital margin (see Figure 12), and this configuration is one of the features that distinguish *Owenetta* from other procolophonids. In other procolophonids the orbit is posteriorly enlarged consequently making the posterior portion of the frontal region narrow. The occipital condyle of *Owenetta* is paired as in other parareptiles (Debraga and Reisz, 1996).

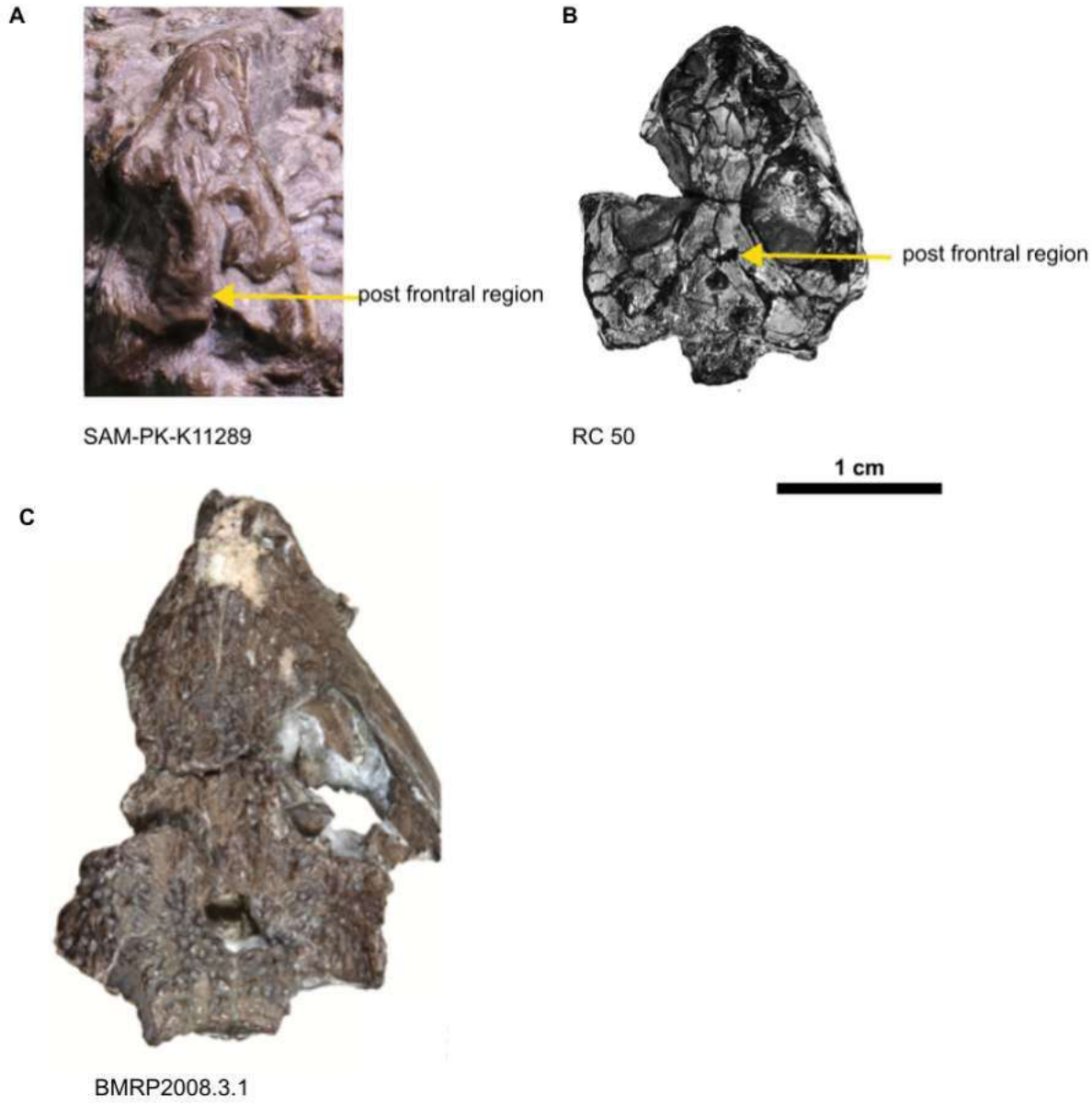

Figure 13: Comparisons of the dermal skull roof.

Comparisons between the dermal skull roof (A) Skull in bonebed SAM-PK-K11289, (B) Holotype of *Owenetta rubidgei* (Reisz and Scott, 2002) and (C) *Colobomycter*

*pholete*r (Modesto and Reisz, 2008). Yellow arrows in A and B indicate the posterior portion of the frontal. Note the surface of the dermal roof in A and B is unornamented, while C is sculptured.

The jugal observed is a simple boomerang-shaped element that contributes to the posterior ventral margin of the orbit (see Figure 14). The jugal in other reptiles is raised posteriorly.

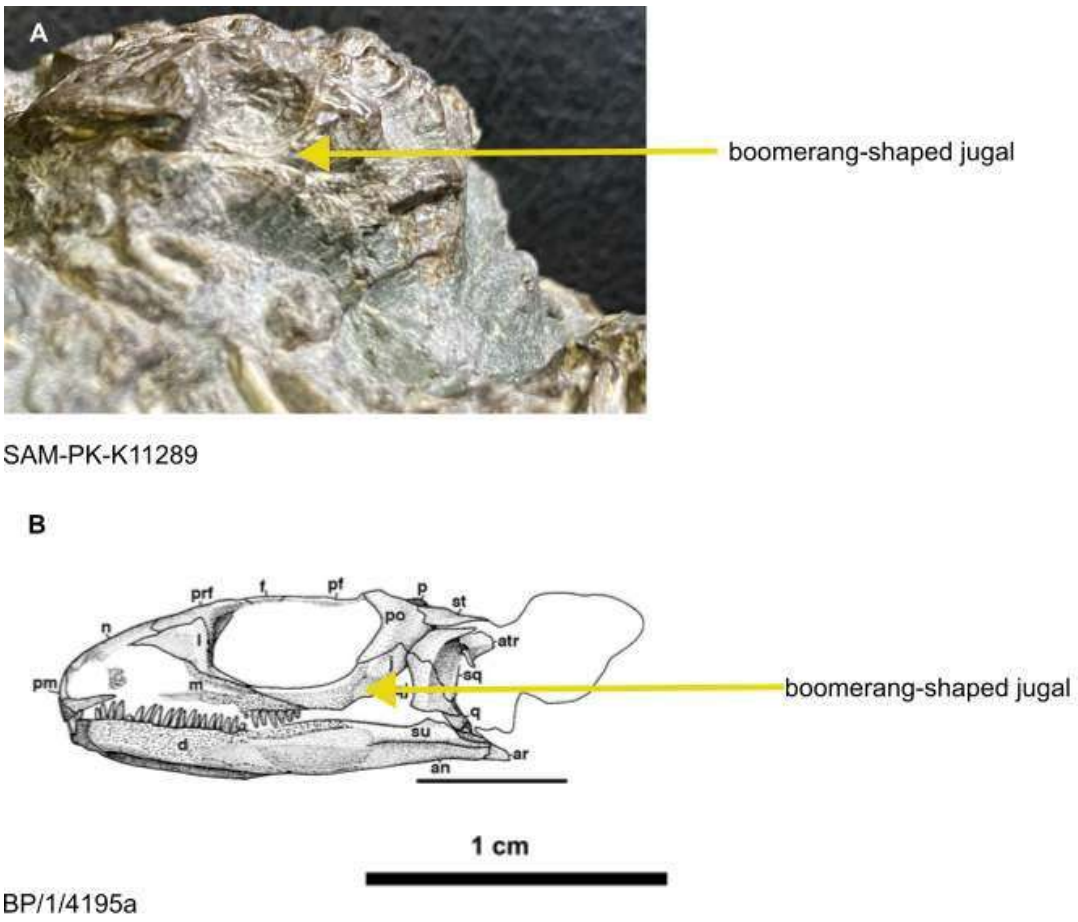

Figure 14: Comparative anatomy of the jugal.

The subtemporal openings in *Owenetta* are teardrop-shaped and short, whereas other parareptiles (e.g., *Colobomycter pholeter*) have almost circular and longer subtemporal openings. The transverse flange of the pterygoid in *Owenetta* lacks dentition, whereas other parareptiles have teeth on the transverse flange of the pterygoid (refer to Figure 15 for comparisons) (Gow, 1972; Gow and Rubidge, 1997; Cisneros et al., 2008; Van den Brandt et al., 2020).

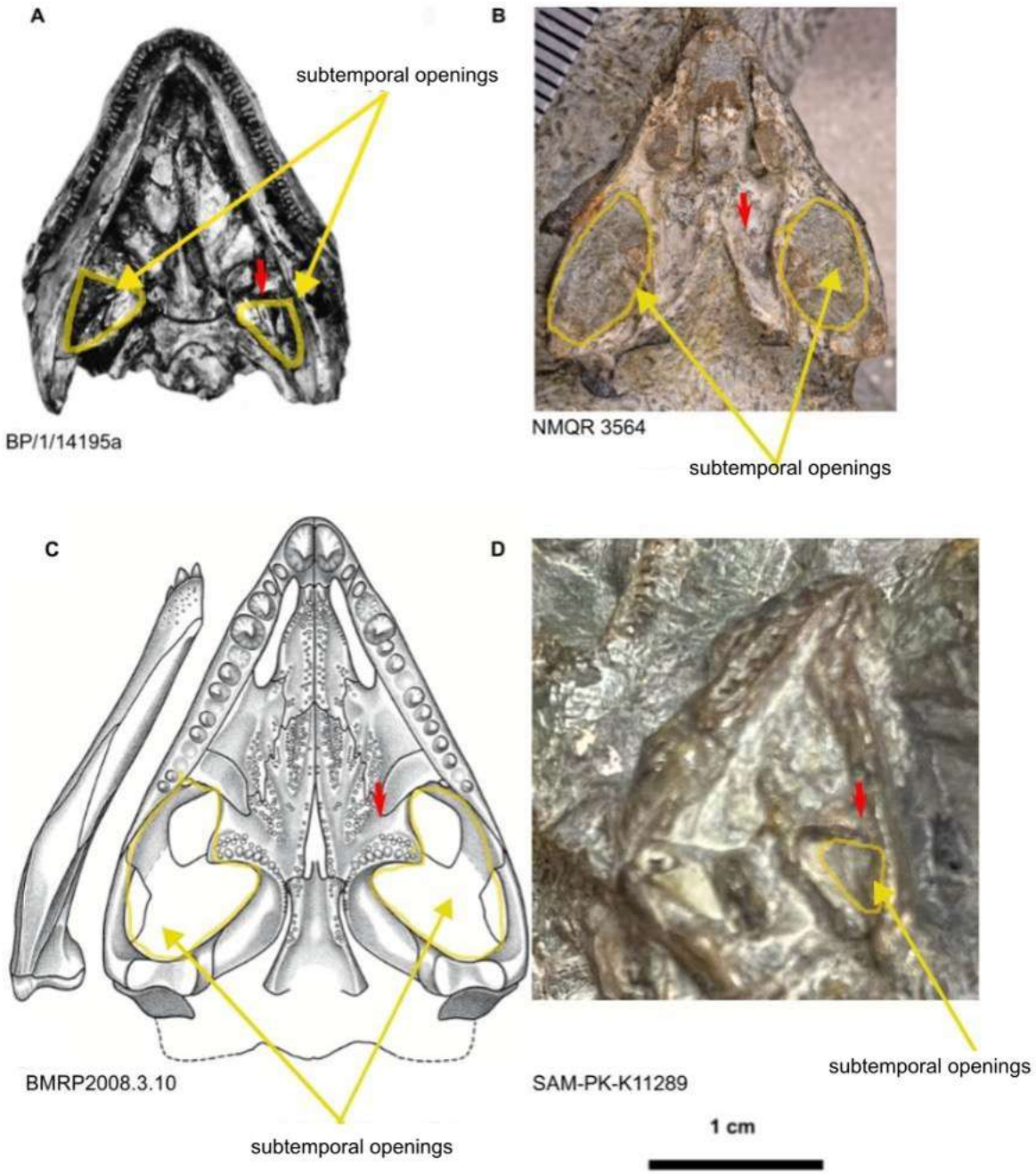

Figure 15: Comparative anatomy of palatal view.

Palatal view of (A) BP/1/4195a (*Owenetta kitchingorum*) (Reisz and Scott, 2002), (B) NMQR 5364 (*Phonodus dutoitorum)* (Modesto et al., 2010*),* (C) BMRP2008.3.10 (*Colobomycter pholeter* (Modesto and Reisz, 2008) and (D) Skull in bonebed SAMPK-K11289. The red arrows indicate the transverse flange of the pterygoid.

The maxilla of *Owenetta* forms the major part of the snout. Its premaxillary process, anterodorsal and suborbital ramus are well developed. The premaxillary process contributes to the border of the external nares (see Figure 16). This is observed in *Owenetta* as seen in BP/1/4195a (see Figure 17). This is an apomorphy of procolophonids, the condition in SAM-PK-K11289 is plesiomorphic. The anterodorsal process is so large that it contacts the prefrontal. This is also observed in *Owenetta rubidgei* and *Saurodektes kitchingorum* (Reisz and Scott,2002). This suborbital ramus observed in SAM-PK-K11289 extends to the midpoint of the orbit. This distinguishes *O.rubidgei* from *Saurodektes kitchingorum* as the suborbital ramus in *Saurodektes kitchingorum* does not extend to this point.

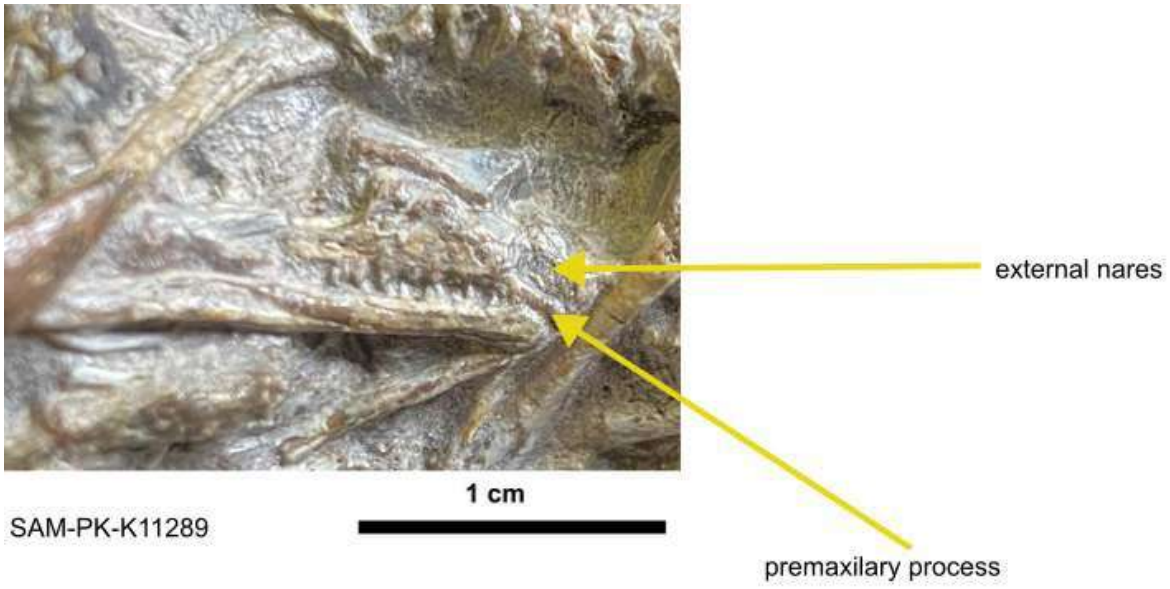

Figure 16: Maxilla in bonebed SAM-PK-K11289.

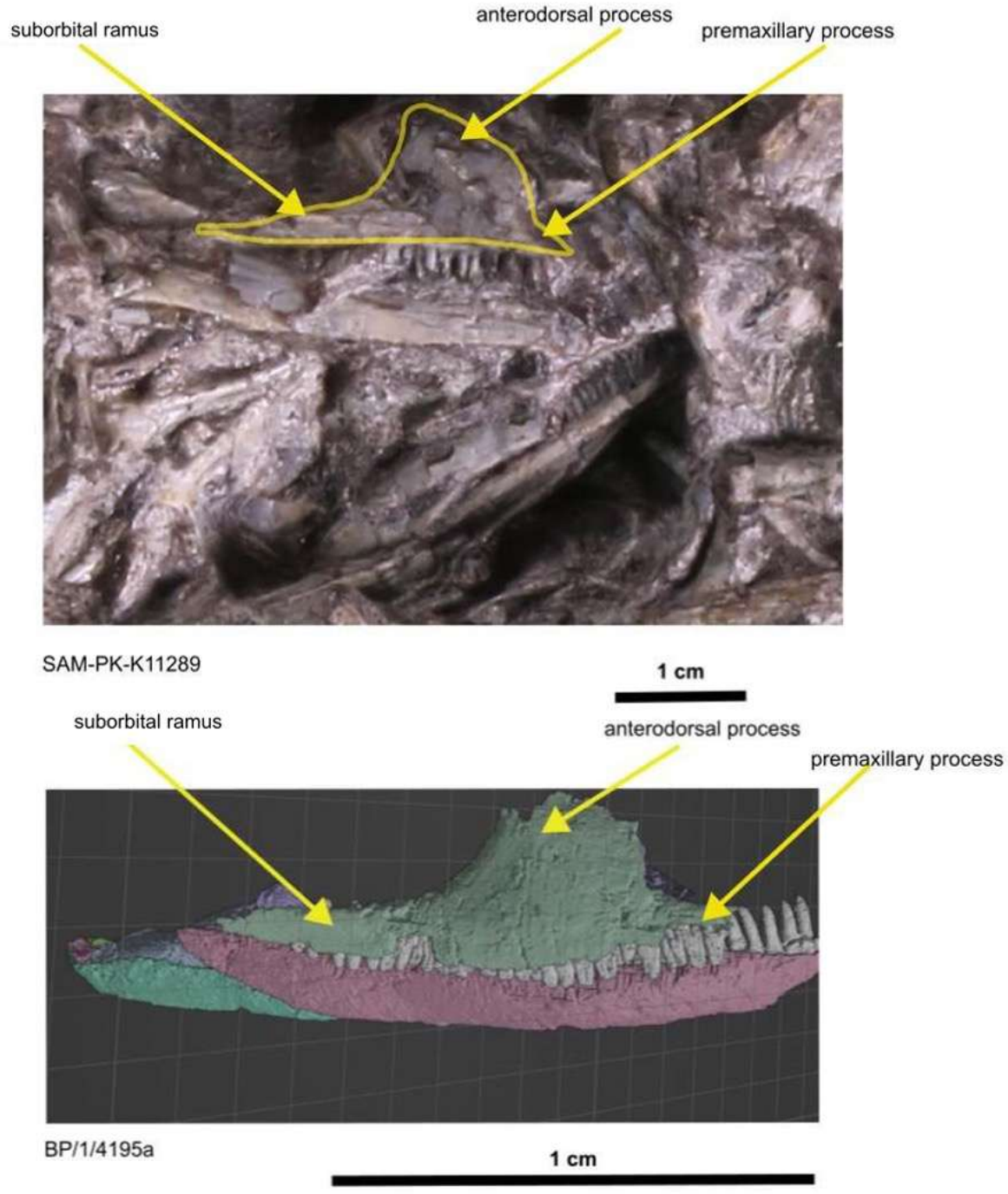

Figure 17: Maxillary comparisons.

Comparisons between the maxilla in bonebed SAM-K-K11289 (A) and (B) maxilla of *Saurodektes kitchingorum*. Reconstruction of B was done by Xavier Jenkins (personal communication).

The labial surface of the maxillae in the bonebed covers the root of the tooth (see yellow arrow in Figure 17A), but its lingual surface exposes the root of the tooth, where the tooth attaches to the maxillary bone (see arrow in Figure 18B). This type of tooth implantation where the labial and lingual walls are asymmetrical is known as pleurodont and is, surprisingly, also observed in the *Saurodektes kitchingorum* holotype (see Figure 14C and B). This sort of tooth implantation is typically observed in crownward reptiles, and to my knowledge is unique among parareptiles - its observation here immediately indicates that it is *Owenetta.* The maxillary and dentary teeth in SAM-PK-K11289 are simple and conical-shaped with no serrations. They are not labio-lingually expanded, this condition is shared by all owenettids and *Sauropareion* (Piñeiro et al., 2004). The morphology of the teeth is what distinguishes *O. rubidgei* from *Saurodektes kitchingorum*, the latter possesses teeth that are recurved and sharp. A caniniform region is not observed in any of the maxilla in SAM-PK-K11289.

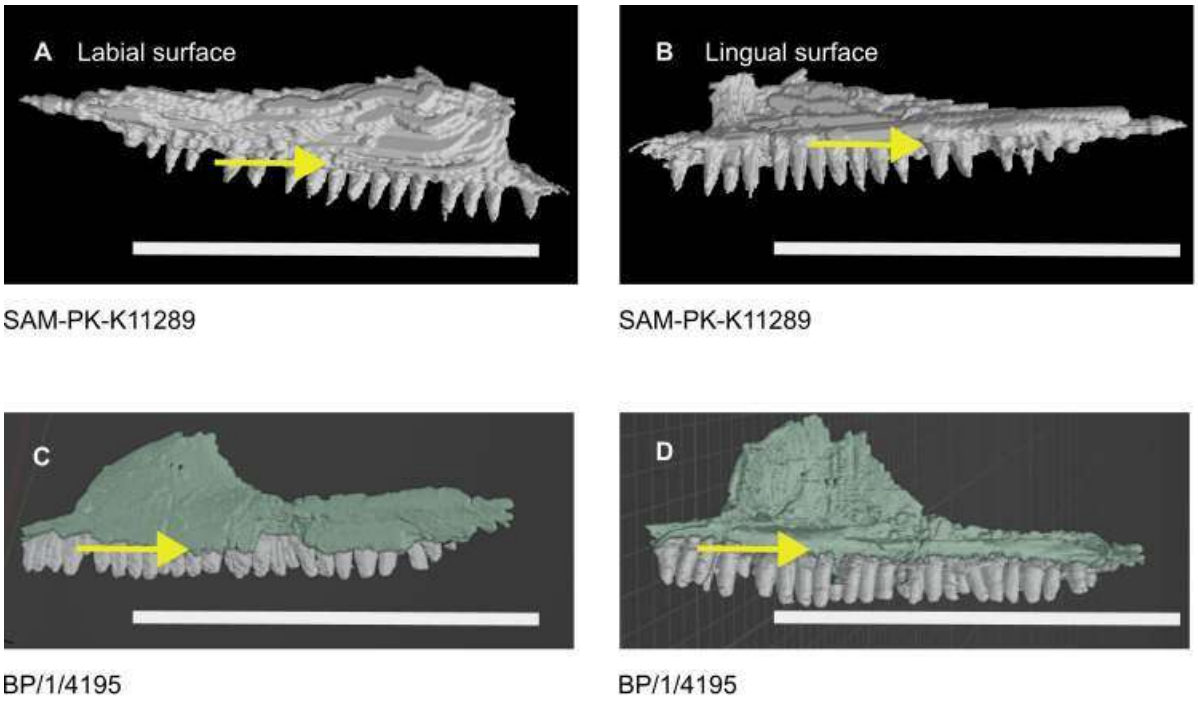

Figure 18: Tooth implantation.

Labial and (D) Lingual surfaces of BP/1/4195 *Saurodektes kitchingorum.* Reconstructions of C and D were done by Xavier Jenkins. Yellow arrows indicate where the tooth implants into the maxilla. In (A), the arrow points anteriorly, and in (B), (C) and (D), it points posteriorly. Scale bars equal to 1 cm.

Comparative description of post crania

The individuals in bonebed SAM-PK-K11289 exhibit several post-cranial morphological features that support its assignment to *Owenetta.* The femora in bonebed SAM-PK-K11289 are elongated and slender. Their proximal and distal ends are only marginally expanded as in *Saurodektes kitchingorum* specimen BP/1/4195a (Reisz and Scott, 2002). The shaft has an evident sigmoidal curve (see Figure 19 for a comparison between the femora in SAM-PK-K11289 and the femur of BP/1/14195a).

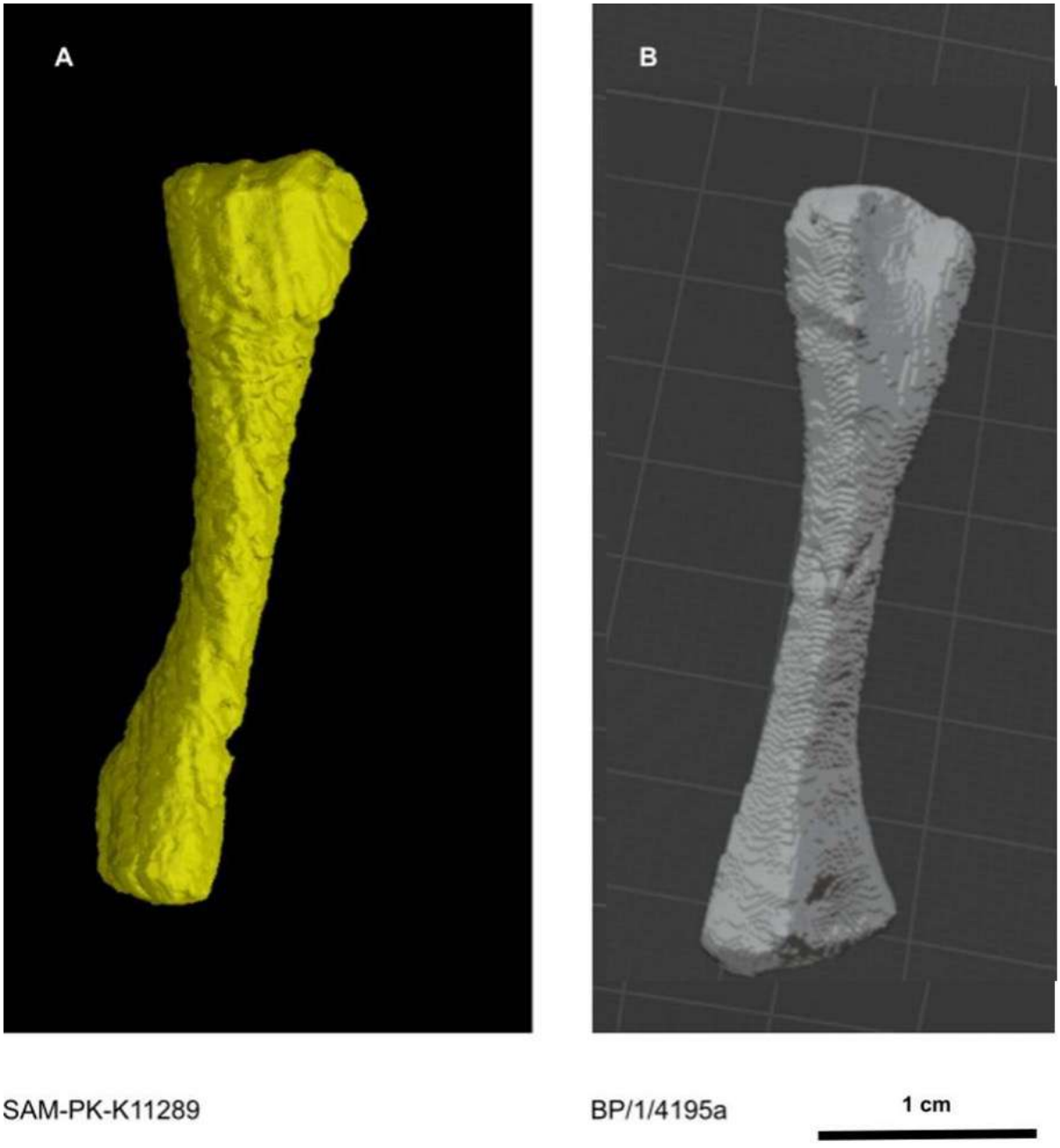

Figure 19: Comparative anatomy of femur.

Comparative anatomy of (A) femur in bonebed SAM-PK-K1289 and (B) femur of *Owenetta kitchingorum* BP/1/4195a.

As in *Owenetta* specimen BP/1/4195a, the humeri in SAM PK-K 11289 are relatively long and slender elements. This morphology is typical for *Owenetta*, as opposed to the broad and robust morphology observed in other procolophonoid parareptiles. The shaft of the humerus rotates midway such that the proximal and distal epiphyses indicated by the yellow arrows in Figure 20 are perpendicular to one another. The entepicondylar foramen is undoubtedly absent in the humeri in bonebed SAM-PK- K11289 and the humerus of BP/1/4195a. This condition is shared between *Owenetta* and its close relative *Barasaurus* (Reisz and Scott, 2002).

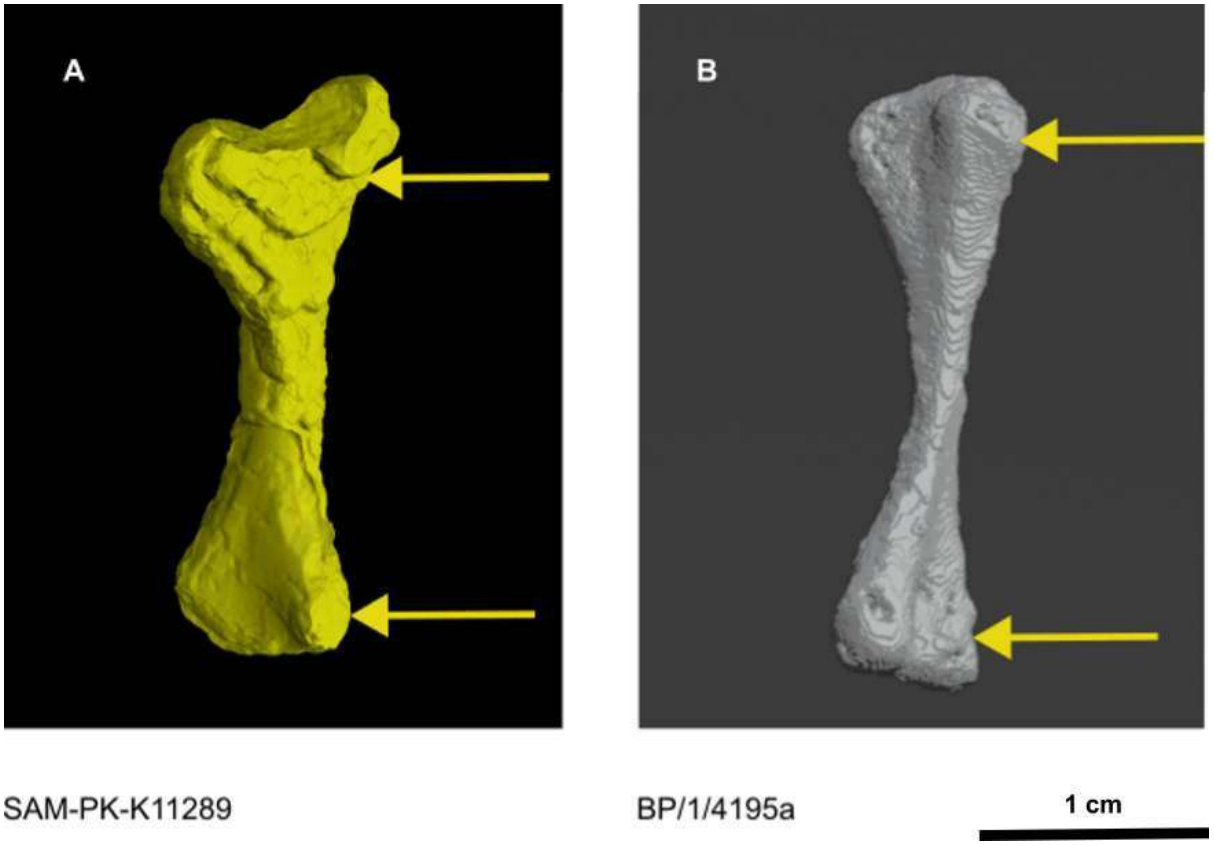

Figure 20: Comparative anatomy of humeri.

Comparative anatomy of humeri in bonebed SAM-PK-K1289 (A) and humeri of BP/1/4195a (B). Yellow arrows indicate slightly expanded and rotated epiphyses.

The pelvic girdle is preserved such that it can only be viewed from above (dorsally). The ilia in bonebed SAM-PK-K11289 present a diagnostic characteristic of *Owenetta*; they are blade-like and are positioned just above the acetabulum; this characteristic is also observed in *Saurodektes kitchingorum.* In bonebed SAM-PKK11289, the iliac blade accommodates 3 sacral vertebrae (see Figure 21). The Iliac blade is substantially more expanded on the posterior end than it is on the anterior end (Reisz and Scott, 2002).

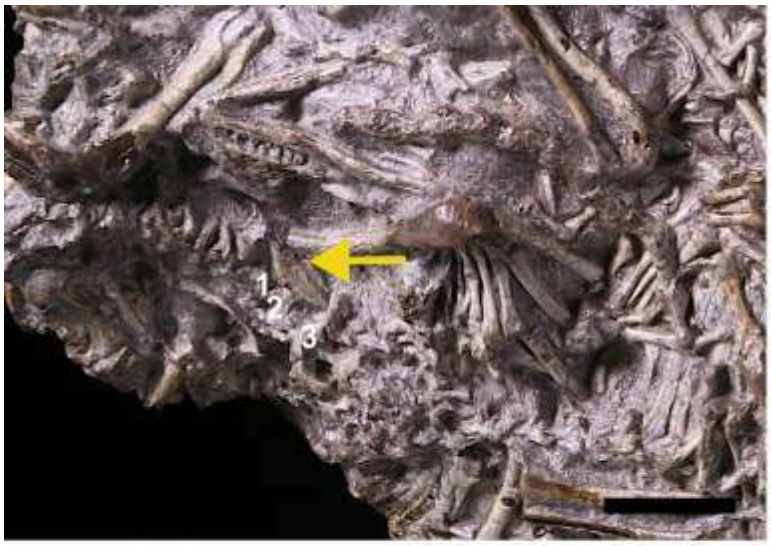

SAM-PK-K11289

Figure 21: Morphology of pelvic girdle.

The yellow arrow indicates the right ilia. Numbers 1,2 and 3 indicate the sacral vertebrae that are associated with the ilia. The scale bar is equal to 2 cm.

The configuration of the caudal vertebrae in bonebed SAM-PK-K11289 suggests a relatively long tail (Figure 22), this configuration matches that of *Saurodektes kitchingorum* BP/1/4195a (Hamley et al.,2021).

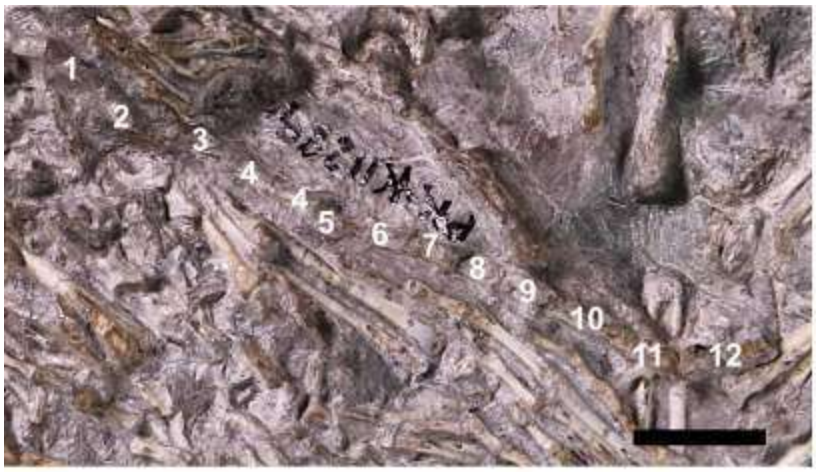

SAM-PK-K11289

Figure 22: Caudal vertebrae series.

Caudal vertebral series indicating an elongated tail. Numbers 1 to 12 indicate articulated caudal vertebrae increasing anteriorly. The scale bar equals 1 cm.

The interclavicle of the bonebed animal is anchor-shaped, with a softly curving anterior end. This is also observed in *Saurodektes kitchingorum* specimen BP/1/14195a (Reisz and Scott, 2002). The stem of the interclavicle of SAM-PK-K11289 is lanceolate (i.e. spear-shaped). This is likely the first report of the stem of the interclavicle as other previous reports of the interclavicle have only described the anterior end.

SAM-PK-K11289

Figure 23: Morphology of interclavicle in SAM-PK-K11289.

Anchor-shaped interclavicle with gently curving anterior end. The yellow arrow indicates the lanceolate-shaped stem. The scale bar equals 1 cm.

Establishing taxonomic identifications by stratigraphic compatibility

Procolophonid parareptiles are a group of small-lizard-like vertebrates from the Permian to the Triassic (Cisneros and Ruta, 2010). Procolophonid fossils are quite abundant in some of the Early Triassic Karoo localities (Botha et al., 2007). In South Africa, the parareptiles present in the latest Permian strata that yielded the bonebed described here (falling within the *L.maccaigi- Moschorhinus* subzone of the *Daptocephalus* Assemblage Zone) include *Owenetta rubidgei*, *Pareiasaurus serridens* and *Spondylestes rubidgei* (Viglietti, 2020). *Owenetta kitchingorum* (Reisz and Scott, 2002) is now synonymised with *Saurodektes rogersum* to form *Saurodektes kitchingorum* (Hamley et al., 2021). This also means the genus *Owenetta* is restricted to Owenetta rubidgei and the Permian.

Radiometric dating places the locality of bonebed SAM-PK-K11289 at the late Permian Lopingian epoch (Rubidge et al., 2013). This age falls within the temporal range that yielded the majority of *Owenetta* in the main Karoo basin. More specifically it falls within the known range of *Owenetta rubidgei*.

Skeletal Representation and Minimum Number of Individuals

Bonebed SAM-PK-K11289 includes numerous skeletal elements belonging to multiple individuals. These elements include limb bones, vertebrae, pedal phalanges, crania, ribs and elements of the girdle. The bonebed is dominated by long bones of the limbs. Notably, the girdle elements and ribs are severely underrepresented. The NISP (Total number of identifiable specimens) is at least 316. This number theoretically represents the highest possible number of individuals in bonebed SAMPK-K11289. However in reality this number grossly exaggerates the MNI as one individual clearly contributes multiple elements to the assemblage. The MNI preserved in bonebed SAM-PK-K11289 was estimated using guidelines outlined by Badgley (1986). Since each individual can only have one left and one right of every limb bone, the MNI based on the left femur is estimated to be 31 (see Table 3).

Table 3: Frequency of skeletal limb elements and their “handedness”.

Skeletal element	Right	Left	Total
Femur	21	31	52
Humerus	24	20	44
Tibia	16	13	19
Fibula	11	13	24
Radius	12	11	23
Ulna	4	7	11

For elements whose exact frequencies in the bonebed could be confidently determined, the expected frequency of the individual element is compared to the actual frequency observed (see Figure 24). Based on the MNI of 31, the expected frequency for the femur, humerus, tibia, fibula, radius and ulna is 62. This value accounts for both the left and right sides of the individual elements. The observed frequency for the femur is 52, representing 83.87% of the expected frequency. The observed frequency for the humeri is 44, representing 70.96% of what is expected. Only 19 out of the expected 62 tibia are present, representing only 30.64% of the tibia. Twenty four out of the expected 62 fibula are present representing 38.70% of what is expected.

Twenty three out of the expected 62 fibula are present representing 37.10% of the expected frequency. Only 11 ulna are present representing 17.74% of the expected frequency. Lastly only 17 crania out of the expected 31 are present, representing a little above half (54.83%) of what is expected.

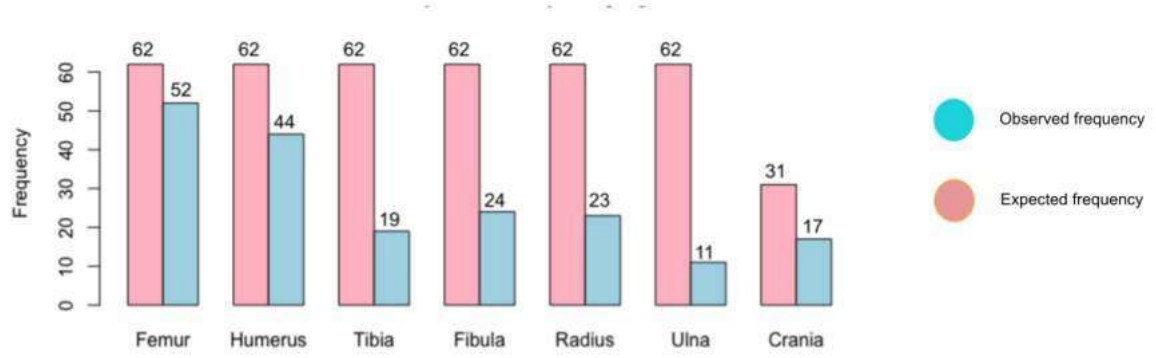

Figure 24: Expected frequency vs Observed frequency of discrete skeletal elements.

Size Distribution and Variation

Body size was used as a proxy for ontogeny in this study. Size does not directly imply growth stage, but can be used to infer the probable age (Merritt, 2015). The size distribution of the humeri and femora were assessed here using standard statistical analysis. We prioritize proximal limb bones because research reveals that they are the most reflective of body size (Campione and Evans, 2012).

The spread/distribution of the femoral and humeral measurements is relatively narrow (Figure 25). The standard deviation for the femoral lengths is 1.613 mm (see Figure 25 A), this indicates very little variation compared to the mean of 33.787 mm. The bonebed was scanned at a resolution of 0.023 mm, the standard deviation accounts for 70 voxels of the difference in the length of the reconstructed humerus. This is vanishingly small considering the number of voxels in each femur. This corresponds to the statistically insignificant standard error mean of 0.223.

The standard deviation for the femoral diameter is 0.206 mm (see Figure 25 D), this indicates very little variation compared to the mean of 2.597 mm. The standard deviation accounts for 9 voxels of the difference in the diameter of the reconstructed femur. This is vanishingly small considering the number of voxels in each femur. This corresponds to the statistically insignificant standard error mean of
0.313.

The standard deviation for the humeral diameter is 0.174 mm (see Figure 25 B), this indicates very little variation compared to the mean of 3.292 mm. The standard deviation accounts for 8 voxels of the difference in the diameter of the reconstructed humerus. This is vanishingly small considering the number of voxels in each humerus. This corresponds to the statistically insignificant standard error mean of 0.020.

The standard deviation for the humeral lengths is 2.077 mm (see Figure 25 C), this indicates very little variation compared to the mean of 21.928 mm. The standard

deviation accounts for 90 voxels of the difference in the length of the reconstructed femur. This is vanishingly small considering the number of voxels in each femur. This corresponds to the statistically insignificant standard error mean of 0.313.

The variation observed in SAM-PK-K11289 is statistically insignificant such that it can be concluded that the elements were drawn from the same population, in this case they were drawn from individuals in the same ontogenetic class.

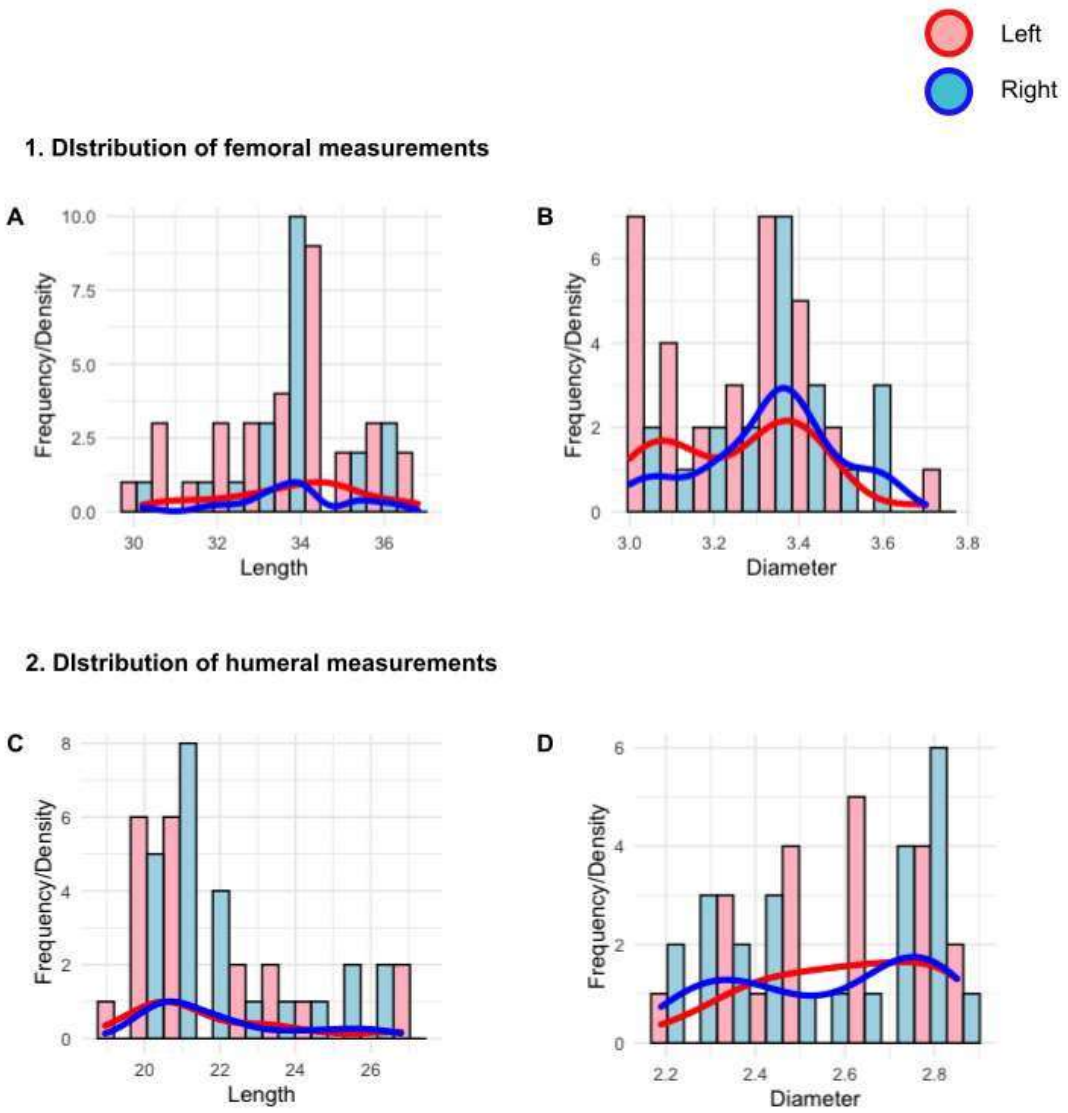

Figure 25: Distribution of humeral and femoral measurements.

Distribution of femoral and humeral measurements including density curve. The left side of each unique element is indicated pink and the right by blue.(A) Distribution of femoral length, (B) Distribution of femoral diameter, (C) Distribution of humeral length and (D) Distribution of humeral diameter.

A t-test was performed on the length of the left and right humeri. The null hypothesis states that there is no significant difference between the left and right humeri therefore we can assume that they come from a single population. The significance level was set at 0.05. The p-value obtained was 0.717, suggesting there is no statistically significant difference between the distribution of right humeral length and left humeral length. This is further supported by a confidence interval of -1.530753 to 1.062670 (see Table 4).

Table 4: t-test Results comparing the left and right humeral length.

Side	n	Mean	SD	df	p	Decisions
Left	20	21.80075	2.205	38.951	0.717	Fail to reject null hypothesis
Right	24	22.03479	2.006			

A t-test was performed on the diameter of the left and right humeri. The null hypothesis states that there is no significant difference between the left and right humeri therefore we can assume that they come from a single population. The significance level was set at 0.05. The p-value obtained was 0.649, suggesting there is no statistically significant difference between the distribution of right humeral diameter and left humeral diameter. This is further supported by a confidence interval of – 0,09747515 to 0.15477515 (see Table 5).

Table 5: t-test Results comparing the left and right humeral diameter.

Side	n	Mean	SD	df	p	Decisions
Left	20	2.59490	0.196	41.763	0.649	Fail to reject null hypothesis
Right	24	2.56625	0.219			

A t-test was performed on the length of the left and right femora. The null hypothesis states that there is no significant difference between the left and right femora therefore we can assume that they come from a single population. The significance level was set at 0.05. The p-value obtained was 0.904, suggesting there is no statistically significant difference between the distribution of right femoral length and left femoral length. This is further supported by a confidence interval of -0.9257782 to 0.8593143 (see Table 6).

Table 6: t-test Results comparing the left and right femoral length.

Side	n	Mean	SD	df	p	Decisions
Left	31	33.774	1.74	47.906	0.940	Fail to reject null hypothesis
Right	21	33.807	1.44			

A t-test was performed on the diameter of the left and right femora. The null hypothesis states that there is no significant difference between the left and right femora therefore we can assume that they come from a single population. The significance level was set at 0.05. The p-value obtained was 0.154, suggesting there

is no statistically significant difference between the distribution of right femoral diameter and left femoral diameter. This is further supported by a confidence interval of -0.016595789 to 0.02707302 (see Table 7).

Table 7: t-test Results comparing the left and right femoral diameter.

Side	n	Mean	SD	df	p	Decisions
Left	31	3.36	0.177	45.43	0.154	Fail to reject null hypothesis
Right	21	3.33	0.163			

The variation between the right and left side of each unique element in the bonebed in the bonebed reveals insignificant variation. This indicates that the left and right sides of a unique element were drawn from the same population, In this case the population is individuals within the same ontogenetic class.

The average humeral diameter is 2.58 mm and the average femoral diameter is 3.29 mm, therefore the ratio of the humeral diameter to the femoral diameter is 0.784. The individual with an articulated femur and humerus (individual O1) has a humeral diameter of 2.26 mm and a femoral diameter of 3.20 mm, indicating that it is slightly smaller than the mean values for these bones in the bonebed. Its humeral/femoral diameter ratio of 0.706 is similar to, but slightly lower than the mean value for the bonebed.

Size Comparisons with other *Owenetta* specimens and ontogeny

Postcranial elements of *Owenetta* specimens are quite rare in the fossil record. We compared the maximum cranial length observed in SAM-PK-K11289 to the maximum cranial length of *Owenetta* and procolophonid specimens whose ontogenetic stage has been identified (see Table 8). The largest cranium (measured at 21 mm maximum cranial length) in bonebed SAM-PK-K11289 is consistent with the maximum cranial length of BP/1/4195. BP/1/4195 has been identified as a subadult. The smallest crania (measured at 17 mm maximum cranial length) in SAM-PK-K11289 is even smaller than juveniles so far described. The largest individual in the bonebed is at least 50% of the largest procolophonid individual observed in this study (*Saurokdektes kitchingorum* RC 845). It is 53.8%, The size of the crania in bonebed SAM-PK-K11289 is consistent with the late Permian *Owenetta* specimens. The bonebed SAM-PK-K11289 therefore preserves some of the smallest *Owenetta* specimens known, and I suggest that the ontogenetic stage represented is juvenility. This is supported by osteological indicators of immaturity such as the poorly developed epiphyseal ends of long bones. The immaturity of the epiphyseal ends of the long bonebed is supported by the high level of abrasion due to the lack of compact bone. This suggests that these elements were not fully ossified when the individuals died. Additionally, the elements of the crania are displaced, suggesting that the cranial sutures were not fully closed. Thus, I conclude that the individuals in bonebed SAM-PK-K11289 had not reached skeletal maturity. It is highly unlikely that the individuals in bonebed SAM-PK-K11289 are neonates, as small and delicate elements such as phalanges are well-ossified. The bones also lack the texture that is usually observed in the bones of neonates. It is also unlikely that bonebed SAM-PK-K11289 is a new small morph of *Owenetta*, as late Permian morphs are known to be relatively smaller than the Triassic forms.

Table 8: *Owenetta* specimens with identified ontogenetic stages.

Taxon	**Specimen number**	**MCL**	**Ontogenetic stage**
Saurodektes kitchingorum	BP/1/4195	23 mm	Subadult
Owenetta rubidgei	SAM-PK-K7582	26 mm	Subadult
Owenetta rubidgei	RC 50	31.1 mm	Juvenile
Saurodeketes kitchingorum	RC 845	39 mm	Juvenile

MCL= Maximum cranial length

Body Mass Estimation

The body mass of the individuals in bonebed SAM-PK-K11289 was inferred from the skeletal; scaling relationships outlined by Campione and Evans (2012). Measurements of the humeral circumference and femoral circumference were fitted into the appropriate equations to get body mass estimates. Based on the circumference of the femur, the body mass estimated ranges from 10.134 grams to 13,135 grams. The body mass estimated from the humeral circumference ranges from 8.211 grams to 11.171 grams. The overall average body mass is 10.661 grams.

Only one individual in the bonebed presented both the femora and humerus in articulation. The equation with both humeral and femoral circumference was used to infer the body mass of this individual. The body mass inferred from this individual (O1) is 9.867 grams. This falls within the range of body mass estimations, albeit slightly smaller than femoral estimates and closer to the mean of humeral size estimates.

Skeletal Articulation and Association

Overall, the degree of articulation and element association of individual skeletons that make up the bonebed is relatively high (see Figures 26 and 27). Only two individuals are preserved in nearly complete articulation, preserving bones of the axial and appendicular skeletons in near-life positions on the dorsal surface of the bonebed. These two individuals are indicated by the white boxes in Figure 26 and are referred to as O1 and O2. Fifteen individuals are represented by an articulated series of presacral and caudal vertebrae. Of the 15 series, 8 are of caudal vertebrae and the remaining seven are of presacral vertebrae. Some of the series preserve the natural curvature of the vertebral column. Five individuals are represented by the stylopod in articulation with the zeugopod. Sixteen individuals are represented by a zeugopod association. Twelve individuals are represented by an articulated autopod. Limb elements are commonly found in close association or articulation however they are clearly isolated from the rest of the skeleton.

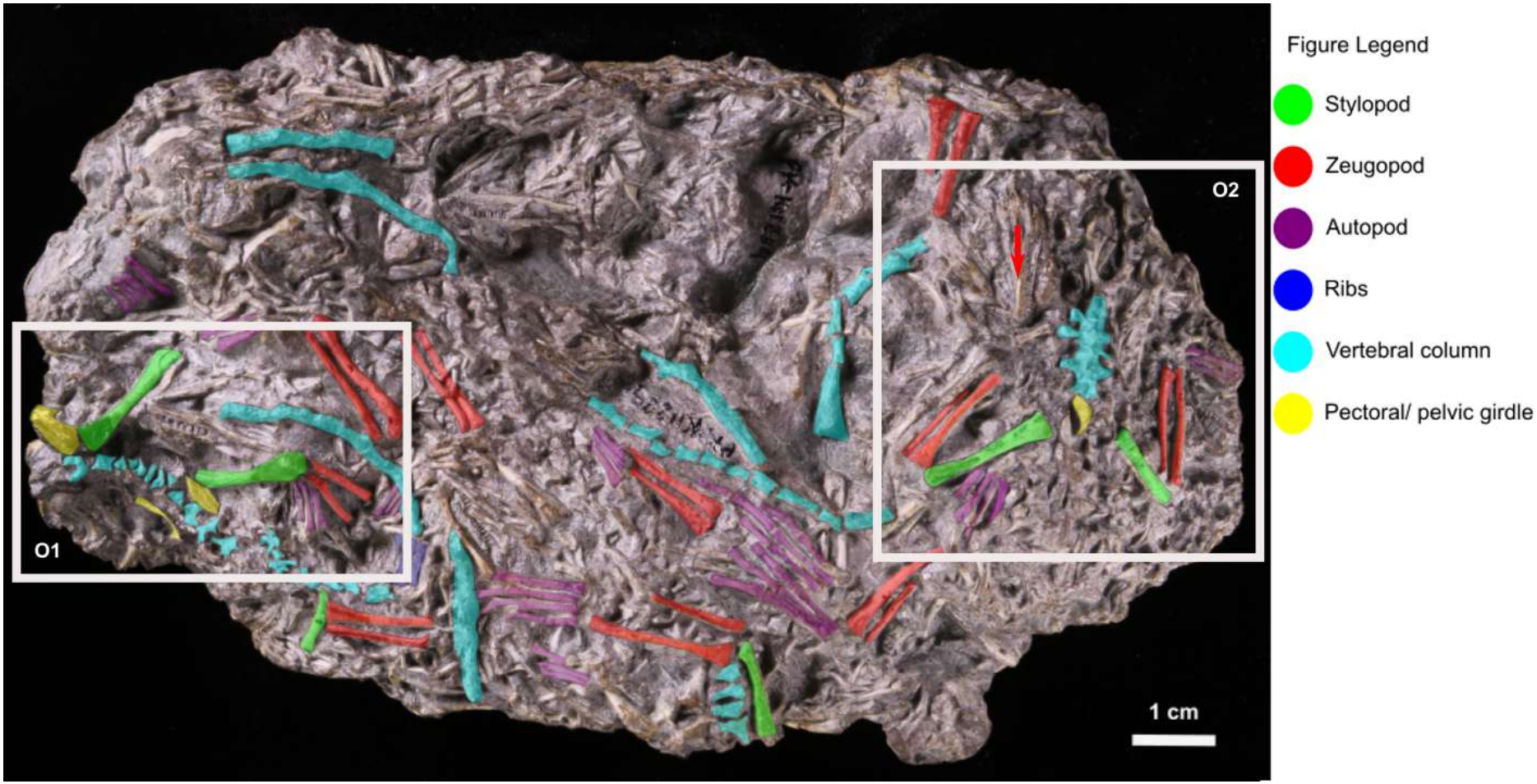

Figure 26: Overall articulation and association in the ventral view.

Individuals O1 and O2 indicated by white boxes. The red arrow indicated the skull that is closely associated with individual O2.

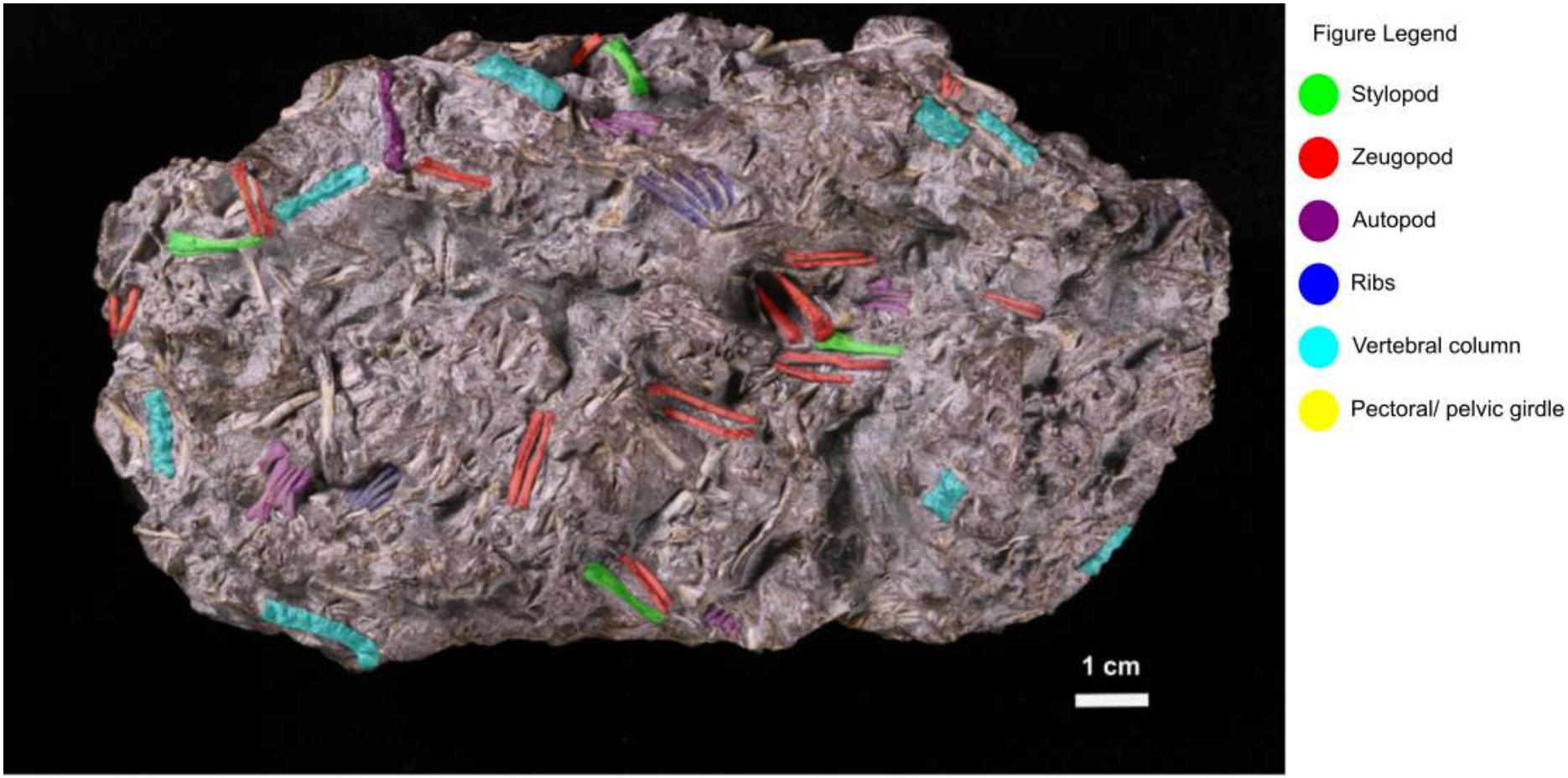

Figure 27: Overall articulation and association observed in the ventral view.

There are two most distinctive partially articulated individuals in the bonebed. For the sake of conciseness, we identify these individuals as O1 and O2 (see Figure 26).

O1 is the most complete individual, the majority of the skeletal elements are present and are either in articulation or very strong association. O1 consists of a vertebral column consisting of most presacral vertebrae, an articulated post-cranial skeleton that includes a left articulated hindlimb and both the left and right ilia. A left forelimb is closely associated with this individual. There is no skull articulated to this individual, however there is a skull that is closely associated and can be confidently assigned to this individual. The skull is lying ventral -up and has a lower jaw and is displaced such that it is nestled under the post-cranial skeleton of this individual and can only be seen on the dorsal side of the bonebed. This individual's vertebral column is curled up. This posture is consistent with taphonomic class A1 outlined by Smith et al. (2022).

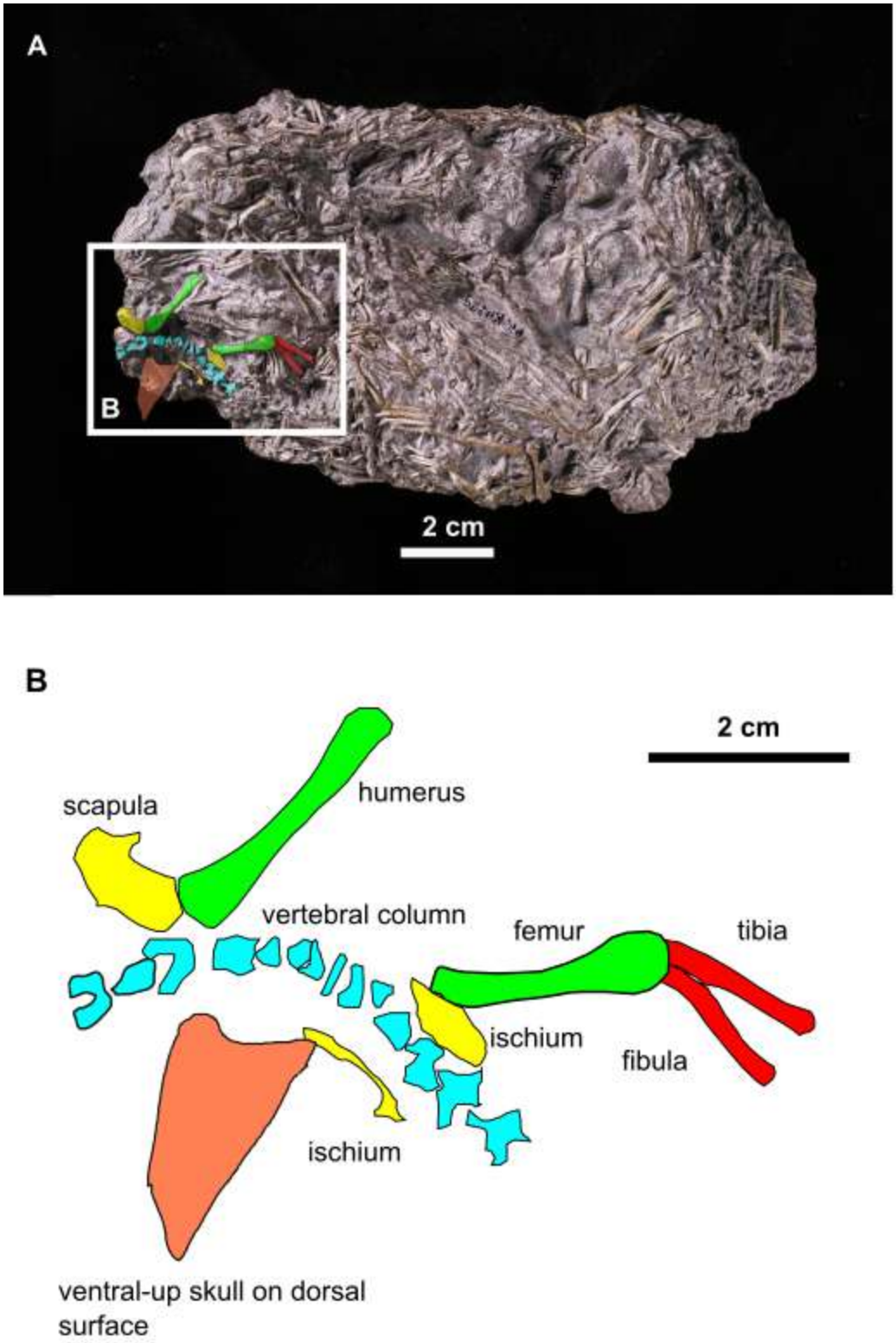

Figure 28: Semi-articulated individual O1 visible on the ventral and dorsal surface of the bonebed.

(B) Individual O1 includes a partial vertebral column, the left and right ischium, the right scapula, the right humerus, the right femur, the right tibia and the right fibula in

articulation. The skull attributable to this individual is lying ventral up on the dorsal surface of the bonebed. O1 can be seen on both the ventral and dorsal surfaces of the bonebed.

Individual O2 is the second most complete individual visible and is preserved on the ventral side of the bonebed. As opposed to O1, this individual is not articulated to a cranium, in fact the anterior most of the skeleton is missing, however there is a skull with an articulated mandible in close association that could be attributed to this individual. The distal end of the vertebral column is preserved and articulated to both the left and right ilia. The humerus, fibula and tibia and preserved in articulation on both sides. This individual's limbs are extended on the side, this spread- eagled posture is typical of that observed in taphonomic class A2 (Smith et al., 2022).

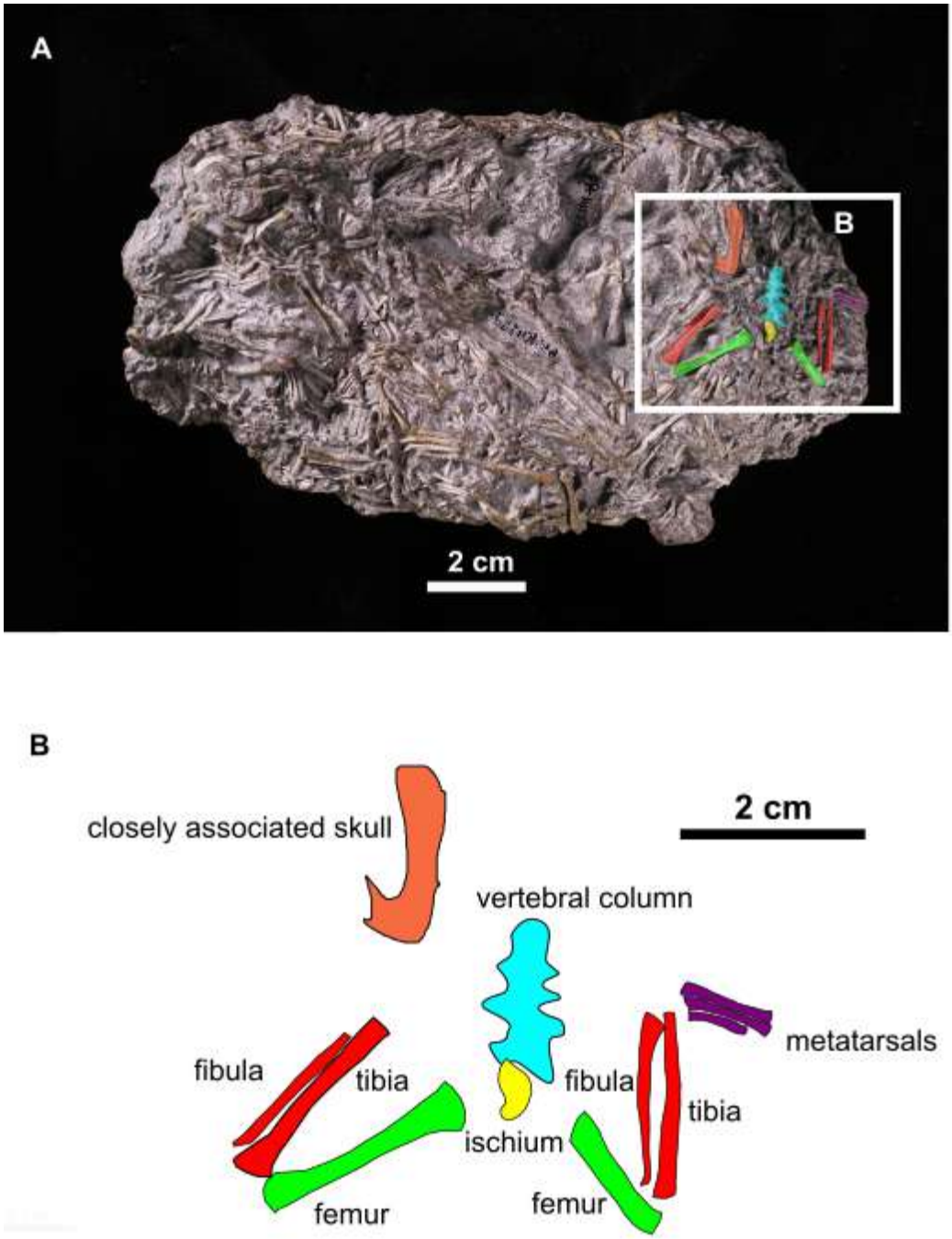

Figure 29: Semi-articulated individual O2 visible on the ventral surface of the bonebed.

(C) Individual O2 includes only the posterior half of the skeleton. Elements in articulation include the vertebral column, the left ischium, the left and right femur, the left and right tibia, left and right fibula and three metatarsals on the right. There is a closely is a partial skull closely associated with this individual.

Another common style of articulation and association observed in the bonebed involves the vertebral column, representing at least 15 individuals (see Figure 30). The articulated segments of different sections of the vertebral column are commonly found in the bonebed. Each series differs in length from the next. The number of individual vertebrae in a series can range from 4 to 12. In some series, the individual vertebral element cannot be determined because the matrix around the vertebral column is not fully prepared in order to preserve the delicate elements. Some vertebral series preserve their true anatomical positions, such that the series forms a curve. And in other series, the vertebral elements have been slightly displaced but remain strongly associated. The caudal vertebrae commonly form longer series than the thoracic, lumbar and cervical vertebrae.

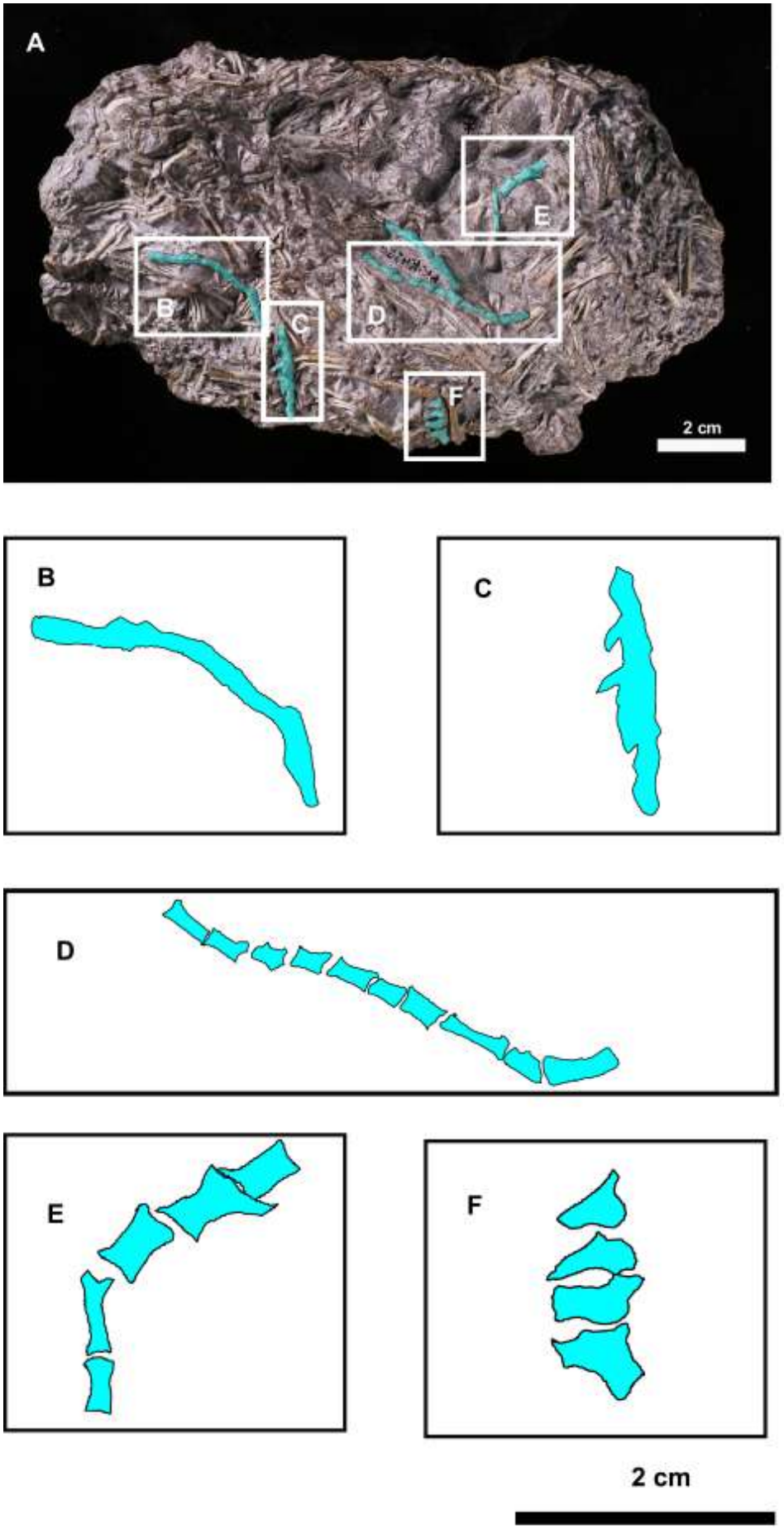
A
B
C
D
E
F
2 cm
B
C
D
E
F
2 cm

Figure 30: Vertebrae articulation modes.

Series of articulated vertebrae in the bonebed. (B) is a series of cervical vertebrae that are closely associated to a skull. The articular ends of each single vertebrae is not fully prepared such that each vertebrae cannot be determined from the next. (C) is a series of thoracic vertebra (D) is a series of caudal vertebrae, each element is distinct from the next. (E) and (F) are a series of presacral vertebrae forming a vertebral series.

The limbs are commonly found isolated from the rest of the skeleton but remain articulated or strongly associated. This is an obvious feature of the bonebed, recorded 21 times on the surface. The ulna and radius (see Figure 31B) are found strongly associated. Their natural anatomical positions are not exactly preserved but the two elements can still be confidently attributed to one individual. In Figure 31C, the femur is articulated (indicated by red) to the tibia and the tibia is strongly associated to the fibula. These three elements can thus be attributed to a single limb of an individual. This articulation mode Involves both the articulation of a zeugopod to a stylopod and the association between two stylopodia. This mode of articulation reflects taphonomic class A4 outlined by (Smith et al., 2022).

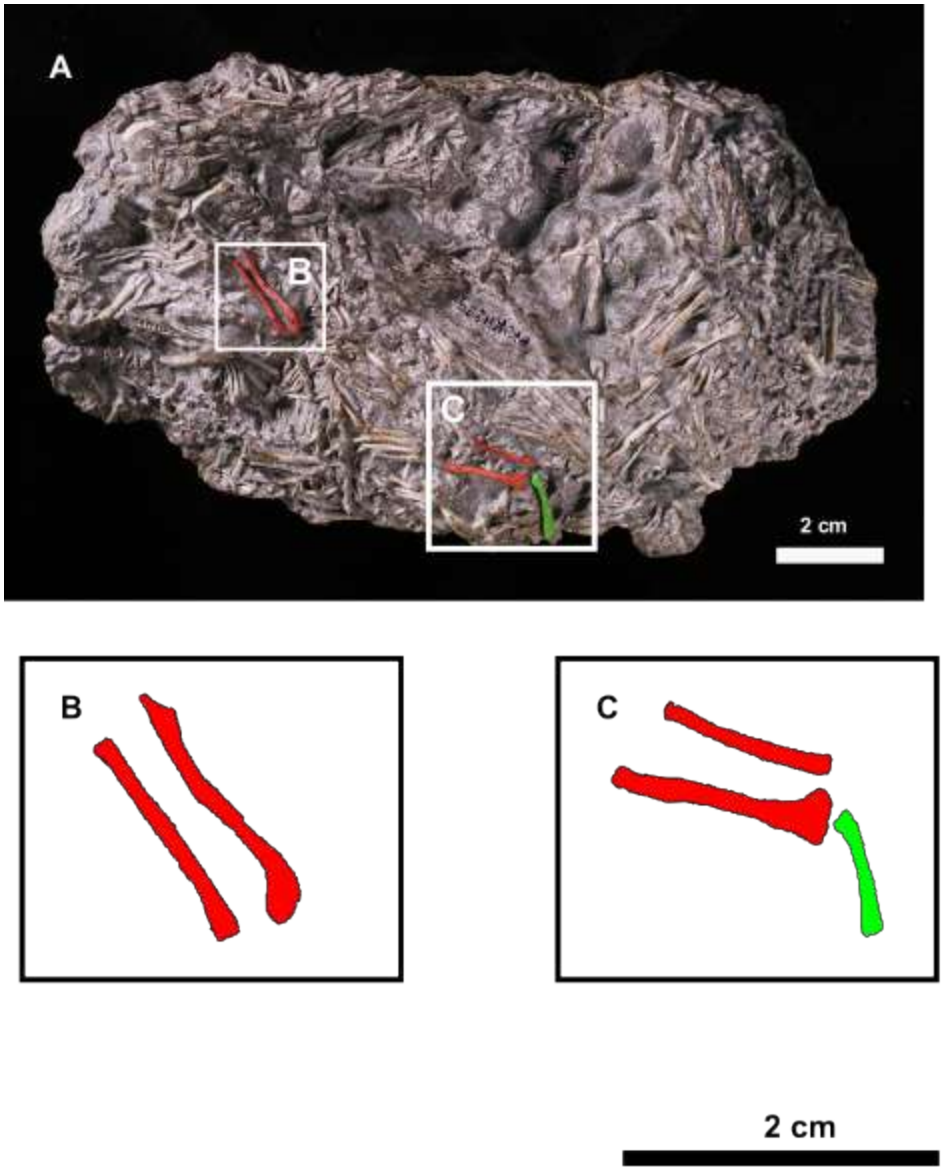

Figure 31: Stylopodial articulation and association modes.

Articulation styles involving the stylopod. (B) Strongly associated ulna and radius, and (C) Femur articulated with tibia, and tibia is strongly associated with fibula.

The most interesting articulation and association style observed in the bonebed involves pedal and manual digit bones. This mode of articulation is relatively abundant in the bonebed, with 12 instances of the autopod in articulation. In Figure 32B, three of the most proximal pedal phalanges are strongly associated. The third proximal phalanx is articulated to the third medial phalanx. The third, likely medial is also present but it is displaced such that it proximal end is tucked under the shaft of the third medial phalanx. This articulation and association of medial pedal and manual digit bones is the most common within the bonebed. The articulation style illustrated in Figure 32C involves the distal, medial and proximal phalanges. Four proximal phalanges are strongly associated. The 1st and 2nd proximal phalanges are articulated to the 1st and 2nd medial phalanges. The third and fourth phalanges are articulated to both the medial and distal phalanges. Figure 32D illustrates metatarsals and phalanges that are clustered. This is common in the bonebed. The cluster illustrated in Figure 32D involves metatarsals and phalanges belonging to more than one manus, most likely two, here annotated as 1 and 2. They are separated by a narrow space. The elements are associated in a fashion resembling their true anatomical positions. There are metatarsal one to three in the first manus (indicated by the number 1). The first metatarsal is articulated to the proximal phalanx. The second and third metatarsals are articulated to the proximal and medial phalanges. The second manus (indicated by the number 2) presents metatarsal one and two that are articulated to the proximal phalanges. The third digit of manus 2 consists of the proximal, medial and distal phalanges.

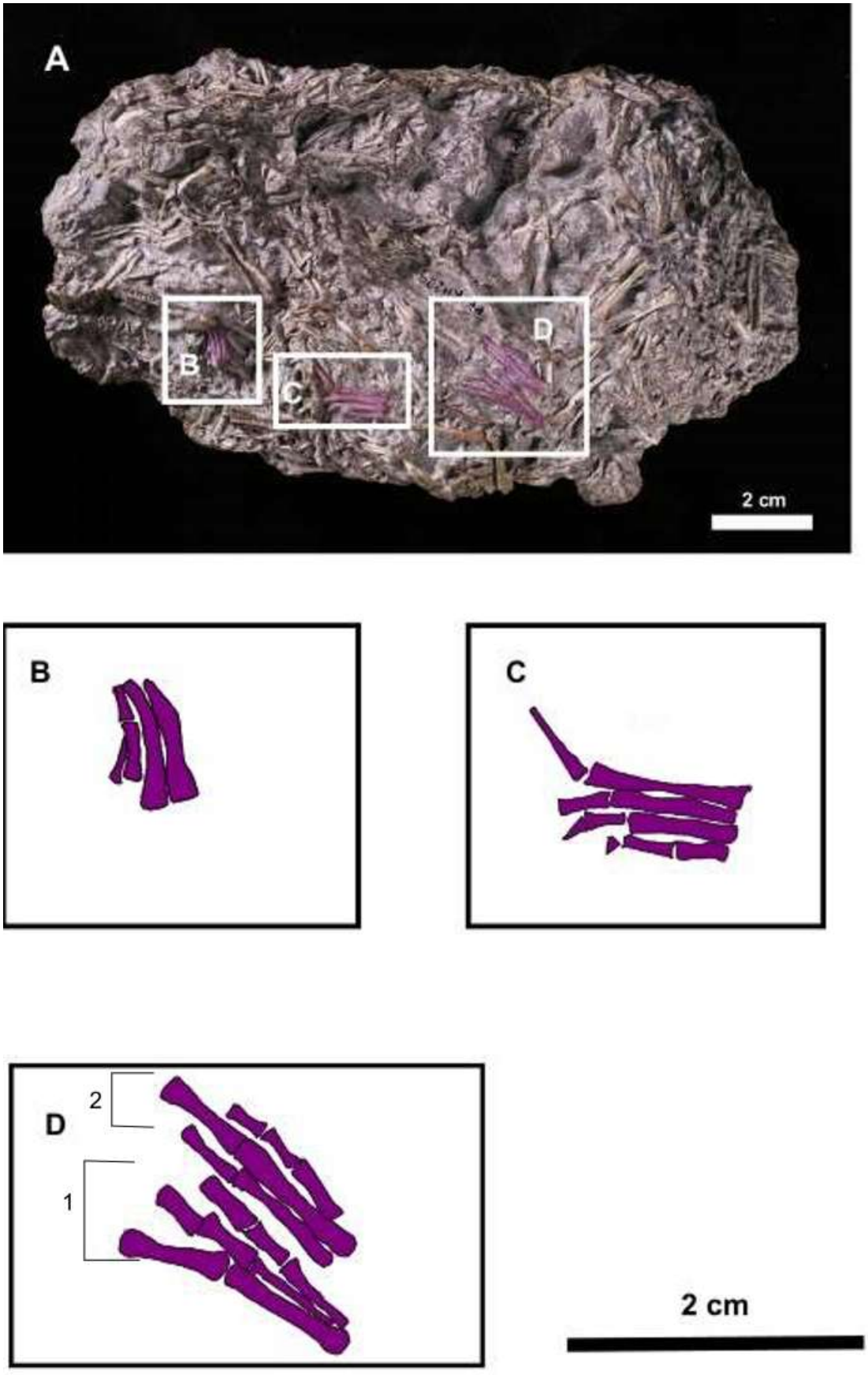

Figure 32: Articulation and association modes of manual and pedal digit bones.

Taphonomic modification

Taphonomic modification data was collected qualitatively from the elements exposed on the surface of the bonebed.

Bioerosion marks

Predators are common accumulators of skeletal material and will leave behind obvious evidence such as tooth marks. Tooth marks are conical-shaped depressions or V-shaped grooves (Fiorillo, 1988, Binford, 1981). There are depressions observed on the long limb bones in bonebed SAM-PK-K11289. Upon superficial observation, these depressions can be mistaken for tooth marks. However, their shapes are entirely inconsistent with tooth marks. The depression observed in Figure 33A, D and F have polygonal shapes, which are shallow and only penetrate the cortical bone. This morphology is not consistent with the V-shaped grooves and conical-shaped pits that are attributed to the actions of teeth. The depression in Figure 33B is circular, this depression is shallow, and the cortical bone has collapsed into it. This is the only depression observed on the vertebrae. The depressions in Figure 33C and E are almost perfectly circular. They only penetrate the cortical bone. None of the depressions exhibit healing. It is, therefore, most likely that these depressions were made during mechanical preparation.

There is no other evidence to suggest that a predator was responsible for the accumulation of bonebed SAM-PK-K11289. No tooth is found lodged into any of the identified depressions nor were any shed teeth recovered during visual or digital investigation. Usually shed teeth are recovered in bone concentrations accumulated by predators. No other taphonomic features that suggest the presence of a predator such as scratch marks were identified on any of the bones. Additionally, the bonebed was not recovered in the skeleton of a host (predator) and the surface of the bones did not exhibit corrosion abrasion, we therefore cannot suggest that the bonebed is a derivation of a predator’s digestive process.

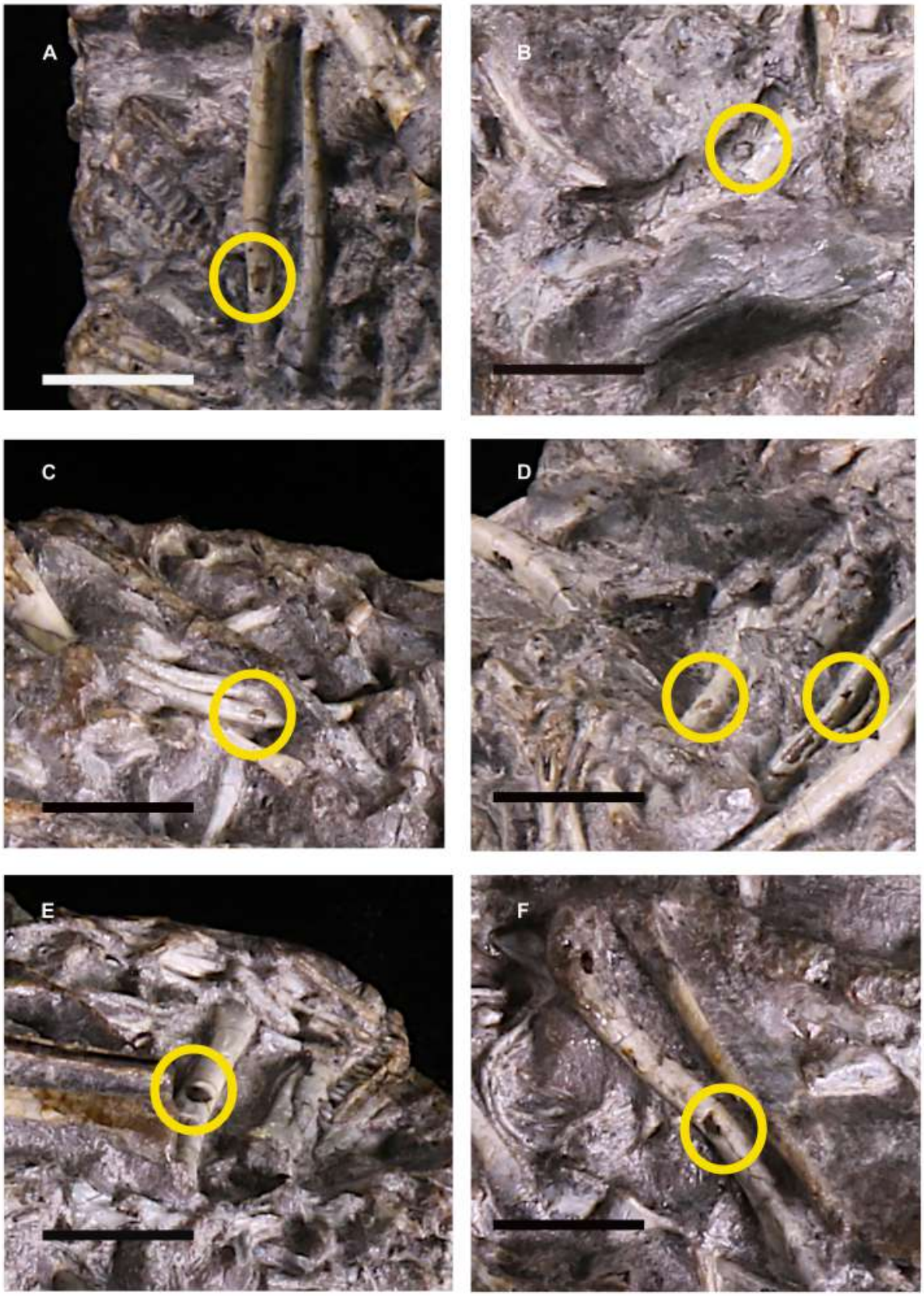

Figure 33: Depressions on the surface of some skeletal elements.

The yellow circle indicates the depressions on the skeletal elements. (A) Polygonal-shaped depression on the distal end of a tibia. (B) Circular-shaped depression on caudal vertebrae, (C) Circular-shaped depression on a pedal phalanx (D) Polygonal-

shaped depression, more likely a chip on the shaft of a tibia, (E) Perfectly circle depression on the shaft of a femur and (F) Polygonal-shaped depression on the shaft on an ulna.

Abrasion, Fractures and Cracking

Abrasion, fracture and weathering categories established by Ryan et al. (2001) were adapted here and used to classify the elements in the bonebed (see Tables 7 and 8). Multiple modes of preservation are observed. The majority of elements exhibit modifications through discolouration, abrasion, polishing and cracking. The preservation quality between elements varies slightly.

Table 9: Fracture definitions adapted from Ryan et al. (2001).

Fracture category	Description
Collection	Fractures that occur during the preparation or collection of a fossil.
Compression	Parallel fractures that may include multiple steps due to crushing.
Intermediate	Fractures that cannot be placed into one category.
Longitudinal	Fractures that are parallel to the long axis of the bone.
Spiral	Saw-toothed fractures, usually occur prior to fossilization.

In Figure 34A, a fracture that is parallel to the long axis of the element is observed. This is referred to as a longitudinal fracture and is relatively uncommon in the bonebed such that it is observed only three other times on the surface of the bonebed. Fractures perpendicular to the long axis of the bone are observed in Figures 34B and C, this fracture is the most common in the bonebed. It is abundantly observed on long bone elements. Almost every single long bone on the surface of the bonebed has a transverse fracture along its shaft. The fractures observed on long bones are consistent in morphology with dry bone fractures (i.e. shivers of Behrensmeyer (1978)). Figure 34D, E and F exhibit compression fractures. This sort of fracture is commonly observed on cranial material but can also occur on long bones that are on the surface. However it is no as abundant as the transverse fracture. This fracture is observed on all of the 5 crania visible on the surface. None of the fractures observed exhibit any sign of healing suggesting that they occurred post-mortem.

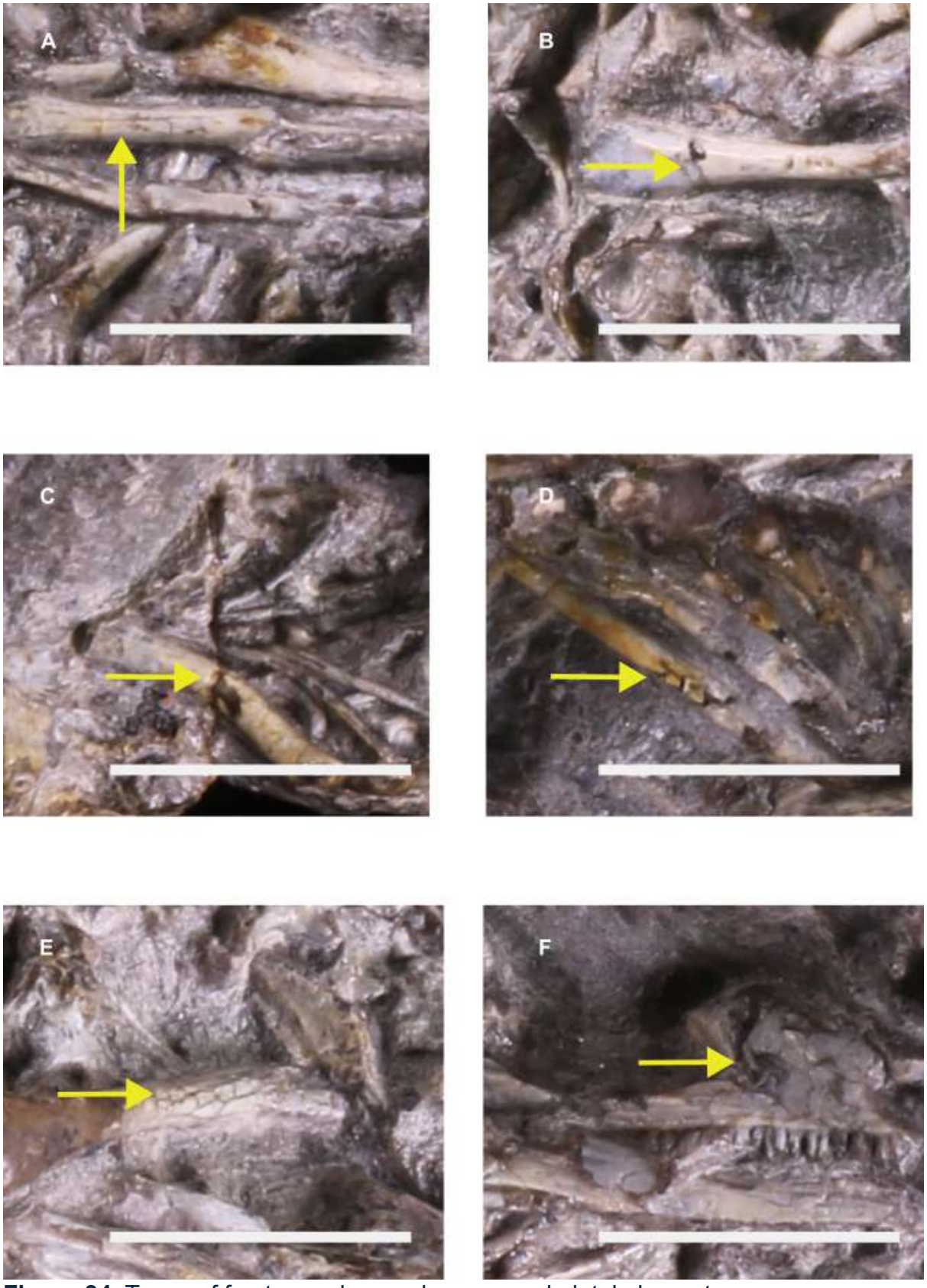

Figure 34: Types of fractures observed on some skeletal elements.

Fractures observed on the surface of the skeletal elements SAM-PK-12289 are variable, the yellow arrow indicates fracture. (A) Longitudinal fracture on the metatarsal, (B) Transverse fracture on the tibia, (C) Transverse fracture on the

metatarsal, (D) Compression fracture on the rib, (E) Compression fracture on the shaft of a femur and (F) Compression fracture on the crania. The scale bar represents 1 cm.

Table 10: : Abrasion and weathering categories adapted from (Ryan et al., 2001).

Taphonomic Category	**Class 0**	**Class 1**	**Class 2**	**Class 3**
Abrasion	Surface of fossil is perfect, no indication of abrasion.	Broken edges of fossils are polished and rounded.	Edges of bone are polished and rounded but the original texture can still be identified.	Surface of bone well rounded and polished, and processes have been reduced to bumps.
Weathering	Fossil surface not cracked and is not flaking.	Epiphyses of bones are not damaged. The surface of the fossil has cracks that are parallel.	Epiphyses are deeply eroded or absent. Cracks are parallel and penetrate the cortical bone. Flaking is observed at the crack.	Surface of the fossil has a high degree of cracking and flaking. Large pieces of the cortical bone are absent.

The elements in bonebed SAM-PK-K11289 are modified, especially at the epiphyses (Figure 35). The trabecular bone has deteriorated and the space is infilled with minerals (see cross-section of bonebed scans in Figure 6). The proximal end of the humerus in Figure 35A is well-polished such that the original texture is not discernible. The surface has cracks that are parallel to the fibrous structure of the bone. The epiphyseal ends are heavily eroded. Moderate flaking can be observed on the bone surface. These taphonomic features are consistent with abrasion stage 3 and weathering stage 2. This sort of modification style is observed in the majority of the long bone elements in bonebed SAM-PK-K11289. Vertebrae material too exhibit this sort of modification. They are heavily eroded, discoloured and polished. Processes of the vertebrae appear as simple bumps.

The distal end of the femur in Figure 35B is extremely rounded such that its original shape is not preserved. There are parallel cracks on the surface of the bone. This is characteristic of abrasion stage 2. A singular weathering stage cannot be determined as the features observed overlap between stages 1 and 2 (Ryan et al., 2001).

Generally the skeletal elements on the surface of the bonebed exhibit a brownish colour (see Figure 35D, E and F).

The weathering style observed in bonebed SAM-PK-K11289 is unique and cannot be characterized into only one of the weathering stages. This can be attributed to the stages being based on mammals larger than 5 kg. Bones belonging to smaller animals and/or different lineages may weather differently.

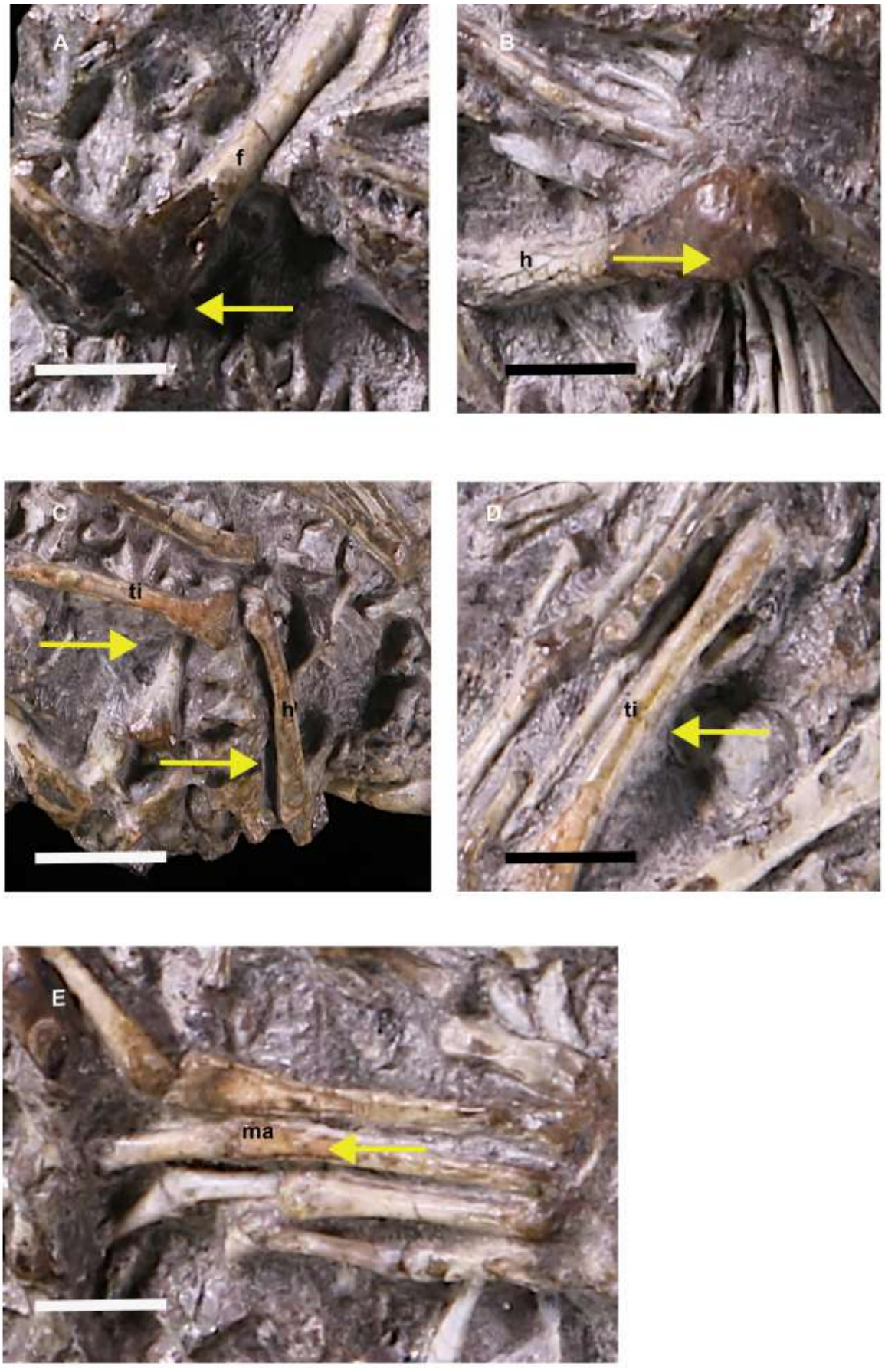
A
f
B
h
C
ti
h'
D
ti
E
ma

Figure 35: Modification features on the surface of some skeletal elements.

Surface modifications observed in the bonebed are variable, the yellow arrow indicates modification. (A) The proximal epiphyseal end of the femur is highly abraded, (B) The distal proximal end of a humerus is highly abraded, (C) Brown discolouration of the surface of a tibia and humerus, (D) Light brown discolouration on the surface of a tibia and (E) Light brown discolouration of metatarsals. Scale bar represents 1 cm.

Bonebed classification and comparisons

The differences between microfossil bonebeds and macrofossil bonebeds is a widely recognized dichotomy in bonebed research (Rogers et al., 2007). Bonebed SAM-PK-K11289 satisfies the criteria to qualify as a microfossil bonebed. The average body mass of the individuals in the bonebed is 10.7 grams. All the identifiable elements (NISP) are smaller than 5 cm in length and width (Wood et al., 1988). All identifiable elements exhibit morphological affinities of one taxon: *Owenetta rubidgei.* Therefore, bonebed SAM-PK-K11289 is a monotaxic or more precisely, a monospecific bonebed. Other monospecific microfossil bonebeds from the Karoo strata include SAM-PK-K8305, SAM-PK-K7710 and SAM-PK-K10818. (see Table 9 for a full list of specimens used for comparative purposes).

Bonebed SAM-PK-K7710 is hypothesized to be an aggregation of juvenile *Youngina* individuals. This bonebed has the same elliptical shape as SAM-PK-K11289, but its taphonomic style is distinctly different (Smith and Evans, 1995). The individuals in this bonebed are fully articulated and arranged in a parallel fashion. The 5 individuals in this bonebed were behaviourally arranged and were buried in their “life positions”. Bonebed SAM-PK-K8305 is a monospecific behavioural aggregation of the varanopid *Heleosaurus scholtzi.* This aggregation too exhibits a high degree of articulation and spatial organisation. The quality of the skeletons suggests that they were not exposed to processes of destruction and dispersion. The presence of dermal osteoderms in this bonebed in their true anatomical positions further supports the idea that the individuals in this bonebed were rapidly buried.

The chaotic melange of bones initially observed in SAM-PK-K11289 appears to be the opposite of the former examples. The individuals in this bonebed are disturbed and not buried in their “life positions”. The skeletons are preserved in different attitudes and orientations and display no obvious alignment. The observation made in SAM-PK-K11289 are not indicative of rapid death and immediate burial as seen in the *Heleosaurus scholtzi* (SAM-PK-K8305) and the *Youngina* (SAM-PK-K7710) aggregations. (see Figure 1 for reference).

Specimens SAM-PK-K10818 (see Figure 35) is an aggregation of *Youngina* that was found less than 3 km away from Osfontein farm where SAM-PK-K11289 was found and 20 m lower in the stratigraphic succession. However even more interesting is that it exhibits a taphonomic style that is similar if not identical to that of SAM-PK-K11289. Both these bonebeds share the same level of articulation. Elements of the limb are strongly associated but not preserved in their anatomical positions. The vertebrae here also form strings and ribs are severely underrepresented as in SAM-PK-K11289. The host lithology of bonebed SAM-PK-K10818 is greenish-grey siltstone which is identical to the rock of SAM-PK-K11289.

Dorsal view

Ventral view

Figure 36: Bonebed SAM-PK-K10818 in dorsal and ventral view.

Table 11: Comparative bonebeds used in the study.

Specimen Number	Taxonomic identification	Description	Source
SAM-PK-K7710	*Youngina capensis*	Four skulls with lower jaws and post crania of 5 individuals.	Iziko Museum
SAM-PK-K10818	*Youngina capensis*	Five articulated juvenile Youngina preserved in their “life positions”	Iziko Museum
RC 845	*Galesaurus and Owenetta kitchingorum* (now *Saurodektes kitchingorum*)	Multi taxic aggregation. Individuals in “life positions. Also with fossil millepedes (Groeneveld and Smith 2023)	Abdala et al. (2006)
BP/1/1395	Youngina capensis	Two skulls found in association	Evolutionary Studies Institute
BP/1/4285	*Owenetta*	Two skull found in association	Evolutionary Studies Institute
SAM-PK-K8305	*Heleosaurus scholtzi*	Five articulated varanopid individuals in "life positions	Botha-Brink and Modesto (2009)

DISCUSSION

Taxonomic identification of individuals in bonebed SAM-PK-K11289

The preserved cranial and post crania in SAM-PK-K11289 agree closely in their shapes, suggesting that all material in the bonebed pertains to a single taxon. Direct comparisons of the maxillae and palate show strong similarities with morphologies observed in *Owenetta*. The lack of cranial ornamentation in any of the specimens strongly refutes identification as other procolophonids or millerettids. Key differences in the shape of the maxilla such as the well-developed anterodorsal and suborbital ramus, and the contribution of the premaxillary process to the external nares, also rule out other potentially contemporaneous early reptiles like *Youngina*. The appendicular skeletal elements most closely resemble *Owenetta* in the following ways: the ilia is blade-like, the interclavicle is anchor-shaped, the humerus exhibits an absence of an entepicondylar foramen and lastly the tail is relatively elongated. The stratigraphic position of the bonebed is entirely consistent with the known distribution of *Owenetta*. These lines of evidence enable a referral of all specimens in the bonebed to *Owenetta*, although a specific diagnosis is less certain. I tentatively refer to the bonebed material as *O. rubidgei* based on these observations.

Body size variation in sample and ontogenetic status

Measurements of the stylopod generated insignificant standard deviation values, indicating a narrow range sizes of individuals in the bonebed. T-tests between the length and diameters of the stylopodial elements indicate that the left and right sides are likely drawn from the same sized populations. The distribution graphs also lacked clear groups of outliers indicating that there is only one group. The individuals in bonebed SAM-PK-K11289 have a smaller maximum cranial length than the smallest reported juvenile *Owenetta* specimens. As per size size-based criterion outlined by Evans et al. (2009), these individuals are at least 50% the size of most procolophonid taxa therefore their assignment to juvenility. Most known specimens of *Owenetta* are subadults. It is unlikely the individuals in SAM-PK-

K1289 are a new small morph of *Owenetta* as there is evidence of immaturity in the crania and postcranial elements. The elements of the crania are displaced, and the epiphyses of long bones are immature, and highly abraded suggesting that they were not fully ossified when the individuals died.

Is bonebed SAM-PK-K11289 a single brood ?

Clutch size (live-bearing species and egg-laying species) is highly variable in reptiles, ranging from 1 to 100 (Meiri et al., 2020). Meiri et al. (2020) tested the relation between clutch size and body size in extant reptiles and revealed that they were significantly positively correlated. They further revealed that reptiles with a body mass of ~10 grams form clutch sizes with approximately a maximum of 11 individuals. Bonebed SAM-PK-K11289 contains 31 individuals with an average body mass of 10.661 grams. This clutch size is unusually high for this body mass and does not reflect the generalized patterns observed in living reptiles, therefore it is highly unlikely that all 31 individuals are from the same set of parents. This scenario can be explained by the communal nesting phenomenon observed in some reptiles and amphibians (J. Sean Doody et al., 2009). Where female reptiles deposit their young in communal sites and dispersal is delayed till after juvenility. I hypothesize that adult female *Owenetta* individuals laid clutches in the same “nests”, as observed in many extant reptile species (Radder and Shine, 2007). Although this is not a single brood of *Owenetta*, it is the largest number of Owenetta individuals found together.

Origin and depositional history of SAM-PK-K11289

Characterisation of the bonebed

The faunal assemblage of bonebed SAM-PK-K1289 can best be described as uniform, monotaxic and consisting of individuals within the same ontogenetic class but not the exact same age and body mass. This satisfies the criteria for an intraspecific biogenetic concentration outlined by Rogers et al. (2007). Behrensmeyer (2007) suggests that such assemblages are due to a behaviour, although the death may be caused by a physical event. I suggest that *Owenetta* was gregarious, and this intrinsic biogenetic aggregation originated from juvenile *Owenetta rubidgei* individuals from different clutches forming aggregations in confined spaces. In physically generated concentrations, the taxa and ontogenetic classes will be random such that it is highly unlikely that a flood will accumulate the disarticulated remains of individuals belonging to the same size class and taxon.

Predator accumulation vs behavioural aggregation?

Predators are responsible for some of the skeletal accumulations in the fossil record (Dodson and Wexlar, 1979, Andrews and Evans, 1983, Mayhew, 2008). Bonebed SAM-PK-K11289 was not recovered in the context of a host (predator). Unique skeletal elements in the bonebed exhibit the same type and level of modification. Predators accumulate skeletal elements in nests, caves, burrows and lairs over time therefore different elements will exhibit different levels of modification. Tooth traces and scratch marks are usually observed in conjunction in the predator-accumulated assemblages. Only isolated puncture marks are present on some of the limb bone elements, and they are consistent in morphology and size with the scribe used during the fossil preparation process. The surface of the skeletal material in bonebed SAM-PK-K11289 reveals no modification features (digestive enzyme corrosion) that indicate that it has passed through the digestive tract of a predator. We therefore cannot suggest that this bonebed has scatological origins. No shed teeth are found in the bonebed. It is also highly unlikely that a predator would be so prey- specific as to only feed on juvenile *Owenetta*. There is not sufficient evidence

suggesting predation therefore it is highly unlikely that bonebed SAM-PK-K11289 originated from predator activity. Behavioural aggregation is therefore deemed to be the most parsimonious explanation for the initial concentration of the bones.

Paleoenvironmental setting of the bonebed

The bonebed forms part of the *Daptocephalus* AZ palaeofauna of latest Permian Changhsingian age (~253 to 252 Ma) (Rubidge et al., 2013, Gastaldo et al., 2020). This sequence is associated with floodplain conditions changing from high water tables with scattered ponds and lakes to well-drained and seasonally dry, consequently this initiated a faunal turnover (Viglietti et al., 2018) that was to culminate in the End-Permian mass extinction. (Viglietti et al., 2018). Brinkman et al. (2007) hypothesized that the appearance of monotaxic bonebeds in the fossil record suggests stressed palaeoenvironmental conditions. For example, Turnbull and Martill (1988) interpreted a monospecific assemblage of *Titanothere mesatirhinus* as a herd killed by a flood event. It is here proposed that the gregarious behaviour represented by this bonebed may have been partially influenced by these changing environmental conditions. Drought events may cause the reptiles to aggregate underground to combat heat and humidity crises. It is also well documented that larger anima*ls* congregate near or around a resource such as water or food *(Shipman, 1975). A monotaxic* hadrosaur bonebed was interpreted as a drought afflicted assemblage due to the abundant representation of juveniles (Rogers, 1990). However, it is unlikely that the shrinking waterhole scenario accounted for the genesis of SAM-PK-K11289 monospecific bonebed. There have been multiple reports of Karoo tetrapods forming behavioural aggregations during and after mass extinction events. Subadult *Lystrosaurus* carcasses were reported in the earliest Triassic behaviourally aggregating around a shrinking pond (Smith et al., 2009a) as well as in underground burrows (Smith et al 2022). *Lystrosaurus* is a much larger animal and is therapsid rather than parareptile however there are some points of comparison between their bonebeds in that they were both monotaxic and both generally disarticulated and form a chaotic melange of bone-on-bone. Species of *Lystrosaurus* and *Saurodektes kitchingorum* both have behaviourally aggregated juveniles within underground burrows during the time that environemental conditiona

are stressed. This strongly suggests that this behaviour likely contributed to their prolonged survival. The scenario presented by these two bonebeds are parallel to what is observed in SAMPK-K11289 such that it may be suggested that *Owenetta* too developed these aggregations for the same reason, which is prolonged survival in stressed environmental conditions. The evidence for a behaviourally driven aggregation for bonebed SAM-PK-K11289 specimen is the strongest, suggesting that juvenile *Owenetta rubidgei* formed relatively large aggregations of at least 31 individuals in underground burrows likely for thermo-regulation and humidity control.

Site of death and burial, Evidence for burial at site of death

The bones in the bonebed are all lining a small shallow depression with more closely packed bone-on-bone and lying horizontally at the base and more spread apart at higher angles towards the top (dorsally). Transportation by a water current tends to disperse, rather than concentrate, such tiny bones. Transport by a water current also transfers some form of hydraulic sorting, for which there is no evidence in the bonebed. The underrepresentation of ribs and girdle elements in the bonebed is likely due to the fact that the individuals were juveniles and these elements were not fully ossified when they died, making them inconspicuous. The bonebed has no other clasts other than bones coming from 31 *Owenetta* skeletons. Transportation will accumulate any material along its path, possibly including other clasts such as small pebbles, remains of plants, or aquatic vertebrates, and will not be taxon- and age-specific. This bonebed is entirely consistent with the passive death of juveniles in a confined space, possibly underground or beneath vegetation.

The fractures observed on the bones are consistent with trampling by small vertebrates and compression due to sedimentation. This is likely what contributed to disarticulation and disturbance in bonebed SAM-PK-K11289. If bonebed SAM-PKK11289 represents a communal nest site, then is possible that *Owenetta* itself damaged the bones while reoccupying the site. SAM-PK-K11289 does not exhibit the undisturbed and life-like articulation style observed in SAM-PK-K7710 and SAMPK-K8305. Rapid burial would have resulted in individuals being spatially

organised in their behavioural disposition commonly, subparallel and in dorsal up attitude (see Figure 1). In this case then skeletons have been disturbed before and/or during burial. Bonebed SAM-PK-K11289 was exposed to subaerial conditions before and during burial. This is evidenced by the preponderance of weathering stage 2 outlined by Ryan et al. (2001). The skeletal elements have compression and transverse fractures. These fractures observed on the bone surface are due to compression during burial. None of the fractures observed exhibit healing, highly suggesting that they occurred after the individuals had perished. Pedal phalanges are found in articulation or strong association. This is also observed in some drought induced assemblages from the late Miocene (Martín-Perea et al., 2021), suggesting high temperatures. This suggests that during decay the pedal phalanges remained in articulation because of the presence of strong connective tissue and possible desiccated skin. The apparent loss of what should have been countless ribs from the bonebed is puzzling considering equally gracile elements such as phalanges are well represented. Some bones potentially identified as ribs have been located and they are lying in parallel as in life (Figures 26 and 27) However, it is possible that at the juvenile stage the ribs were only partially ossified, and thus prone to disintegration during decomposition rendering them unidentifiable in the resultant bone hash at the base of the bonebed.

The sequence of events in the taphonomic pathway

The bonebed of 31 juvenile *Owenetta* individuals originated from a social behaviour. Indicated by the presence of a single taxon and single age class. The individuals most likely came from different sets of parents, suggested by the MNI greatly exceeding expected brood size for living squamates with similar body sizes.

The individuals in the bonebed died within a short space of time possibly from heat stress ssociated with environmental changes during the early extinction phase of the end-Permian mass extinction in the Karoo Basin. The bonebed decomposed and disarticulated within a relatively confined space such as a burrow or shelter structure. It is plausible that this bonebed represents a communal nesting site, and if so it is likely that the disarticulation and disturbance of bones was a result of

subsequent generations of *Owenetta* reoccupying the site. However, some of the distortion observed can confidently be attributed to sedimentation processes. Prior to burial the bonebed was exposed to subaerial conditions and desiccation, during which time the skeletons were further disturbed but not significantly broken. I hypothesize that this exposure period was relatively short, otherwise elements would have been displaced, especially delicate ones such as the phalanges.

Wind or a gentle water flow from the floodplain surface deposited silt that buried the bone accumulation. The deposition of silt onto the bone accumulation during initial burial is responsible for some of the fractures observed on the bone. Paedogenic precipitation of microcrystalline calcite occurred in the “decomposition halo” around the buried bonebed. The micrite cementation around and within the bonebed minimised further crushing and compaction of bone during deeper burial. The preferential precipitation of micrite also ensured that the entire bonebed stayed intact through recent natural exhumation and weathering with a short distance transport along the rock bed gully of an ephermeral stream.

Aggregations of *Owenetta* and other reptiles in the fossil record

Owenetta has never been explicitly described as gregarious, however there are multiple reports of *Owenetta* in aggregations, where some of these aggregations are monotaxic and others involve other taxa. BP/1/4195 is an aggregation of two *Owenetta* individuals that are behaviourally aligned, although not described as an aggregation this may have well been the first report of gregariousness in *Owenetta* (Reisz and Scott, 2002). Official reports of *Owenetta* aggregating with other taxa have been reported. Abdala et al. (2006) reported an aggregation of *Galesaurus* and *Owenetta kitchingorum* (now *Saurodektes kitchingorum*) alluding to a shelter sharing scenario. Even though not interpreted as a behavioural association, Groenewald et al. (2023) also reported an association between *Owenetta kitchingorum* and fossil millipedes. This description of bonebed SAM-PK-K11289 is the first official report of a monotaxic aggregation of *Owenetta*. Reports of monospecific microvertebrate aggregations of other reptile taxa have been made but none present this large number of individuals. Bonebed SAM-PK-K7710 includes only 5 individuals.

Bonebed SAM-PK-K8305 too includes only 5 individuals (refer to Figure 1). There are a minimum of 31 individuals in this bonebed which is the largest number of *Owenetta* found together to date.

Does the juvenile aggregation of SAM-PK-K11289 provide evidence for sociality in owenettids?

Juvenile aggregation SAM-PK-K11289 presents compelling evidence for sociality in owenettids. The monospecificity of the bone bed and its single age class indicates a very deliberate accumulation mechanism. This pattern is only observed in biogenetic concentrations. Although *Owenetta* is not explicitly reported in literature as gregarious, it has been found in monotaxic and multitaxic associations. The evolution of social aggregations during stressed environmental conditions is not unusual. Bonebed SAMPK-K11289 fall within the concomitant climatic warming and drying heralding the onset of the End-Permian mass extinction. This behaviour likely possessed an adaptive value as it is observed in other taxa from overlying strata. There is not sufficient evidence for scatological origins or fluvial processes. Sociality is observed in extant reptiles therefore it is highly possible that it might have been present in ancient diminutive parareptiles.

Juvenile aggregations as an indicator of sociality

Sociality is a behaviour that occurs when two or more individuals of the same species interact with one another (Allaby, 2014). Aggregations are thought to have first appeared 517 million years ago in vertebrates (Burrow and Turner, 2012), and possibly even earlier in other life forms. Hsieh and Plotnick (2020) noted that some of the oldest examples of fossil aggregations depicting some form of sociality date as far back as the Ordovician and possibly the Cambrian (Purcell and Kitting, 1982, Fortey and Hughes, 1998, Droser and Gehling, 2008, Hou et al., 2008, Carbone and Narbonne, 2014, Caron and Vannier, 2016, Fu et al., 2018, Mizumoto et al., 2019). The interpretation of this *Owenetta* bonebed provides evidence that supports that sociality existed well before the branching of crown diapsids. Social aggregations are a common occurrence in modern animals. Social aggregations are a common

occurrence in modern animals. For example, newborn Timber rattlesnakes (*Crotalus horridus)* are often observed in communal dens (Schuett et al., 2016). Mixed species aggregations are observed in large African herbivores and birds (Morse, 1970, Montgomery, 1981, Stears et al., 2020, Saltz et al., 2023). The configuration of aggregations ranges from random to organized (Gardner et al., 2016), with some species aggregating opportunistically, and others forming lifelong aggregations with consistent and permanent members. The number of individuals within an aggregation can range from ten to a million (Parrish and Edelstein-Keshet, 1999). Aggregations can occur between members of the same species and across members of different species. Bonebed SAM-PK-K11289 is strictly organized in terms of the taxon and ontogeny. It is an aggregation between members of the same species and ontogeny.

Sociality in extant relatives

Research on extant reptiles reveals that they have an advanced sensory system that is equipped with the necessary tools to perform social behaviours (Doody et al., 2021). It has also revealed that reptiles exhibit a diverse range of social repertoires. For instance, lizards alone exhibit both simple forms of sociality such as monogamy and more complex forms such as permanent group living (see Figure 37 range of sociality in reptiles). This makes them the perfect candidates for modelling transitions of social behaviours from simple to more complex forms and understanding the overall evolution of sociality (Whiting and While, 2017). *Ergenia* lizards form complex social structures and some species of this genus exhibit family structures. This structure includes adult male and adult female tending to their offspring. This is observed in other organisms such as birds but is quite unusual for reptiles (O'connor and Shine, 2003). Eastern garter snakes purposefully seek social interactions and will form part of large social aggregation with non-random consistent individuals (Skinner and Miller, 2020). This configuration is consistent with what is observed in bonebed SAM-PK-K11289.

A review by Doody et al. (2009) reports that communal nesting is observed in 258 species of extant reptile lizards, 52 species of snakes, 30 turtle species, 6

crocodilian species and the tuatara. These communal nests usually occur in a network of nests, a crevice, a hole, or under the shelter of an object. SAM-PK-K11289 assumes that spatial organization that it typical of a communal nest. This coupled with the population configuration highly suggests that bonebed SAM-PK-K11289 might have been a communal nest. I hypothesize that SAM-PK-K11289 likely represents what is exemplified in living skinks. The individuals in SAM-PK-K11289 nested communally in a substrate depression, protected by some objects, possibly the vegetation on the floodplain of the meandering river (Doody et al., 2021).

Figure 37: Examples of sociality in extant reptiles.

(A) Arizona black rattlesnake (*Crotalus cerberus*) social aggregation photograph taken by Jeff Smith, (B) Group living in Cunningham's skinks (*Ergenia cunninghami*) (Watson and Watson, 2020), (C) Adult Cunningham's skink (*Ergenia cunninghami*) with offspring -resembling parental care (Watson et al., 2020), and (D), Family living in *Egernia* lizards (*Ergenia saxatilis*) (O'connor and Shine, 2003). Pictures are not scaled.

CONCLUSION

Bonebed SAM-PK-K11289 from the latest Permian rocks of the South African Karoo is a mono-specific juvenile aggregation of *Owenetta rubidgei*. Mechanical preparation and synchrotron X-ray tomography reveal that the bonebed contains skeletal remains of 31 juvenile individuals of *Owenetta rubidgei.* This is the largest aggregation of this taxon found to date. This aggregation was behaviourally generated probably in a sheltered structure such as an underground depression and shared some characteristics with drought-induced bonebeds recovered from the overlying Early Triassic strata. Between death, possibly from heat stress, and final burial the exposed skeletons were desiccated and disturbed but not transported. Trampling by small tetrapods and sedimentation are the most probable agents of the observed disarticulation patterns. The concomitant climatic warming and drying heralding the onset of the End-Permian mass extinction were likely the environmental drivers of this underground aggregation behaviour. Such aggregation of this nature are observed in other taxa in similar environmental conditions. Juveniles of this aggregation were most likely from different sets of parents living in the vicinity or sharing nesting sites, thus *Owenetta rubidgei* is exhibiting a form of sociality common in lizard species today. Configuration and organisation of aggregation is consistent with communal nests observed in extant taxa.

REFERENCES

ABDALA, F., CISNEROS, J. C. & SMITH, R. M. 2006. Faunal aggregation in the Early Triassic Karoo Basin: earliest evidence of shelter-sharing behavior among tetrapods? *Palaios,* 21**,** 507-512.

ALLABY, M. 2014. *A Dictionary of Zoology*, Oxford University Press.

ALLULEE, J. L. & HOLLAND, S. M. 2005. The sequence stratigraphic and environmental context of primitive vertebrates: Harding Sandstone, Upper Ordovician, Colorado, USA. *Palaios,* 20**,** 518-533.

ANDERSON, J. F., HALL-MARTIN, A. & RUSSELL, D. A. 1985. Long-bone circumference and weight in mammals, birds and dinosaurs. *Journal of Zoology,* 207**,** 53-61.

ANDREWS, P. & EVANS, E. M. N. 1983. Small mammal bone accumulations produced by mammalian carnivores. *Paleobiology,* 9**,** 289 - 307.

AR, A. & YOM-TOV, Y. 1978. The evolution of parental care in birds. *Evolution***,** 655-669.

BADGLEY, C. 1986. Counting individuals in mammalian fossil assemblages from fluvial environments. *Palaios***,** 328-338.

BAJDEK, P., OWOCKI, K., SENNIKOV, A. G., GOLUBEV, V. K. & NIEDŹWIEDZKI, G. 2017. Residues from the Upper Permian carnivore coprolites from Vyazniki in Russia-key questions in reconstruction of feeding habits. *Palaeogeography, Palaeoclimatology, Palaeoecology,* 482**,** 70-82.

BALSHINE, S. 2012. Patterns of parental care in vertebrates. *The evolution of parental care,* 62**,** 80.

BARNARD, C. 2007. Ethical regulation and animal science: why animal behaviour is special. *Animal Behaviour,* 74**,** 5-13.

BARNARD, C. J. 2012. *Animal behaviour: ecology and evolution*, Springer Science & Business Media.

BEHRE, C. H. & JOHNSON, J. H. 1933. Ordovician and Devonian fish horizons in Colorado. *American Journal of Science,* 5**,** 477-486.

BEHRENSMEYER, A. K. 1978. Taphonomic and ecologic information from bone weathering. *Paleobiology,* 4**,** 150-162.

BEHRENSMEYER, A. K. 2007. Bonebeds through time. *Bonebeds: Genesis, analysis, and paleobiological significance***,** 65-101.

BELL, P. R. & CAMPIONE, N. E. 2014. Taphonomy of the Danek Bonebed: a monodominant Edmontosaurus (Hadrosauridae) bonebed from the Horseshoe Canyon Formation, Alberta. *Canadian Journal of Earth Sciences,* 51**,** 992-1006.

BENOIT, J. 2023. Synchrotron scanning reveals the deep evolutionary root of the mammalian brain: The surprisingly advanced endocast morphology of *Lumkuia fuzzi* (Cynodontia: Probainognathia). *Palaeontologica Africana,* 56**,** 103-110.

BENOIT, J., ANGIELCZYK, K. D., MIYAMAE, J. A., MANGER, P., FERNANDEZ, V. & RUBIDGE, B. 2018. Evolution of facial innervation in anomodont therapsids (Synapsida): Insights from X-ray computerized microtomography. *Journal of Morphology,* 279**,** 673-701.

BENOIT, J., MANGER, P. & RUBIDGE, B. 2016. Palaeoneurological clues to the evolution of defining mammalian soft tissue traits. *Scientific reports,* 6**,** 25604.

BENOIT, J., RUF, I., MIYAMAE, J. A., FERNANDEZ, V., RODRIGUES, P. G. & RUBIDGE, B. S. 2020. The evolution of the maxillary canal in Probainognathia (Cynodontia, Synapsida): reassessment of the homology of

the infraorbital foramen in mammalian ancestors. *Journal of Mammalian Evolution,* 27**,** 329-348.

BENSON, R. B., CAMPIONE, N. E., CARRANO, M. T., MANNION, P. D., SULLIVAN, C., UPCHURCH, P. & EVANS, D. C. 2014. Rates of dinosaur body mass evolution indicate 170 million years of sustained ecological innovation on the avian stem lineage. *PLoS Biology,* 12**,** e1001853.

BENTON, M. J. 2010. Studying function and behavior in the fossil record. *PLoS biology,* 8**,** e1000321.

BENTON, M. J. & TWITCHETT, R. J. 2003. How to kill (almost) all life: the end-Permian extinction event. *Trends in Ecology & Evolution,* 18**,** 358-365.

BINFORD, L. 1981. Patterns of bone modifications produced by nonhuman agents. *Bones: Ancient Men and Modern Myths: Academic Press, New York***,** 35-86.

BLACKBURN, T. M. & GASTON, K. J. 1994. Animal body size distributions: patterns, mechanisms and implications. *Trends in Ecology & Evolution,* 59**,** 471-474.

BLACKBURN, T. M., HARVEY, P. H. & PAGEL, M. D. 1990. Species number, population density and body size relationships in natural communities. *The Journal of Animal Ecology,* 59**,** 335-345.

BLOB, R. W., BADGLEY, C., ROGERS, R., EBERTH, D. & FIORILLO, A. 2007. Numerical methods for bonebed analysis. *Bonebeds: genesis, analysis, and paleobiological significance***,** 333-396.

BLUMER, L. S. 1979. Male Parental Care in the Bony Fishes. *The Quarterly Review of Biology,* 54**,** 149 - 161.

BLUMER, L. S. 1982. A bibliography and categorization of bony fishes exhibiting parental care. *Zoological Journal of the Linnean Society,* 75**,** 1-22.

BONNET, X., SHINE, R. & LOURDAIS, O. 2002. Taxonomic chauvinism. *Trends in Ecology & Evolution,* 17**,** 1-3.

BOTHA, J., MODESTO, S. P. & SMITH, R. M. 2007. Extended procolophonoid reptile survivorship after the end-Permian extinction. *South African Journal of Science,* 103**,** 54-56.

BOTHA-BRINK, J. & MODESTO, S. P. 2009. Anatomy and relationships of the Middle Permian varanopid *Heleosaurus scholtzi* based on a social aggregation from the Karoo Basin of South Africa. *Journal of Vertebrate Paleontology,* 29**,** 389-400.

BRANDT, D. S. 1989. Taphonomic grades as a classification for fossiliferous assemblages and implications for paleoecology. *Palaios,* 4

, 303-309.

BRASSEY, C. A. 2016. Body-mass estimation in paleontology: a review of volumetric techniques. *The Paleontological Society Papers,* 22**,** 133-156.

BRINK, A. 1954. Thrinaxodon and some other Lystrosaurus Zone Cynodonts in the Collection ofThe National Museum, Bloemfontein. *Navorsinge van die Nasionale Museum: Researches of the National Museum,* 1**,** 115-125.

BRINKMAN, D. B., EBERTH, D. A., CURRIE, P. J., ROGERS, R. & FIORILLO, A. 2007. From bonebeds to paleobiology: applications of bonebed data. *Bonebeds: genesis, analysis, and paleobiological significance***,** 221-263.

BROOM, R. 1939. A new type of cotylosaurian, *Owenetta rubidgei*. *Annals of the Transvaal Museum,* 19**,** 319-321.

BROWN, J. H., MARQUET, P. A. & TAPER, M. L. 1993. Evolution of body size: consequences of an energetic definition of fitness. *The American Naturalist,* 142**,** 573-584.

BURNESS, G. P., DIAMOND, J. & FLANNERY, T. 2001. Dinosaurs, dragons, and dwarfs: the evolution of maximal body size. *Proceedings of the National Academy of Sciences,* 98**,** 14518-14523.

BURROW, C. J. & TURNER, S. 2012. Fossil fish taphonomy and the contribution of microfossils in documenting Devonian vertebrate history, Springer

CAMPBELL, K. E. & MARCUS, L. 1992. The relationship of hindlimb bone dimensions to body weight in birds. *Natural History Museum of Los Angeles County Science Series,* 36**,** 395-412.

CAMPIONE, N. E. & EVANS, D. C. 2012. A universal scaling relationship between body mass and proximal limb bone dimensions in quadrupedal terrestrial tetrapods. *BMC biology,* 10**,** 1-22.

CAMPIONE, N. E. & EVANS, D. C. 2020. The accuracy and precision of body mass estimation in non-avian dinosaurs. *Biological Reviews,* 95**,** 1759-1797.

CAMPIONE, N. E., EVANS, D. C., BROWN, C. M. & CARRANO, M. T. 2014. Body mass estimation in non-avian bipeds using a theoretical conversion to quadruped stylopodial proportions. *Methods in Ecology and Evolution,* 5**,** 913-923.

CARBONE, C. & NARBONNE, G. M. 2014. When life got smart: the evolution of behavioral complexity through the Ediacaran and early Cambrian of NW Canada. *Journal of Paleontology,* 88**,** 309-330.

CARON, J.-B. & VANNIER, J. 2016. Waptia and the diversification of brood care in early arthropods. *Current Biology,* 26**,** 69-74.

CATUNEANU, O., WILLIS, A. J. & MIALL, A. D. 1998. Temporal significance of sequence boundaries. *Sedimentary Geology,* 121**,** 157-178.

CATUNEANU, O., WOPFNER, H., ERIKSSON, P., CAIRNCROSS, B., RUBIDGE, B., SMITH, R. & HANCOX, P. 2005. The Karoo basins of south-central Africa. *Journal of African Earth Sciences,* 43**,** 211-253.

CISNEROS, J. C., DAMIANI, R., SCHULTZ, C., DA ROSA, A., SCHWANKE, C., NETO, L. W. & AURÉLIO, P. L. 2004. A procolophonoid reptile with temporal fenestration from the Middle Triassic of Brazil. *Proceedings of the Royal Society of London. Series B: Biological Sciences,* 271**,** 1541-1546.

CISNEROS, J. C., RUBIDGE, B. S., MASON, R. & DUBE, C. 2008. Analysis of millerettid parareptile relationships in the light of new material of *Broomia perplexa Watson*, 1914, from the Permian of South Africa. *Journal of Systematic Palaeontology,* 6**,** 453-462.

CISNEROS, J. C. & RUTA, M. 2010. Morphological diversity and biogeography of procolophonids (Amniota: Parareptilia). *Journal of Systematic Palaeontology,* 8**,** 607-625.

CLOETENS, P., BARRETT, R., BARUCHEL, J., GUIGAY, J.-P. & SCHLENKER, M. 1996. Phase objects in synchrotron radiation hard x-ray imaging. *Journal of physics D: applied physics,* 29**,** 133.

CLUTTON-BROCK, T. H. 1991. *The evolution of parental care*, Princeton University Press.

COLE, D. Evolution and development of the Karoo Basin. Conference on inversion tectonics of the Cape Fold Belt, 1992. 87-99.

COOMBS, W. P. 1982. Juvenile specimens of the ornithischian dinosaur *Psittacosaurus*.

CURRIE, D. J. 1993. What shape is the relationship between body size and population density? *Oikos***,** 353-358.

DARWIN, C. 1965. The expression of the emotions in man and animals University of Chicago press.

DARWIN, C. & QUAMMEN, D. 2008. *On the Origin of Species:\the Illustrated Edition*, ICON Group International.

DAVIDOWITZ, G. & NIJHOUT, H. F. 2004. The physiological basis of reaction norms: the interaction among growth rate, the duration of growth and body size. *Integrative and Comparative Biology,* 44**,** 443-449.

DAVIES, N. B., KREBS, J. R. & WEST, S. A. 2012. An introduction to behavioural ecology, John Wiley & Sons.

DAWKINS, M. S. 2003. Behaviour as a tool in the assessment of animal welfare. *Zoology,* 106**,** 383-387.

DE ESTEBAN-TRIVIGNO, S., MENDOZA, M. & DE RENZI, M. 2008. Body mass estimation in Xenarthra: a predictive equation suitable for all quadrupedal terrestrial placentals? *Journal of Morphology,* 269**,** 1276-1293.

DEBRAGA, M. & REISZ, R. R. 1996. The Early Permian reptile *Acleistorhinus pteroticus* and its phylogenetic position. *Journal of Vertebrate Paleontology,* 16**,** 384-395.

DODSON, P. & WEXLAR, D. 1979. Taphonomic investigations of owl pellets. *Paleobiology,* 5**,** 275 - 284.

DOODY, J. S., BURGHARDT, G. M. & DINETS, V. 2013. Breaking the social–non-social dichotomy: a role for reptiles in vertebrate social behavior research? *Ethology,* 119**,** 95-103.

DOODY, J. S., DINETS, V. & BURGHARDT, G. M. 2021. The secret social lives of reptiles, JHU Press.

DOODY, J. S., FREEDBERG, S. & KEOGH, J. S. 2009. Communal egg-laying in reptiles and amphibians: evolutionary patterns and hypotheses. *The Quarterly review of biology,* 84**,** 229-252.

DROSER, M. L. & GEHLING, J. G. 2008. Synchronous aggregate growth in an abundant new Ediacaran tubular organism. *Science,* 319**,** 1660-1662.

EBERTH, D. A. & CURRIE, P. J. 2010. Stratigraphy, sedimentology, and taphonomy of the Albertosaurus bonebed (upper Horseshoe Canyon Formation; Maastrichtian), southern Alberta, CanadaThis article is one of a series of papers published in this Special Issue on the theme *Albertosaurus*. *Canadian Journal of Earth Sciences,* 47**,** 1119-1143.

EBERTH, D. A., ROGERS, R. R., FIORILLO, A. R., ROGERS, R., EBERTH, D. & FIORILLO, A. 2007. A practical approach to the study of bonebeds. *Bonebeds: genesis, analysis, and paleobiological significance***,** 265-331.

EBERTH, D. A., SHANNON, M. & NOLAND, B. G. 2010. A Bonebeds Database: Classification, Biases, and Patterns of Occurrence. *Bonebeds: Genesis, analysis, and paleobiological significance***,** 103.

EFREMOV, J. 1940. Taphonomy: a new branch of paleontology: Pan-American Geologist, v. 74.

ELLIOTT, J. & HURLEY, M. 1995. The functional relationship between body size and growth rate in fish. *Functional Ecology***,** 625-627.

ERWIN, D. 1990. The end-Permian mass extinction. *Annual Review of Ecology and Systematics,* 21**,** 69-91.

ERWIN, D. H. 2015. *Extinction: How Life on Earth Nearly Ended 250 Million Years Ago-Updated Edition*, Princeton University Press.

EVANS, D. C., BAVINGTON, R. & CAMPIONE, N. E. 2009. An unusual hadrosaurid braincase from the Dinosaur Park Formation and the biostratigraphy of *Parasaurolophus* (Ornithischia: Lambeosaurinae) from southern Alberta. *Canadian Journal of Earth Sciences,* 46**,** 791-800.

EVANS, S. E. 1987. The braincase of *Youngina capensis* (Reptilia: Diapsida; Permian). *Neues Jahrbuch für Geologie und Paläontologie-Monatshefte***,** 193-203.

FERNANDEZ, V., ABDALA, F., CARLSON, K. J., COOK, D. C., RUBIDGE, B. S., YATES, A. & TAFFOREAU, P. 2013. Synchrotron reveals Early Triassic odd couple: injured amphibian and aestivating therapsid share burrow. *PLoS One,* 8**,** e64978.

FERNÁNDEZ-JALVO, Y., SCOTT, L. & ANDREWS, P. 2011. Taphonomy in palaeoecological interpretations. *Quaternary Science Reviews,* 30**,** 1296-1302.

FINARELLI, J. A. & FLYNN, J. J. 2006. Ancestral state reconstruction of body size in the Caniformia (Carnivora, Mammalia): the effects of incorporating data from the fossil record. *Systematic Biology,* 55**,** 301-313.

FIORILLO, A. R. 1988. Taphonomy of Hazard Homestead Quarry (Ogallala Group), Hitchcock County, Nebraska. *Rocky Mountain Geology,* 26**,** 57-97.

FOLLAND, J. P., MC CAULEY, T. M. & WILLIAMS, A. G. 2008. Allometric scaling of strength measurements to body size. *European journal of applied physiology,* 102**,** 739-745.

FORTEY, R. A. & HUGHES, N. C. 1998. Brood pouches in trilobites. *Journal of Paleontology,* 72**,** 638-649.

FRANK, S. A. 2007. All of life is social. *Current Biology,* 17**,** R648-R650.

FRASER, D. 2009. Animal behaviour, animal welfare and the scientific study of affect. *Applied Animal Behaviour Science,* 118**,** 108-117.

FU, D., ORTEGA-HERNÁNDEZ, J., DALEY, A. C., ZHANG, X. & SHU, D. 2018. Anamorphic development and extended parental care in a 520 million-year-old stem-group euarthropod from China. *BMC Evolutionary Biology,* 18**,** 1-17.

GANGLOFF, R. A. & FIORILLO, A. R. 2010. Taphonomy and paleoecology of a bonebed from the Prince Creek Formation, North Slope, Alaska. *Palaios,* 25**,** 299-317.

GARDNER, M., BULL, C., COOPER, S. & DUFFIELD, G. 2001. Genetic evidence for a family structure in stable social aggregations of the Australian lizard Egernia stokesii. *Molecular Ecology,* 10**,** 175-183.

GARDNER, M. G., PEARSON, S. K., JOHNSTON, G. R. & SCHWARZ, M. P. 2016. Group living in squamate reptiles: a review of evidence for stable aggregations. *Biological Reviews,* 91**,** 925-936.

GARDNER, N. M., HOLLIDAY, C. M. & O'KEEFE, F. R. 2010. The braincase of *Youngina capensis* (Reptilia, Diapsida): new insights from high-resolution CT scanning of the holotype.

GASTALDO, R. A., KAMO, S. L., NEVELING, J., GEISSMAN, J. W., LOOY, C. V. & MARTINI, A. M. 2020. The base of the *Lystrosaurus* Assemblage Zone, Karoo Basin, predates the end-Permian marine extinction. *Nature Communications,* 11**,** 1428.

GASTON, K. J. 1992. Taxonomy of taxonomists. *Nature,* 356**,** 281-282.

GILLOOLY, J. F., BROWN, J. H., WEST, G. B., SAVAGE, V. M. & CHARNOV, E. L. 2001. Effects of size and temperature on metabolic rate. *science,* 293**,** 2248-2251.

GINGERICH, P. D. 1990. Prediction of body mass in mammalian species from long bone lengths and diameters. 28**,** 72-92.

GOODRICH, E. 1942. The hind foot of *Youngina* and fifth metatarsal in Reptilia. *Journal of Anatomy,* 76**,** 308.

GOW, C. 1972. The osteology and relationships of the Millerettidae (Reptilia: Cotylosauria). *Journal of Zoology,* 167**,** 219-264.

GOW, C. E. & RUBIDGE, B. S. 1997. The oldest Procolophonoid (Amniota: Parareptilia)-New discovery from the lower Beaufort of South Africa. *Palaentologica africana*

, 34**,** 49-53.

GREGGOR, A. L., BERGER-TAL, O., BLUMSTEIN, D. T., ANGELONI, L., BESSA-GOMES, C., BLACKWELL, B. F., ST CLAIR, C. C., CROOKS, K., DE SILVA, S. & FERNÁNDEZ-JURICIC, E. 2016. Research priorities from animal behaviour for maximising conservation progress. *Trends in ecology & evolution,* 31**,** 953-964.

GROENEWALD, D. P., BOTHA, J. & SMITH, R. M. 2023. Fossil millipedes associated with articulated tetrapod skeletons in the Early Triassic Karoo Basin, South Africa. *Palaeogeography, Palaeoclimatology, Palaeoecology,* 617**,** 111508.

GUBERNICK, D. J. 2013. *Parental care in mammals*, Springer Science & Business Media.

HAFEZ, B. & HAFEZ, E. 2000. Reproductive behavior. *Reproduction in farm animals***,** 291-306.

HAMLEY, T., CISNEROS, J. C. & DAMIANI, R. 2021. A procolophonid reptile from the Lower Triassic of Australia. *Zoological Journal of the Linnean Society,* 192**,** 554-609.

HANCOX, P. & RUBIDGE, B. 2001. Breakthroughs in the biodiversity, biogeography, biostratigraphy, and basin analysis of the Beaufort Group. *Journal of African Earth Sciences,* 33**,** 563-577.

HONĚK, A. 1993. Intraspecific variation in body size and fecundity in insects: a general relationship. *Oikos,* 66**,** 483-492.

HOU, X.-G., SIVETER, D. J., ALDRIDGE, R. J. & SIVETER, D. J. 2008. Collective behavior in an early Cambrian arthropod. *Science,* 322**,** 224-224.

HSIEH, S. & PLOTNICK, R. E. 2020. The representation of animal behaviour in the fossil record. *Animal Behaviour,* 169**,** 65-80.

HUNT, A. K., FORD, D. P., FERNANDEZ, V., CHOINIERE, J. N. & BENSON, R. B. 2023. A description of the palate and mandible of *Youngina* capensis (Sauropsida, Diapsida) based on synchrotron tomography, and the phylogenetic implications. *Papers in Palaeontology,* 9**,** e1521.

IBIRICU, L. M., MARTINEZ, R. D., CASAL, G. A. & CERDA, I. A. 2013. The behavioral implications of a multi-individual bonebed of a small theropod dinosaur. *PLoS One,* 8**,** e64253.

J. SEAN DOODY, B., STEVE FREEDBERG & J. SCOTT KEOGH 2009. Communal Egg-Laying in Reptiles and Amphibians: Evolutionary Patterns and Hypotheses. *The Quarterly Review of Biology,* 84**,** 229-252.

JANAWAY, R. C., PERCIVAL, S. L. & WILSON, A. S. 2009. Decomposition of human remains. *Microbiology and aging: clinical manifestations***,** 313-334.

JASINOSKI, S. C. & ABDALA, F. 2017. Aggregations and parental care in the Early Triassic basal cynodonts Galesaurus planiceps and *Thrinaxodon liorhinus*. *PeerJ,* 5**,** e2875.

JOHNSON, M., VAN VUUREN, C., VISSER, J., COLE, D., WICKENS, H. D. V., CHRISTIE, A. & ROBERTS, D. 1997. The Foreland Karoo Basin, South Africa. *Sedimentary basins of the world.* Elsevier.

JOHNSON, M. R. 1976. Stratigraphy and sedimentology of the Cape and Karoo sequences in the Eastern Cape Province.

KAMIL, A. C., KREBS, J. R. & PULLIAM, H. R. 2012. *Foraging behavior*, Springer Science & Business Media.

KLEIBER, M. 1947. Body size and metabolic rate. *Physiological reviews,* 27**,** 511-541.

KORTH, W. W. 1979. Taphonomy of microvertebrate fossil assemblages.

KOZŁOWSKI, J., KONARZEWSKI, M. & CZARNOLESKI, M. 2020. Coevolution of body size and metabolic rate in vertebrates: a life-history perspective. *Biological Reviews,* 95**,** 1393-1417.

LAFFERTY, K. D. & KURIS, A. M. 2002. Trophic strategies, animal diversity and body size. *Trends in Ecology & Evolution,* 17**,** 507-513.

LAWRENCE, D. R. 1968. Taphonomy and information losses in fossil communities. *Geological Society of America Bulletin,* 79**,** 1315-1330.

LEEDMAN, A. & MAGRATH, R. D. 2003. Long-term brood division and exclusive parental care in a cooperatively breeding passerine. *Animal Behaviour,* 65**,** 1093-1108.

LYCKEGAARD, A., JOHNSON, G. & TAFFOREAU, P. 2011. Correction of ring artifacts in X-ray tomographic images. *Int J Tomogr Stat,* 18**,** 1-9.

LYMAN, R. L. 1994. *Vertebrate taphonomy*, Cambridge University Press.

MARQUET, P. A., NAVARRETE, S. A. & CASTILLA, J. C. 1995. Body size, population density, and the energetic equivalence rule. *Journal of Animal Ecology*, 325-332.

MARTIN, A. P. & PALUMBI, S. R. 1993. Body size, metabolic rate, generation time, and the molecular clock. *Proceedings of the National Academy of Sciences,* 90, 4087-4091.

MARTÍN-PEREA, D. M., MORALES, J., CANTERO, E., COURTENAY, L. A., HERNÁNDEZ FERNÁNDEZ, M. & DOMINGO, M. S. 2021. Taphonomic analysis of Batallones-10, a Late Miocene drought-induced mammalian assemblage (Madrid basin, Spain) within the Cerro de los Batallones complex. *Palaeogeography, Palaeoclimatology, Palaeoecology,* 578, 110576.

MAYHEW, D. F. 2008. Avian predators as accumulators of fossil mammal material. *Boreas,* 6, 25-31.

MEIRI, S., AVILA, L., BAUER, A. M., CHAPPLE, D. G., DAS, I., DOAN, T. M., DOUGHTY, P., ELLIS, R., GRISMER, L., KRAUS, F., MORANDO, M., OLIVER, P., PINCHEIRA-DONOSO, D., RIBEIRO-JUNIOR, M. A., SHEA, G., TORRES-CARVAJAL, O., SLAVENKO, A. & ROLL, U. 2020. The global diversity and distribution of lizard clutch sizes. *Global Ecology and Biogeography,* 29, 1515-1530.

MELLETT, J. S. 1974. Scatological origin of microvertebrate fossil accumulations. *Science,* 185, 349-350.

MENG, Q., LIU, J., VARRICCHIO, D. J., HUANG, T. & GAO, C. 2004. Parental care in an ornithischian dinosaur. *Nature,* 431, 145-146.

MERRITT, C. E. 2015. The influence of body size on adult skeletal age estimation methods. *American Journal of Physical Anthropology,* 156**,** 35-57.

MILLIEN, V. & BOVY, H. 2010. When teeth and bones disagree: body mass estimation of a giant extinct rodent. *Journal of Mammalogy,* 91**,** 11-18.

MIRONE, A., BRUN, E., GOUILLART, E., TAFFOREAU, P. & KIEFFER, J. 2014. The PyHST2 hybrid distributed code for high speed tomographic reconstruction with iterative reconstruction and a priori knowledge capabilities. *Nuclear Instruments and Methods in Physics Research Section B: Beam Interactions with Materials and Atoms,* 324**,** 41-48.

MIZUMOTO, N., MIYATA, S. & PRATT, S. C. 2019. Inferring collective behaviour from a fossilized fish shoal. *Proceedings of the Royal Society B,* 286**,** 20190891.

MODESTO, S. & SMITH, R. M. 2001. A new Late Permian captorhinid reptile: a first record from the South African Karoo. *Journal of Vertebrate Paleontology,* 21**,** 405-409.

MODESTO, S. P. & REISZ, R. R. 2008. New material of *Colobomycter pholeter*, a small parareptile from the Lower Permian of Oklahoma. *Journal of Vertebrate Paleontology,* 28**,** 677-684.

MODESTO, S. P., SCOTT, D. M., BOTHA-BRINK, J. & REISZ, R. R. 2010. A new and unusual procolophonid parareptile from the Lower Triassic Katberg Formation of South Africa. *Journal of Vertebrate Paleontology,* 30**,** 715-723.

MONTGOMERY, W. L. 1981. Mixed-species schools and the significance of vertical territories of damselfishes. *Copeia,* 1981**,** 477-481.

MORSE, D. H. 1970. Ecological aspects of some mixed-species foraging flocks of birds. *Ecological monographs,* 40**,** 119-168.

NELSON, X. J. 2014. Animal behavior can inform conservation policy, we just need to get on with the job–or can it?

O'CONNOR, D. & SHINE, R. 2003. Lizards in ‘nuclear families’: a novel reptilian social system in *Egernia saxatilis* (Scincidae). *Molecular Ecology,* 12**,** 743-752.

OKASHA, S. 2003. Biological altruism.

OLSON, E. C. 1936. Notes on the skull of *Youngina capensis* Broom. *The Journal of Geology,* 44**,** 523-533.

ORD, T. J., MARTINS, E. P., THAKUR, S., MANE, K. K. & BÖRNER, K. 2005. Trends in animal behaviour research (1968–2002): ethoinformatics and the mining of library databases. *Animal Behaviour,* 69**,** 1399-1413.

PAGANIN, D., MAYO, S. C., GUREYEV, T. E., MILLER, P. R. & WILKINS, S. W. 2002. Simultaneous phase and amplitude extraction from a single defocused image of a homogeneous object. *Journal of microscopy,* 206**,** 33-40.

PARRISH, J. K. & EDELSTEIN-KESHET, L. 1999. Complexity, pattern, and evolutionary trade-offs in animal aggregation. *Science,* 284**,** 99-101.

PAWAR, S. 2003. Taxonomic chauvinism and the methodologically challenged. *Bioscience,* 53**,** 861-864.

PETERS, R. H. 1986. *The ecological implications of body size*, Cambridge university press.

PIÑEIRO, G., ROJAS, A. & UBILLA, M. 2004. A new procolophonoid (Reptilia, Parareptilia) from the Upper Permian of Uruguay. *Journal of Vertebrate Paleontology,* 24**,** 814-821.

PREZIOSI, R. F., FAIRBAIRN, D. J., ROFF, D. A. & BRENNAN, J. M. 1996. Body size and fecundity in the waterstrider *Aquarius remigis*: a test of Darwin's fecundity advantage hypothesis. *Oecologia,* 108**,** 424-431.

PURCELL, J. E. & KITTING, C. L. 1982. Intraspecific aggression and population distributions of the sea anemone Metridium senile. *The Biological Bulletin,* 162**,** 345-359.

QVARNSTRÖM, M., FIKÁČEK, M., WERNSTRÖM, J. V., HULD, S., BEUTEL, R. G., ARRIAGA-VARELA, E., AHLBERG, P. E. & NIEDŹWIEDZKI, G. 2021. Exceptionally preserved beetles in a Triassic coprolite of putative dinosauriform origin. *Current Biology,* 31**,** 3374-3381. e5.

QVARNSTRÖM, M., NIEDŹWIEDZKI, G., TAFFOREAU, P., ŽIGAITĖ, Ž. & AHLBERG, P. E. 2017. Synchrotron phase-contrast microtomography of coprolites generates novel palaeobiological data. *Scientific Reports,* 7**,** 2723.

QVARNSTRÖM, M., WERNSTRÖM, J. V., PIECHOWSKI, R., TAŁANDA, M., AHLBERG, P. E. & NIEDŹWIEDZKI, G. 2019. Beetle-bearing coprolites possibly reveal the diet of a Late Triassic dinosauriform. *Royal Society Open Science,* 6**,** 181042.

RADDER, R. S. & SHINE, R. 2007. Why do female lizards lay their eggs in communal nests? *Journal of Animal Ecology,* 76**,** 881-7.

REISZ, R. R. & SCOTT, D. 2002. *Owenetta kitchingorum*, sp. nov., a small parareptile (Procolophonia: Owenettidae) from the Lower Triassic of South Africa. *Journal of Vertebrate Paleontology,* 22**,** 244-256.

RETALLACK, G. 1995. Permian-Triassic life crisis on land. *Science,* 267**,** 77-80.

ROGERS, R. & KIDWELL, S. M. 2007. A conceptual framework for the genesis and analysis. *Bonebeds: Genesis, Analysis, and Paleobiological Significance*, 1-63.

ROGERS, R. R. 1990. Taphonomy of three dinosaur bone beds in the Upper Cretaceous Two Medicine Formation of northwestern Montana: evidence for drought-related mortality. *Palaios,* 5, 394-413.

ROGERS, R. R. & BRADY, M. E. 2010. Origins of microfossil bonebeds: insights from the Upper Cretaceous Judith River Formation of north-central Montana. *Paleobiology,* 36, 80-112.

ROGERS, R. R., EBERTH, D. A. & FIORILLO, A. R. 2010. *Bonebeds: genesis, analysis, and paleobiological significance*, University of Chicago Press.

ROGERS, R. R., KIDWELL, S. M., EBERTH, D. A. & FIORILLO, A. R. 2007. A conceptual framework for the genesis and analysis of vertebrate skeletal concentrations. *Bonebeds: Genesis, analysis, and paleobiological significance*, 1-63.

ROMANO, M. & RUBIDGE, B. 2021. First 3D reconstruction and volumetric body mass estimate of the tapinocephalid dinocephalian *Tapinocaninus pamelae* (Synapsida: Therapsida). *Historical Biology,* 33, 498-505.

RUBIDGE, B. S., ERWIN, D. H., RAMEZANI, J., BOWRING, S. A. & DE KLERK, W. J. 2013. High-precision temporal calibration of Late Permian vertebrate biostratigraphy: U-Pb zircon constraints from the Karoo Supergroup, South Africa. *Geology,* 41, 363-366.

RUSCIO, M. G. & ADKINS-REGAN, E. 2004. Immediate early gene expression associated with induction of brooding behavior in Japanese quail. *Hormones and Behavior,* 46, 19-29.

RYAN, M. J., RUSSELL, A. P., EBERTH, D. A. & CURRIE, P. J. 2001. The taphonomy of a *Centrosaurus* (Ornithischia: Certopsidae) bone bed from the Dinosaur Park Formation (Upper Campanian), Alberta, Canada, with comments on cranial ontogeny. *Palaios,* 16**,** 482-506.

SALTZ, J., PALMER, M. & BEAUDROT, L. 2023. Identifying the social context of single-and mixed-species group formation in large African herbivores. *Philosophical Transactions of the Royal Society B,* 378**,** 20220105.

SANDER, P. M. 1992. The Norian *Plateosaurus* bonebeds of central Europe and their taphonomy. *Palaeogeography, Palaeoclimatology, Palaeoecology,* 93**,** 255-299.

SAUER, J. & SLADE, N. 1987. Size-based demography of vertebrates. *Annual Review of Ecology and Systematics,* 18**,** 71-90.

SCHUETT, G. W., CLARK, R. W., REPP, R. A., AMARELLO, M., SMITH, C. F. & GREENE, H. W. 2016. Social behavior of rattlesnakes: a shifting paradigm. *Rattlesnakes of arizona,* 2**,** 161-244.

SHIPMAN, P. 1975. Implications of drought for vertebrate fossil assemblages. *Nature,* 257**,** 667-668.

SKINNER, M. & MILLER, N. 2020. Aggregation and social interaction in garter snakes (*Thamnophis sirtalis sirtalis*). *Behavioral Ecology and Sociobiology,* 74**,** 1-13.

SMITH, R. 1990a. A review of stratigraphy and sedimentary environments of the Karoo Basin of South Africa. *Journal of African Earth Sciences (and the Middle East),* 10**,** 117-137.

SMITH, R. & BOTHA, J. 2005. The recovery of terrestrial vertebrate diversity in the South African Karoo Basin after the end-Permian extinction. *Comptes Rendus Palevol,* 4**,** 623-636.

SMITH, R., ERIKSSON, P. & BOTHA, W. 1993. A review of the stratigraphy and sedimentary environments of the Karoo-aged basins of Southern Africa. *Journal of African Earth Sciences (and the Middle East),* 16**,** 143-169.

SMITH, R. M. 1987. Helical burrow casts of therapsid origin from the Beaufort Group (Permian) of South Africa. *Palaeogeography, Palaeoclimatology, Palaeoecology,* 60**,** 155-169.

SMITH, R. M. 1990b. Alluvial paleosols and pedofacies sequences in the Permian Lower Beaufort of the southwestern Karoo Basin, South Africa. *Journal of Sedimentary Research,* 60**,** 258-276.

SMITH, R. M. 1995. Changing fluvial environments across the Permian-Triassic boundary in the Karoo Basin, South Africa and possible causes of tetrapod extinctions. *Palaeogeography, Palaeoclimatology, Palaeoecology,* 117**,** 81-104.

SMITH, R. M., ANGIELCZYK, K. D., BENOIT, J. & FERNANDEZ, V. 2021. Neonate aggregation in the Permian dicynodont *Diictodon* (Therapsida, Anomodontia): evidence for a reproductive function for burrows? *Palaeogeography, Palaeoclimatology, Palaeoecology,* 569**,** 110311.

SMITH, R. M., BOTHA, J. & VIGLIETTI, P. A. 2022. Taphonomy of drought afflicted tetrapods in the early Triassic Karoo Basin, South Africa. *Palaeogeography, Palaeoclimatology, Palaeoecology,* 604**,** 111207.

SMITH, R. M. & BOTHA-BRINK, J. 2014. Anatomy of a mass extinction: sedimentological and taphonomic evidence for drought-induced die-offs at the

Permo-Triassic boundary in the main Karoo Basin, South Africa. *Palaeogeography, Palaeoclimatology, Palaeoecology,* 396**,** 99-118.

SMITH, R. M. & EVANS, S. E. 1995. An Aggregation of Juvenile *Yougina* from the Beaufort Group, Karoo Basin, South Africa. *Palaeontologia africana,* 32**,** 45-49.

SMITH, R. M. & EVANS, S. E. 1996. New material of *Youngina*: evidence of juvenile aggregation in Permian diapsid reptiles. *Palaeontology,* 39**,** 289-304.

SMITH, R. M. & WARD, P. D. 2001. Pattern of vertebrate extinctions across an event bed at the Permian-Triassic boundary in the Karoo Basin of South Africa. *Geology,* 29**,** 1147-1150.

SMITH, S. Y., COLLINSON, M. E., RUDALL, P. J., SIMPSON, D. A., MARONE, F. & STAMPANONI, M. 2009a. Virtual taphonomy using synchrotron tomographic microscopy reveals cryptic features and internal structure of modern and fossil plants. *Proceedings of the National Academy of Sciences,* 106**,** 12013-12018.

SMITH, T. M., OLEJNICZAK, A. J., KUPCZIK, K., LAZZARI, V., VOS, J. D., KULLMER, O., SCHRENK, F., HUBLIN, J.-J., YAKOB, T. & TAFFOREAU, P. 2009b. Taxonomic assessment of the Trinil molars using non-destructive 3D structural and development analysis.

SNIGIREV, A., SNIGIREVA, I., KOHN, V., KUZNETSOV, S. & SCHELOKOV, I. 1995. On the possibilities of x-ray phase contrast microimaging by coherent high-energy synchrotron radiation. *Review of scientific instruments,* 66**,** 5486-5492.

SPARKS, J. 1984. Animal Behaviour: an Evolutionary Approach, 3rd editionJohn Alcock Sinauer Associates, Massachusetts, 1984,£ 19· 80. *Oryx,* 18**,** 251-251.

SPEAKMAN, J. R. 2005. Body size, energy metabolism and lifespan. *Journal of Experimental Biology,* 208**,** 1717-1730.

STAMPS, J. 1994. Territorial behavior: testing the assumptions. *Advances in the Study of Behavior,* 23**,** 232.

STANLEY, S. M. & YANG, X. 1994. A double mass extinction at the end of the Paleozoic Era. *Science,* 266**,** 1340-1344.

STEARS, K., SCHMITT, M. H., WILMERS, C. C. & SHRADER, A. M. 2020. Mixed-species herding levels the landscape of fear. *Proceedings of the Royal Society B,* 287**,** 20192555.

SUTTON, M. D. 2008. Tomographic techniques for the study of exceptionally preserved fossils. *Proceedings of the Royal Society B: Biological Sciences,* 275**,** 1587-1593.

TAFFOREAU, P., BOISTEL, R., BOLLER, E., BRAVIN, A., BRUNET, M., CHAIMANEE, Y., CLOETENS, P., FEIST, M., HOSZOWSKA, J. & JAEGER, J.-J. 2006. Applications of X-ray synchrotron microtomography for non-destructive 3D studies of paleontological specimens. *Applied Physics A,* 83**,** 195-202.

TANKARD, A., JACKSON, M., ERIKSSON, K., HOBDAY, D., HUNTER, D., MINTER, W., TANKARD, A., JACKSON, M., ERIKSSON, K. & HOBDAY, D. 1982. *The Intracratonic Karoo Basin,* New York Springer

TATE, J. R. & CANN, C. E. 1982. High-resolution computed tomography for the comparative study of fossil and extant bone. *American Journal of Physical Anthropology,* 58**,** 67-73.

TINBERGEN, J. 2012. *Social behaviour in animals: with special reference to vertebrates*, Springer Science & Business Media.

TURNBULL, W. D. & MARTILL, D. M. 1988. Taphonomy and preservation of a monospecific titanothere assemblage from the Washakie Formation (late

Eocene), southern Wyoming. An ecological accident in the fossil record. *Palaeogeography, Palaeoclimatology, Palaeoecology,* 63**,** 91-108.

VAN DEN BRANDT, M. J., ABDALA, F. & RUBIDGE, B. S. 2020. Cranial morphology and phylogenetic relationships of the Middle Permian pareiasaur *Embrithosaurus schwarzi* from the Karoo Basin of South Africa. *Zoological Journal of the Linnean Society,* 188**,** 202-241.

VAN SCHAIK, C. P. 2010. Social learning and culture in animals. *Animal behaviour: Evolution and mechanisms.* Berlin: Springer.

VARRICCHIO, D. J., SERENO, P. C., XIJIN, Z., LIN, T., WILSON, J. A. & LYON, G. H. 2008. Mud-trapped herd captures evidence of distinctive dinosaur sociality. *Acta Palaeontologica Polonica,* 53**,** 567-578.

VIGLIETTI, P. 2020. Biostratigraphy of the Daptocephalus Assemblage Zone (Beaufort Group, Karoo Supergroup), South Africa. *South African Journal of Geology 2020,* 123**,** 191-206.

VIGLIETTI, P., RUBIDGE, B. & SMITH, R. 2017. Revised lithostratigraphy of the upper Permian Balfour and Teekloof formations of the main Karoo Basin, South Africa. *South African Journal of Geology,* 120**,** 45-60.

VIGLIETTI, P. A. 2016. Stratigraphy and sedimentary environments of the late Permian *Dicynodon* Assemblage Zone (Karoo Supergroup, South Africa) and implications for basin development. University of the Witwatersrand, Faculty of Science, School of Geosciences.

VIGLIETTI, P. A., SMITH, R. M., ANGIELCZYK, K. D., KAMMERER, C. F., FRÖBISCH, J. & RUBIDGE, B. S. 2016. The *Daptocephalus* Assemblage Zone (Lopingian), South Africa: a proposed biostratigraphy based on a new

compilation of stratigraphic ranges. *Journal of African Earth Sciences,* 113**,** 153-164.

VIGLIETTI, P. A., SMITH, R. M. & COMPTON, J. S. 2013. Origin and palaeoenvironmental significance of *Lystrosaurus* bonebeds in the earliest Triassic Karoo Basin, South Africa. *Palaeogeography, Palaeoclimatology, Palaeoecology,* 392**,** 9-21.

VIGLIETTI, P. A., SMITH, R. M. & RUBIDGE, B. S. 2018. Changing palaeoenvironments and tetrapod populations in the *Daptocephalus* Assemblage Zone (Karoo Basin, South Africa) indicate early onset of the Permo-Triassic mass extinction. *Journal of African Earth Sciences,* 138**,** 102-111.

VON DER HEYDEN, B. P., BENOIT, J., FERNANDEZ, V. & ROYCHOUDHURY, A. N. 2020. Synchrotron X-ray radiation and the African earth sciences: a critical review. *Journal of African Earth Sciences,* 172**,** 104012.

WARD, A. & WEBSTER, M. 2016. *Sociality: the behaviour of group-living animals*, Springer.

WATSON, G. & WATSON, J. 2020. Scientists capture rare footage of mother skink fighting a deadly brown snake to protect her babies. *The Conversation,* 3.

WATSON, G. S., GREEN, D. W. & WATSON, J. A. 2020. Observations supporting parental care by a viviparous reptile: aggressive behaviour against predators demonstrated by Cunningham's skinks. *Australian Journal of Zoology,* 67**,** 180-183.

WEY, T., BLUMSTEIN, D. T., SHEN, W. & JORDÁN, F. 2008. Social network analysis of animal behaviour: a promising tool for the study of sociality. *Animal behaviour,* 75**,** 333-344.

WHITE, E. P., ERNEST, S. M., KERKHOFF, A. J. & ENQUIST, B. J. 2007. Relationships between body size and abundance in ecology. *Trends in ecology & evolution,* 22**,** 323-330.

WHITING, M. J. & WHILE, G. M. 2017. 13 Sociality in Lizards. *Comparative social evolution***,** 390.

WOOD, J. M., THOMAS, R. G. & VISSER, J. 1988. Fluvial processes and vertebrate taphonomy: the upper cretaceous Judith River formation, south-central dinosaur Provincial Park, Alberta, Canada. *Palaeogeography, Palaeoclimatology, Palaeoecology,* 66**,** 127-143.

XU, X. & NORELL, M. A. 2004. A new troodontid dinosaur from China with avian-like sleeping posture. *Nature,* 431**,** 838-841.

APPENDICES

Appendix 1

Table 12: Measurements of stylopodia and appropriate body mass equations.

UNIQUE ROI	ID	SIDE	LENGTH	DIAMETER	CIRCUMFERENCE	APPROPRIATE EQUATION	BODY MASS IN GRAMS
R1,P4,P2	Humerus	R	24.110	2.335	7.335619	logBM=2.6861*logCH-0.1438	8.853826
R1,P14	Humerus	L	24.600	2.356	7.401592	logBM=2.6861*logCH-0.1438	8.946785
R1,P14	Humerus	R	25.100	2.70	8.482300	logBM=2.6861*logCH-0.1438	10.488511
R1,P13	Humerus	L	20.079	2.429	7.630929	logBM=2.6861*logCH-0.1438	9.270999
R1,P19,P1	Humerus	L	21.100	2.36	7.414159	logBM=2.6861*logCH-0.1438	8.964508
R1,P23,P1	Humerus	R	22.190	2.29	7.194247	logBM=2.6861*logCH-0.1438	8.655096
R1,P24	Humerus	L	18.950	2.336	7.338760	logBM=2.6861*logCH-0.1438	8.858249
R1,P26,P2	Humerus	R	20.070	2.23	7.005752	logBM=2.6861*logCH-0.1438	8.391137
R1,P40	Humerus	R	20.390	2.35	7.382743	logBM=2.6861*logCH-0.1438	8.920212
R1,P77	Humerus	R	20.580	2.60	8.168141	logBM=2.6861*logCH-0.1438	10.036758
R1,P79,P1	Humerus	L	22.850	2.63	8.262389	logBM=2.6861*logCH-0.1438	10.171986

R1,P91	Humerus	L	20.071	2.53	7.948229	logBM=2.6861*logCH-0.1438	9.722242
R1,P94	Humerus	R	25.361	2.670	8.388052	logBM=2.6861*logCH-0.1438	10.352687
R1,P96,P1	Humerus	L	20.480	2.67	8.388052	logBM=2.6861*logCH-0.1438	10.352687
R1,P111,P1	Humerus	L	20.420	2.64	8.293805	logBM=2.6861*logCH-0.1438	10.217119
R1,P123	Humerus	R	20.030	2.24	7.037168	logBM=2.6861*logCH-0.1438	8.435049
R1,P153	Humerus	L	20.085	2.80	8.796459	logBM=2.6861*logCH-0.1438	10.943059
R1.P183,P4	Humerus	L	23.300	2.80	8.796459	logBM=2.6861*logCH-0.1438	10.943059
R1,P194	Humerus	L	20.680	2.50	7.853982	logBM=2.6861*logCH-0.1438	9.587891
R1,P195	Humerus	R	22.220	2.809	8.824734	logBM=2.6861*logCH-0.1438	10.984104
R1,P216,P10	Humerus	L	20.510	2.475	7.775442	logBM=2.6861*logCH-0.1438	9.476136
R1,P225	Humerus	R	20.830	2.302	7.231946	logBM=2.6861*logCH-0.1438	8.708028
R1,P234	Humerus	R	21.608	2.269	7.128274	logBM=2.6861*logCH-0.1438	8.562578
R1,P237,P1	Humerus	L	20.700	2.660	8.356636	logBM=2.6861*logCH-0.1438	10.307469
R1,P240	Humerus	R	20.326	2.76	8.670796	logBM=2.6861*logCH-0.1438	10.760911
R1,P245,P4	Humerus	R	22.300	2.80	8.796459	logBM=2.6861*logCH-0.1438	10.943059
R1,P253	Humerus	R	23.730	2.821	8.862433	logBM=2.6861*logCH-0.1438	11.038863
R1,P255,P1	Humerus	L	22.800	2.68	8.419468	logBM=2.6861*logCH-0.1438	10.397934
R1,P268,P1	Humerus	R	20.900	2.44	7.665486	logBM=2.6861*logCH-0.1438	9.319995
R1,P271	Humerus	R	26.140	2.44	7.665486	logBM=2.6861*logCH-0.1438	9.319995

R1,P274	Humerus	L	20.960	2.84	8.922123	logBM=2.6861*logCH-0.1438	11.125643
R1,P275	Humerus	R	20.680	2.80	8.796459	logBM=2.6861*logCH-0.1438	10.943059
R1,P285,P1	Humerus	R	20.250	2.70	8.482300	logBM=2.6861*logCH-0.1438	10.488511
R1,P289.P7	Humerus	R	21.200	2.53	7.948229	logBM=2.6861*logCH-0.1438	9.722242
R1,P183,P4	Humerus	L	23.300	2.189	6.876946	logBM=2.6861*logCH-0.1438	8.211440
R1,294,P1	Humerus	L	26.800	2.809	8.824734	logBM=2.6861*logCH-0.1438	10.984104
R1,P294,P3	Humerus	R	22.220	2.801	8.799601	logBM=2.6861*logCH-0.1438	10.947619
R2,P4	Humerus	R	20.560	2.70	8.482300	logBM=2.6861*logCH-0.1438	10.488511
R2,P8	Humerus	R	26.340	2.74	8.607964	logBM=2.6861*logCH-0.1438	10.670000
R2,P7,P1	Humerus	L	26.770	2.85	8.953539	logBM=2.6861*logCH-0.1438	11.171356
R2,P7,P2	Humerus	L	21.080	2.814	8.840442	logBM=2.6861*logCH-0.1438	11.006915
R2,P19	Humerus	R	21.170	2.834	8.903274	logBM=2.6861*logCH-0.1438	11.098229
R5,P8	Humerus	L	20.480	2.53	7.948229	logBM=2.6861*logCH-0.1438	9.722242
R5,P9	Humerus	R	20.530	2.429	7.630929	logBM=2.6861*logCH-0.1438	9.270999
R1,P1	Femur	R	32.200	3.341	10.496061	logBM=2.8479*logCF-0.4587	11.57770
R1,P3,P2	Femur	R	36.050	3.6	11.309734	logBM=2.8479*logCF-0.4587	12.69778
R1,P4	Femur	L	34.700	3.38	10.618583	logBM=2.8479*logCF-0.4587	11.74509
R1,P4	Femur	L	36.700	3.42	10.744247	logBM=2.8479*logCF-0.4587	11.91724
R1,P5	Femur	R	34.100	3.413	10.722256	logBM=2.8479*logCF-0.4587	11.88708

R1,P7	Femur	R	34.100	3.36	10.555751	logBM=2.8479*logCF-0.4587	11.65919
R1,P1	Femur	L	33.200	3.35	10.524335	logBM=2.8479*logCF-0.4587	11.61629
R1,P14	Femur	R	33.110	3.09	9.707521	logBM=2.8479*logCF-0.4587	10.51167
R1,P14	Femur	L	34.530	3.02	9.487610	logBM=2.8479*logCF-0.4587	10.21794
R1,P14	Femur	R	33.370	3.47	10.901327	logBM=2.8479*logCF-0.4587	12.13310
R1,P14	Femur	L	33.140	3.29	10.335840	logBM=2.8479*logCF-0.4587	11.35951
R1,P14	Femur	R	34.040	3.35	10.524335	logBM=2.8479*logCF-0.4587	11.61629
R1,P12	Femur	L	35.800	3.30	10.367256	logBM=2.8479*logCF-0.4587	11.40223
R1,P12	Femur	R	36.300	3.38	10.618583	logBM=2.8479*logCF-0.4587	11.74509
R1,P18	Femur	L	36.200	3.41	10.712831	logBM=2.8479*logCF-0.4587	11.87416
R1,P18	Femur	R	33.140	3.41	10.712831	logBM=2.8479*logCF-0.4587	11.87416
R1,P23	Femur	R	35.600	3.35	10.524335	logBM=2.8479*logCF-0.4587	11.61629
R1,P33	Femur	L	34.280	3.27	10.273008	logBM=2.8479*logCF-0.4587	11.27416
R1,P76	Femur	L	34.800	3.468	10.895043	logBM=2.8479*logCF-0.4587	12.12445
R1,P77	Femur	L	36.800	3.394	10.662565	logBM=2.8479*logCF-0.4587	11.80528
R1,P80	Femur	L	31.100	3.34	10.492919	logBM=2.8479*logCF-0.4587	11.57341
R1,P1	Femur	L	35.030	3.442	10.813362	logBM=2.8479*logCF-0.4587	12.01213
R1,P108	Femur	L	34.740	3.03	9.519026	logBM=2.8479*logCF-0.4587	10.25980
R1,P108	Femur	L	34.700	3.339	10.489778	logBM=2.8479*logCF-0.4587	11.56913

R1,P116	Femur	R	30.200	3.00	9.424778	logBM=2.8479*logCF-0.4587	10.13431
R1,P177	Femur	R	32.700	3.547	11.143229	logBM=2.8479*logCF-0.4587	12.46697
R1,P188	Femur	L	33.400	3.490	10.964158	logBM=2.8479*logCF-0.4587	12.21965
R1,P178	Femur	L	32.840	3.066	9.632123	logBM=2.8479*logCF-0.4587	10.41078
R1,P179	Femur	R	31.770	3.050	9.581858	logBM=2.8479*logCF-0.4587	10.34363
R1,P179,P3	Femur	L	34.900	3.10	9.738937	logBM=2.8479*logCF-0.4587	10.55376
R1,P183	Femur	R	33.800	3.6	11.309734	logBM=2.8479*logCF-0.4587	12.69778
R1,P183,P4	Femur	L	33.720	3.45	10.838495	logBM=2.8479*logCF-0.4587	12.04667
R1,P1184,P6	Femur	L	34.500	3.36	10.555751	logBM=2.8479*logCF-0.4587	11.65919
R1,P188,P1	Femur	R	34.080	3.25	10.210176	logBM=2.8479*logCF-0.4587	11.18894
R1,P203,P3	Femur	L	32.050	3.019	9.484468	logBM=2.8479*logCF-0.4587	10.21375
R1,P209,P1	Femur	L	34.380	3.10	9.738937	logBM=2.8479*logCF-0.4587	10.55376
R1,P216,P6	Femur	L	35.800	3.7	11.623893	logBM=2.8479*logCF-0.4587	13.13545
R1,P230	Femur	L	32.100	3.157	9.918008	logBM=2.8479*logCF-0.4587	10.79429
R1,P232	Femur	L	30.600	3.01	9.456194	logBM=2.8479*logCF-0.4587	10.17611
R1,P237,P1	Femur	R	35.290	3.263	10.251017	logBM=2.8479*logCF-0.4587	11.24432
R1,P237,P2,P1	Femur	R	34.090	3.183	9.999689	logBM=2.8479*logCF-0.4587	10.90435
R1,P245,P4	Femur	L	31.638	3.12	9.801769	logBM=2.8479*logCF-0.4587	10.63804
R1,P252	Femur	L	33.600	3.37	10.587167	logBM=2.8479*logCF-0.4587	11.70212

R1,P268	Femur	R	35.300	3.21	10.084512	logBM=2.8479*logCF-0.4587	11.01886
R1,273,P4	Femur	L	32.602	3.134	9.845751	logBM=2.8479*logCF-0.4587	10.69711
R1,P274	Femur	L	30.400	3.032	9.525309	logBM=2.8479*logCF-0.4587	10.26818
R1,P294,P1	Femur	L	34.325	3.205	10.068804	logBM=2.8479*logCF-0.4587	10.99764
R2,P4	Femur	R	33.380	3.45	10.838495	logBM=2.8479*logCF-0.4587	12.04667
R2,P7	Femur	L	30.830	3.072	9.650973	logBM=2.8479*logCF-0.4587	10.43599
R2,P8	Femur	R	33.670	3.343	10.502344	logBM=2.8479*logCF-0.4587	11.58627
R2,P15	Femur	R	33.670	3.345	10.508627	logBM=2.8479*logCF-0.4587	11.59485
R2,P16	Femur	L	33.601	3.35	10.524335	logBM=2.8479*logCF-0.4587	11.61629

Appendix 2

R Code for t-test

```
#Loading the necessary packages
library(ggplot2) library(readr)
library(dplyr) library(tidyverse)

#Setting directory  getwd()
list.files()
setwd("/Users/lutendomukwevho/Downloads")
C1=read.csv("/Users/lutendomukwevho/Downloads/HUMERUS.csv",sep = ';')

#T-TEST FOR THE HUMERAL LENGTH
LENGTH_L <- C1$LENGTH.[C1$SIDE == "L"]
LENGTH_R <- C1$LENGTH.[C1$SIDE == "R"]

# Perform t-test t_test_result <-
t.test(LENGTH_L, LENGTH_R)

# View the result print(t_test_result)

LENGTH_sd <- C1 %>% group_by(SIDE)
%>%
summarise(sd_LENGTH = sd(LENGTH.)) print(LENGTH_sd)

#T-TEST FOR THE HUMERAL DIAMETER
DIAMETER_L <- C1$DIAMETER.[C1$SIDE == "L"]
DIAMETER_R <- C1$DIAMETER.[C1$SIDE == "R"]
```

```
# Perform t-test t_test_result <- t.test(DIAMETER_L,
DIAMETER_R)

# View the result print(t_test_result)

DIAMETER_sd <- C1 %>% group_by(SIDE) %>%
summarise(sd_DIAMETER = sd(DIAMETER.))
print(DIAMETER_sd)

side_counts <- C1 %>%
count(SIDE) print(count)

C2=read.csv("/Users/lutendomukwevho/Downloads/FEMUR.csv",sep = ';')

#T-TEST FOR THE FEMORAL LENGTH
LENGTH_L <- C2$LENGTH[C1$SIDE == "L"]
LENGTH_R <- C2$LENGTH[C1$SIDE == "R"]

# Perform t-test t_test_result <-
t.test(LENGTH_L, LENGTH_R)

# View the result print(t_test_result)

LENGTH_sd <- C2 %>% group_by(SIDE)
%>% summarise(sd_LENGTH =
sd(LENGTH)) print(LENGTH_sd)

#T-TEST FOR THE FEMORAL DIAMETER
DIAMETER_L <- C1$DIAMETER[C2$SIDE == "L"]
DIAMETER_R <- C1$DIAMETER[C2$SIDE == "R"]
```

```
# Perform t-test t_test_result <- t.test(DIAMETER_L,
DIAMETER_R)

# View the result print(t_test_result)

DIAMETER_sd <- C2 %>% group_by(SIDE) %>%
summarise(sd_DIAMETER = sd(DIAMETER))
print(DIAMETER_sd)

side_counts <- C2 %>%
count(SIDE) print(count)
```

Appendix 3

R Code for plotting histograms

```
#Distribution of femoral diameter ggplot(C2, aes(x = DIAMETER))
+ # Specifying x-axis as DIAMETER.
geom_histogram(aes(fill = factor(SIDE)), color = "black", bins = 10, position = "dodge")
# Adding histogram layer with dodged bars geom_density(aes(color = factor(SIDE)), size
= 1.5) + # Adding density curve with diZerent colors for sides
labs(x = "Diameter", y = "Frequency/Density", title = "Histogram of Diameter by Side with
Density Curve") + # Adding labels scale_fill_manual(values = c("pink", "lightblue"), labels
= c("SIDE L", "SIDE R")) + # Setting colors and labels for sides scale_color_manual(values
= c("red", "blue"), labels = c("SIDE L", "SIDE R")) + # Setting colors and labels for sides in
density curve theme_minimal() # Applying minimal theme

#Distribution of femoral length ggplot(C2, aes(x = LENGTH)) + geom_histogram(aes(fill
= factor(SIDE)), color = "black", bins = 10, position = "dodge") + geom_density(aes(color
= factor(SIDE), y = ..scaled..), size = 1.5, position = "identity") + labs(x = "Length", y =
"Frequency/Density", title = "Histogram of Length by Side with Density Curve") +
scale_fill_manual(values = c("pink", "lightblue"), labels = c("SIDE L", "SIDE R")) +
scale_color_manual(values = c("red", "blue"), labels = c("SIDE L", "SIDE R")) +
theme_minimal()

#Distribution of humeral diameter ggplot(C1, aes(x =
DIAMETER.)) + # Specifying x-axis as DIAMETER.
geom_histogram(aes(fill = factor(SIDE)), color = "black", bins = 10, position = "dodge") +
# Adding histogram layer with dodged bars geom_density(aes(color = factor(SIDE)), size
= 1.5) + # Adding density curve with diZerent colors for sides
```

```
labs(x = "Diameter", y = "Frequency/Density", title = "Histogram of Diameter by Side with Density Curve") + # Adding labels scale_fill_manual(values = c("pink", "lightblue"), labels = c("SIDE L", "SIDE R")) + # Setting colors and labels for sides scale_color_manual(values = c("red", "blue"), labels = c("SIDE L", "SIDE R")) + # Setting colors and labels for sides in density curve  theme_minimal() # Applying minimal theme

#Distribution humeral length ggplot(C1, aes(x = LENGTH.)) +  geom_histogram(aes(fill = factor(SIDE)), color = "black", bins = 10, position = "dodge") +  geom_density(aes(color = factor(SIDE), y = ..scaled..), size = 1.5, position = "identity") +  labs(x = "Length", y = "Frequency/Density", title = "Histogram of Length by Side with Density Curve") + scale_fill_manual(values = c("pink", "lightblue"), labels = c("SIDE L", "SIDE R")) + scale_color_manual(values = c("red", "blue"), labels = c("SIDE L", "SIDE R")) + theme_minimal()
```